REGULATION OF CELLULAR GROWTH AND DIFFERENTIATION BY MICRORNAS -21 AND -451

APPROVED BY SUPERVISORY COMMITTEE

Eric N. Olson, Ph.D.

Raymond J. MacDonald, Ph.D.

Joseph A. Hill, M.D, Ph.D.

Jane E. Johnson, Ph.D.

Lily Jun-Shen Huang, Ph.D.

To my wife Anna

Acknowledgements

I am grateful to many individuals who enhanced my training and contributed to my efforts. I must thank Jim Richardson and John Shelton for their service and advice; Cheryl Nolan and Sasha Qi for their help with animals and cell culture. I must also thank Dr. Joseph Hill and his laboratory for advice and support in all things cardiovascular. The surgeons in his laboratory, Yongli and Herman, performed all TAC and MI studies in the miR-21 story. Young-Jae Nam was very generous and performed the surgeries for the transient deletion story.

I also would like to acknowledge Eva van Rooij, who generated the miR-21 knockout mice and guided me during the genesis of my microRNA projects. She along with Rusty Montgomery, were essential to the miR-21 story and continue to be essential in the support of my ongoing work. I also must thank Alec Zhang who taught me how to work with hematopoietic cells and perform flow cytometry. He was essential to the original miR-451 discoveries. Mitchell Weiss was very generous in his assistance with the miR-451 story. He delayed publication of his work and shared both reagents and his own advice with us during the preparation of our manuscript. His kindness was unexpected and essential to our success in the publication of that story. I am deeply indebted to Lily Huang and Huiyu Yao who helped me perform many of the miR-451 phenotyping studies. Lily continues to advise me on many of the miR-451 experiments. Lily and Huiyu are essential for the continuing studies on miR-451 and PV.

The advice, scientific insight, and day-to-day hard work of Rhonda Bassel-Duby was critical for my training. Without Rhonda, my work would not have been possible.

My mentor Eric Olson has given me an invaluable training experience. The caliber of the science being performed in his laboratory deserves the distinguished reputation. My training in

experimental technique and design has been excellent. I must also express my gratitude for the scientific training that I have gained working with Eric on manuscripts, grants, presentations, and patents. These experiences are not common for graduate students and have given me a set of skills that will assist me in much more than the experimental side of science. Finally, Eric fosters an environment that encourages ingenuity, which, as he has taught me, is essential for discovery. He always entertains unconventional ideas.

I must also thank my undergraduate mentor Jonathan King for sparking my interest in basic science and contributing greatly to my decision to pursue a combined degree. The report that we published together has helped me in many ways that I did not expect. Johannes Backs continues to be a positive influence on my scientific career. Johannes trained me early in my graduate career and has always been enthusiastic about our work together.

Finally, I could not have accomplished this without my family. Specifically, my wife Anna who has given me her love and support unconditionally.

REGULATION OF CELLULAR GROWTH AND DIFFERENTIATION BY MICRORNAS -21 AND -451

by

David M. Patrick

DISSERTATION

Presented to the Faculty of the Graduate School of Biomedical Sciences

The University of Texas Southwestern Medical Center at Dallas

In Partial Fulfillment of the Requirements

For the Degree of

DOCTOR OF PHILOSOPHY

The University of Texas Southwestern Medical Center at Dallas

Dallas, Texas

April, 2011

REGULATION OF CELLULAR GROWTH AND DIFFERENTIATION BY MICRORNAS -21 AND -451

David M. Patrick

The University of Texas Southwestern Medical Center at Dallas, 2011

Mentor: Eric N. Olson, Ph.D.

MicroRNAs are small RNAs approximately 20-24 nucleotides in length that are conserved throughout evolution. MicroRNA genes are transcribed by RNA polymerase II and are processed both in the nucleus and the cytoplasm from longer precursor RNAs. Functionally, microRNAs interact with Argonaute proteins and guide the formation of a complex with messenger RNAs by Watson-Crick base-pair formation between the microRNA and mRNA. This association stimulates the formation of the microRNA-RNA-induced silencing complex which, upon association with essential adaptor molecules such as GW182, recruits transcriptional repressors and mRNA destabilizers. Essential developmental processes such as embryonic stem cell differentiation and cardiovascular development have been shown to be dependent upon microRNAs. MicroRNAs also participate in a variety of disease processes including tumorigenesis and cardiovascular disease.

MicroRNA-451 (miR-451) is regulated during erythrocyte terminal differentiation. The expression of miR-451 is restricted to late erythrocyte precursors and terminally differentiated erythrocytes. We therefore hypothesized that miR-451 plays a role in terminal erythroid differentiation. Deletion of miR-451 in mice results in a terminal erythroid differentiation defect both embryonically and in adulthood. These animals display a reduction in hematocrit and an inability to sustain a high erythropoietic rate. Transient inhibition of miR-451 results in the same defect. Transcript profiling of *miR-451*$^{-/-}$ erythroblasts revealed upregulation of 14-3-3ζ, a molecule

implicated in the regulation of hematopoiesis. Knockdown of 14-3-3ζ with shRNA in *miR-451*$^{-/-}$ erythroblasts attenuates the differentiation defect. These data show the essential role of miR-451 repression of 14-3-3ζ during terminal erythrocyte differentiation. Finally, the potent effect of miR-451 inhibition on erythrocyte production suggests that this strategy may be efficacious for the treatment of polycythemia vera, a myeloproliferative neoplasm characterzed by excessive erythrocyte production. Inhibition of miR-451 in a mouse model of PV significantly reduces disease burden.

MicroRNA-21 (miR-21) is regulated in a variety of both human and mouse models of disease. MiR-21 has been widely reported as a driver of tumorigenesis and is consistently upregulated in cardiac remodeling. It has been suggested that miR-21 plays a protective role during cardiac hypertrophy, however, an opposing report suggests that miR-21 inhibition is beneficial in a mouse model of cardiac remodeling. We therefore hypothesized that miR-21 played an essential role in cardiac hypertrophy and remodeling. Deletion of miR-21 in mice resulted in no observable phenotype. *MiR-21*$^{-/-}$ displayed cardiac remodeling, cardiac stress-responsive gene activation, and reduction in cardiac function in response to four cardiac stress models: thoracic aortic constriction, angiotensin II infusion, calcineurin overexpression, and myocardial infarction. Moreover, inhibition of miR-21 with an LNA-modified miR-21 inhibitor did not modify cardiac remodeling. Finally, inducible genetic deletion of miR-21 did not modify the cardiac response to TAC. These data do not support a role for miR-21 in cardiac disease, however, further analyses of *miR-21*$^{-/-}$ mice show that these animals are protected from non-small-cell lung cancer (NSCLC). Furthermore, *miR-21*$^{-/-}$ mouse embryonic fibroblasts are sensitized to doxorubicin-induced apoptosis. These data suggest that inhibition of miR-21 will be efficacious in the treatment of NSCLC while having minimal effects on other tissue types.

Table of Contents

List of Publications

Patrick, D.M., Zhang, C.C., Tao, Y., Yao, H., Qi, X., Schwartz, R.J., Jun-Shen Huang, L., and Olson, E.N. 2010b. Defective erythroid differentiation in miR-451 mutant mice mediated by 14-3-3zeta. *Genes Dev* **24**(15): 1614-1619.

Patrick, D.M., Montgomery, R.L., Qi, X., Obad, S., Kauppinen, S., Hill, J.A., van Rooij, E., and Olson, E.N. 2010a. Stress-dependent cardiac remodeling occurs in the absence of microRNA-21 in mice. *J Clin Invest* **120**(11): 3912-3916.

Hatley, M.E., **Patrick, D.M.,** Garcia, M.R., Richardson, J.A., Bassel-Duby, R., van Rooij, E., and Olson, E.N. 2010. Modulation of K-Ras-dependent lung tumorigenesis by MicroRNA-21. *Cancer Cell* **18**(3): 282-293.

Backs, J., Backs, T., Neef, S., Kreusser, M.M., Lehmann, L.H., **Patrick, D.M.,** Grueter, C.E., Qi, X., Richardson, J.A., Hill, J.A. et al. 2009. The delta isoform of CaM kinase II is required for pathological cardiac hypertrophy and remodeling after pressure overload. *Proc Natl Acad Sci U S A* **106**(7): 2342-2347.

Patrick, D.M., Leone, A.K., Shellenberger, J.J., Dudowicz, K.A., and King, J.M. 2006. Proinflammatory cytokines tumor necrosis factor-alpha and interferon-gamma modulate epithelial barrier function in Madin-Darby canine kidney cells through mitogen activated protein kinase signaling. *BMC Physiol* **6**: 2.

List of Figures

List of Abbreviations

mRNA	Messenger ribonucleic acid
miR	MicroRNA
nt	Nucleotides
pri-microRNA	Primary micro-ribonucleic acid
RISC	RNA-Induced Silencing Complex
Ago1-4	Argonaute proteins 1 through 4
siRNA	Small interfering ribonucleic acid
ES cells	Embryonic stem sells
HCV	Hepatitis C virus
bp	Base pairs
LNA	Locked nucleic acid
MEP	Megakaryocyte/erythrocyte precursor cells
CD71	Cluster of differentiation 71, transferrin receptor protein 1
TER119	Glycophorin A, erythrocyte terminal differentiation marker
EPO	Erythropoietin
BFU-E	Burst forming unit erythroblast
CFU-E	Colony forming unit erythroblast
JAK2	Janus kinase 2
PI3K	Phosphatidylinositol 3-kinase
MAPK	Mitogen activated protein kinase
STAT5	Signal transducer and activator of trancription 5
MX1-Cre	Hematopoietic cell-specfic inducible Cre-recombinase
ENU	*N*-ethyl-*N*-nitrosourea
GATA1/2	GATA-binding factor 1 or 2
β-Gal	β-Galactosidase
HCT	Hematocrit
d.p.c.	Days post coitus
MACS	Magnetic cell separation
UTR	Unstranslated region

shRNA	Small hairpin RNA
GFP	Green fluorescent protein
IRES	Internal ribosomal entry site
MI	Myocardial infarction
TAC	Thoracic aortic constriction
βMHC	β myosin heavy chain
PDCD4	Programmed cell death 4
CnA	Calcineurin
AngII	Angiotensin II
LAD	Left anterior descending coronary artery
HW/BW	Heart weight to body weight ratio
VW/TL	Ventricular weight to tibial length ratio
CAG-Cre-ESR1	Ubiquitously expressed inducible cre recombinase
IC_{50}	Half maximal inhibitory concentration
tTA	Tetracycline responsive transactivator
NSCLC	Non-small-cell lung cancer
PV	Polycythemia vera
HSC	Hematopoietic stem cell
JAK2-WT	Mice harboring a bone marrow graft that overexpresses wild-type human JAK2
JAK2-VF	Mice harboring a bone marrow graft that overexpresses human JAK2-V617F constitutively active kinase

Chapter I

Introduction

Evolution of microRNAs

The presence of a protein product in an organism is the result of the expression of one or more genes. The process of gene expression includes multiple transcriptional and post-transcriptional events that modify numerous properties of the final protein product. The regulation of protein abundance is dependent upon the level of transcription of a specific genomic locus, the stability of the processed messenger RNA (mRNA), the efficiency of its translation, and the stability of the protein product (Jaenisch and Bird 2003; Raj and van Oudenaarden 2008). Transcription factors and associated molecules are responsible for both activation and repression of transcription of genetic loci and therefore contribute significantly to the final expression of genes. Recently, however, factors that affect spliced, fully processed mRNAs have also been strongly implicated as important modulators of gene expression. Specifically, a highly conserved family of small RNA molecules termed microRNAs has been shown to contribute to the regulation of gene expression by inducing a cascade of events that lead to the modification of fully processed mRNA molecules (Ambros 2001; Ambros 2010).

MicroRNAs are a group of small non-translated RNA molecules that are approximately 20-24 nt in length. These molecules evolved at the onset of multicellularity and are present in both plant and animal species (Lagos-Quintana et al. 2001; Lau et al. 2001; Lee and Ambros 2001). The first microRNA discovered, lin-4, was described in *C. elegans* in 1993, where it was shown to play a role in diverse post-embryonic developmental events by repressing expression of the lin-14 protein (Lee et al. 1993). Further studies in invertebrates revealed diverse developmental functions for microRNAs including roles in cell proliferation and stage progression (Moss et al. 1997; Hipfner et al. 2002). With the exception of the let-7 family, few microRNAs are conserved throughout all metazoans. Significant divergence of microRNA

sequences occurred with the rise of vertebrates and in general, the functions and sequences of many microRNA families have been conserved within this group (Liu et al. 2008).

MicroRNA biogenesis and maturation

MicroRNAs are transcribed by RNA polymerase II as large primary transcripts ranging in size from 500 to 10,000 nt (pri-microRNA). Although microRNAs are typically processed from unique non-protein coding transcripts, many microRNAs are processed out of an intron of a protein coding gene, referred to as the host gene. In this case, both the host gene and the microRNA share regulatory elements. Often, intronic microRNAs and their host genes participate in the regulation of similar molecular pathways (Bartel 2004; Kim 2005). Greater than one microRNA may be encoded and processed from the same pri-microRNA. Appropriate processing of the pri-microRNA requires the formation of stem-loop secondary structure which includes the mature microRNA sequence. The hairpin structure is recognized in the nucleus by the RNAse III drosha/DGCR8 enzyme complex that then cleaves the loop structure from the pri-microRNA to generate an approximately 70 nt hairpin termed the pre-microRNA. The pre-microRNA is then recognized by the nuclear export receptor exportin 5 which facilitates its translocation to the cytoplasm (Bartel 2004; Bartel 2009).

Typical cytoplasmic processing of pre-microRNAs is carried out by the Dicer. Dicer recognizes the hairpin secondary structure and cleaves it, yielding a duplex consisting of the mature microRNA and its partially antisense strand which is termed the star strand designated with an asterisk in the nomenclature (Kim 2005). The biological significance of the microRNA* strand varies with each microRNA. Studies profiling the abundance of small RNA species have shown that the majority of microRNA* strands are selectively degraded, however, specific

examples of stable microRNA* strands have been reported. In these cases, the microRNA* strand likely functions as a separate microRNA (Chiang et al. 2010). After Dicer mediated cleavage, the microRNA-microRNA* duplex is recognized by the members of the Argonaute family of RNA binding proteins (Lee et al. 2002; Kim 2005). Due to this association, stable microRNA* molecules are unlikely to freely base-pair with mature microRNAs and therefore do not act as endogenous microRNA inhibitors (Figure 1.1).

Loading of the microRNA into argonaute is the critical step in the formation of a functional RNA-induced-silencing-complex (RISC) (Meister et al. 2004). Argonaute proteins unwind the duplex and load the microRNA into its RNA binding pocket with the 5' end oriented into the nucleic-acid-binding channel between the PAZ and PIWI domains. Crystallographic studies of the ternary Argonaute-microRNA-target complex revealed an alpha-helical-like Watson-Crick paired duplex between 5' nucleotides 2-8 of the microRNA with the target molecule (Boland et al. 2010; Frank et al. 2010). Other regions of the microRNA do not participate in the microRNA-target interaction. These structural studies are supported by experimental analyses showing that nucleotides 2-8 are required for appropriate microRNA induced slilencing of target molecules (Lewis et al. 2003; Brennecke et al. 2005; Krek et al. 2005; Lewis et al. 2005). These nucleotides are called the "seed" region of the microRNA. MicroRNAs that share the same seed region are considered members of the same family due to the likelihood of shared target genes. Bioinformatic algorithms that predict likely microRNA target mRNAs utilize this seed sequence as a primary determinant (Bartel 2009). Several other determinants of efficient microRNA-mRNA interactions have been noted, including mRNA secondary structure and the location of the microRNA binding sites. Binding sites within the 3'-UTR near the stop codon or near the poly-A tail are most effective (Lewis et al. 2005).

It should be noted that only a single identified microRNA, miR-451, bypasses Dicer-mediated processing. The biogenesis and function of this unique microRNA will be discussed in detail in Chapter II.

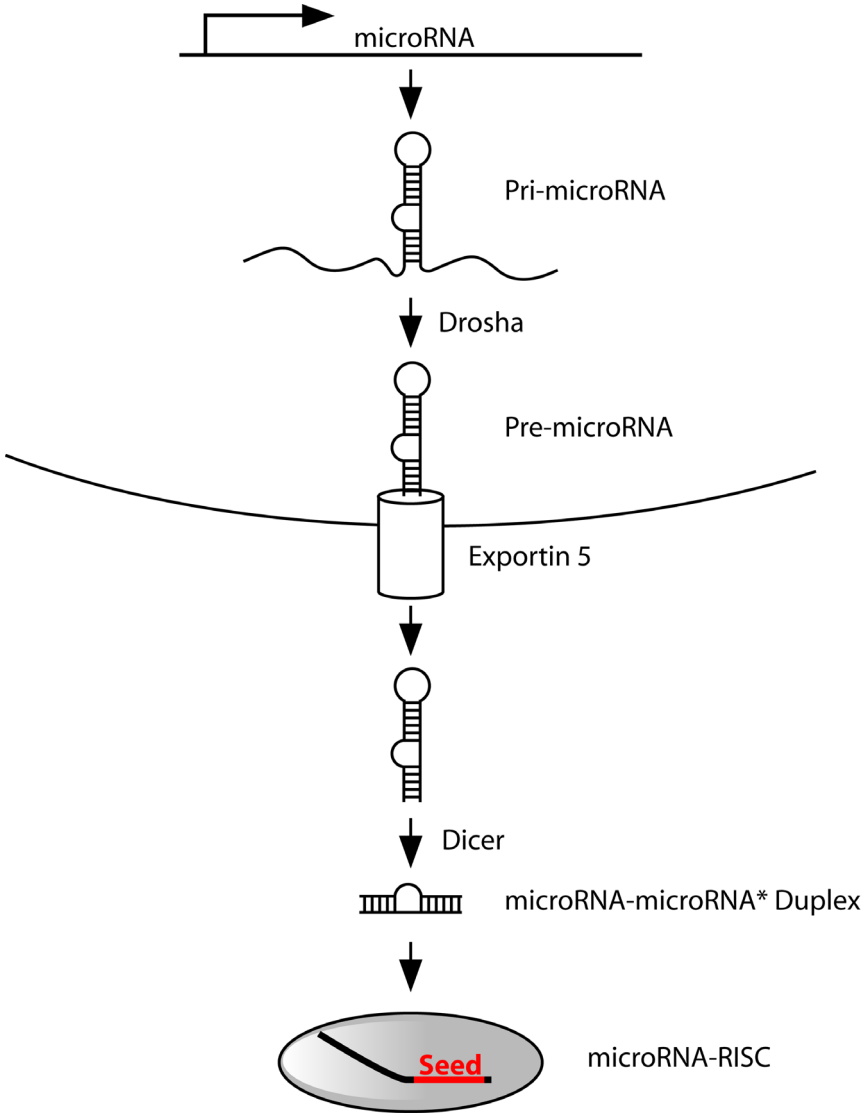

Figure 1.1- MicroRNA biogenesis. MicroRNA genes are transcribed by RNA polymerase II as a large primary transcript termed a pri-microRNA. The pri-microRNA is processed within the nucleus by the Drosha complex into an approximately 70 nucleotide hairpin termed the pre-microRNA. The pre-microRNA is then exported from the nucleus to the cytoplasm where it is further processed by Dicer into the microRNA-microRNA* duplex. The mature microRNA is then preferentially loaded into the microRNA-RNA-Induced-Silencing-Complex (microRNA-RISC).

The microRNA RNA-Induced-Silencing-Complex (microRNA-RISC): mechanism of microRNA-mediated mRNA repression

The miRISC is built upon the mature microRNA bound to a target mRNA within the binding pocket of an Argonaute family member. Argonautes are members of the PIWI domain containing family of RNA binding proteins. In mammals, there are four Argonaute isoforms, Ago1-Ago4, of which only Ago2 possesses the critical residues required for slicer activity (O'Carroll et al. 2007). Although the active cleavage (slicing) of double-stranded RNA is the critical mechanism mediating the small-interfering RNA (siRNA) response, microRNA induced mRNA silencing is independent of this function. In this regard, microRNAs have been shown to be equally associated with all Argonaute isoforms, suggesting their redundancy in this process (Su et al. 2009). Once the microRNA is bound to Argonaute, a number of protein components interact with the complex and mediate mRNA translational inhibition or destabilization.

Many Argonaute associated proteins have been identified including TSN-1, VIG-1, and Mov10; however, their functions as modifiers of Argonaute function and microRNA mediated mRNA repression have not been described (Mourelatos et al. 2002; Meister et al. 2005). It is clear, however, that the GW182 family of proteins is essential for microRNA-mediated mRNA repression. GW182 proteins strongly interact with all Argonaute family members and are conserved amongst metazoans. Knockdown of GW182 in *Drosophila* leads to mRNA profiles that are similar to Argonaute knockdown experiments, suggesting similar functions (Rehwinkel et al. 2005; Schneider et al. 2006; Ding and Han 2007). The ultimate importance of GW182 family members is suggested to be their function as a critical component for the formation of subcellular compartments termed P bodies.

The P body is a collection of RNA associated proteins that is polysome poor. Debate exists as to the actual size of a P body. Indeed, large P bodies have been documented that are visible by light-microscopy, however, a P body may be loosely defined as the collection of P body component proteins on an RNA scaffold (Parker and Sheth 2007). Therefore, functional P body components may not always be visible by light microscopy. P body protein components include the translational repressor molecules Rbp1 and TTP, which have been suggested to interact with ribosomes due to the documentation of mRNA re-entry into the polysome pool upon changes in conditions (Fenger-Gron et al. 2005; Jang et al. 2006). Many mRNAs within the P body are associated with mRNA destabilizing enzymes, the best characterized components of which are the Ccr4p/Pop2p/Not1-5 complex of deadenylases, the Xrn1p exonuclease, and the Dhh1p/Me31B/RCK/p54 decapping complex (Ingelfinger et al. 2002; Cougot et al. 2004; Andrei et al. 2005; Parker and Sheth 2007). Combined, these factors contribute to the destabilization and degradation of mRNA molecules within the P body (Figure 1.2). Despite a significant number of studies suggesting the functions of P bodies and their role in microRNA-mediated mRNA repression, very little is known about the interplay of P body components and their interactions with the ribosome. We can conclude that microRNA binding to an mRNA target gene may result in either translational inhibition or degradation of the target, however, it is likely that this process is dynamic and is regulated upon stress.

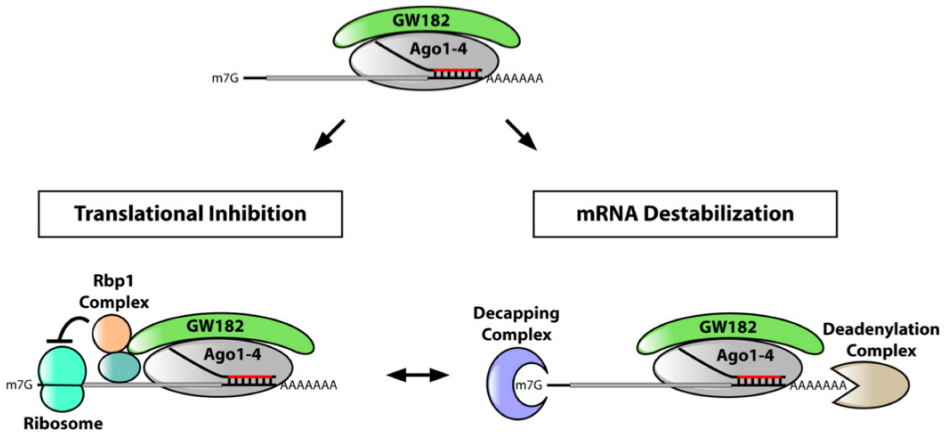

Figure 1.2-MicroRNAs function to repress mRNA expression. Once bound to an Argonaute protein (Ago1-4) the complex is targeted to a target mRNA. Next, the adaptor molecule GW182 is recruited. GW182 facilitates interactions with both the Rbp1 translational repression complex, deadenylation complexes, and decapping complexes. These interactons are dynamic and result in a repression of mRNA expression.

The role of microRNAs in mammalian development

The global role of microRNAs as regulators of development has been established. Deletion of both Dicer and DGCR8 in embryonic stem (ES) cells lead to dramatic defects in cellular differentiation. Deletion of Dicer in ES cells leads to severe differentiation defects and reduced silencing of centromeric repeat sequences, which is required for genomic stability (Kanellopoulou et al. 2005). DGCR8 null ES cells lack the capacity to fully differentiate. Upon induction of differentiation, these cells retain the expression of pluripotency markers (Wang et al. 2007). Tissue specific deletion of Dicer typically results in a non-specific, global disruption of tissue function (Stefani and Slack 2008).

To date, approximately 30 reports describe the targeted deletion of specific microRNAs in mice. The diversity of the function of specific microRNAs is highlighted by a review of these reports (Park et al. 2010). Congruent with this observation is the description of both developmental abnormailites and embryonic lethality in individual microRNA knockout mice. For instance, genetic deletion of the miR-17-92 family results in 100% postnatal death due to cardiac and lung defects (Ventura et al. 2008). MiR-1-2 knockout mice exhibit 50% embryonic lethality due to cardiac defects (Kwon et al. 2005). MiR-126 knockout mice display 40-50% lethality resulting from perinatal hemorrhages due to defects in vascular integrity (Kuhnert et al. 2008; Wang et al. 2008b). Apart from these examples, the majority of microRNA knockout mice are homozygous viable; however, many display stress responsive abnormalities.

MicroRNAs as modifiers of disease

Dysregulation of microRNAs is a hallmark of disease processes. Several studies have elucidated both the microRNA profiles and the function of individual microRNAs in major disease states including neoplastic, autoimmune, infectious, and essential diseases. Overexpression of miRs -346, -146, -155, and -16 has been shown in patients with active rheumatoid arthritis (Alevizos and Illei 2010). Many of these microRNAs have been suggested to play a role in inflammatory cell differentiation and function. MiRs -1, -30, -128, -196, -296, -351, -431, and -448 have been shown to be upregulated in response to interferon cytokines (Pedersen et al. 2007). Each of these microRNAs binds directly to viral RNAs expressed by the hepatitis C virus (HCV), inhibiting expression of these viral genes. Most famously, miR-122 has been shown to be essential for HCV viral processing (Jopling et al. 2005). MiR-122 inhibitors have been shown to have efficacy against HCV in primate models and are now in clinical trials in humans (Elmen et al. 2008a; Lanford et al. 2010).

A landmark study profiling microRNA expression levels in 334 human tissue samples, both normal and neoplastic, showed that human tumor types express a specific profile of microRNAs, the diagnostic power of which is significant. In this same study, 17 poorly differentiated tumor samples were diagnosed based upon microRNA profile, whereas mRNA profiling was significantly less accurate (Lu et al. 2005). Specific microRNAs have been shown to be modified in a large number of unrelated cancers, suggesting their role as global oncogenes or tumor supressors. Specifically, the miR-17-92 cluster has been shown to be amplified in many cancers and functions as an oncogene, whereas the miR-15-16-1 cluster is typically deleted (Calin and Croce 2006). miR-21 has been found to be a overexpressed in a number of tumors including glioblastomas, acute myelogenous leukemia, chronic lymphocytic leukemia, breast,

colon, pancreatic, lung, prosate, liver, and stomach cancers (Pan et al. 2010). Functionally, microRNAs that play a role in tumorigenesis or the repression thereof have been suggested to modify the expression of characterized oncogenes or tumor supressors. Specifically, miR-17-92 has been shown to inhibit the tumor supressors Bim and Pten, whereas miR-15-16-1 has been shown to target the oncogenes BCL2, WT1, RAB9B, and MAGE83 (Cimmino et al. 2005; Mendell 2008; Croce 2009; Roccaro et al. 2009). The specific role of miR-21 in tumorigenesis will be discussed in Chapter IV.

MicroRNA profiles of tissue specific diseases such as hepatic fibrosis, atherosclerosis, and cardiac hypertrophy have revealed specific patterns of microRNA dysregulation. In a mouse model of steatofibrotic hepatitis, miRs -34a, -155, -200b, and -221 were upregulated, whereas, microRNAs 29c, 122, 192, and 203 were downregulated (Pogribny et al. 2010). Expression of miRs -155, -21, and -126 has been shown to be modified in vascular disease (Urbich et al. 2008). MicroRNAs have been shown to play an essential role in cardiac hypertrophy. The role of microRNAs and their role in cardiac hypertrophy will also be discussed in Chapter III.

Methods used to study microRNA function

Multiple biological and biochemical methods have been developed that allow for the interrogation of both microRNA expression and microRNA function. Many of these methods are similar to those used for interrogation of traditional gene function. In fact, due to the nature of microRNA gene structure and processing, gain and loss-of-function analyses are simplified in comparison to mRNA gain and loss-of-function studies. Most important to the elucidation of microRNA function is the identification of target mRNA molecules. As discussed above, there are many factors that determine the efficiency of microRNA-mRNA interactions, and this

interaction may result in pleiotropic effects. Therefore predicted microRNA target mRNAs must be validated experimentally.

Early methods to characterize microRNA expression utilized custom array based platforms. Today these microarrays are available commercially and constitute the most common method of microRNA expression profiling. These arrays depend on the hybridization of a labeled pool of total RNA to a chip containing labeled antisense RNAs corresponding to the specific microRNA (Lopez-Romero et al. 2010). These arrays are accurate but are limited by the specific set of probes present on the chip. The second primary method utilized to profile microRNA expression is small RNA deep sequencing. This method utilizes sequencing data that is filtered bioinformatically to generate cohorts of sequences for individual molecules (Hafner et al. 2008). This allows for the determination of exact copy number of individual molecules of the same sequence. This method is more precise and the species of microRNAs that may be interrogated is unlimited. This method is, however, expensive and labor intensive. Due to these limitations, this method is less convenient and most commonly used in large bioinformatic laboratories.

Methods for the overexpression of microRNAs are very similar to that of mRNAs. Since microRNA loci are transcribed by RNA-Polymerase II, typical expression vectors and enhancers may be used. Typically, the pre-miR hairpin sequence must be expressed for efficient processing of the microRNA and its loading into the microRNA-RISC, however, in practice, inclusion of 100-200 base-pairs (bp) of both 5' and 3' flanking sequence increases processing efficiency. Genetically, loss-of-function studies are performed in a similar fashion. Due to the primary importance of the pre-microRNA hairpin structure, intergenic microRNAs may be easily targeted for either conditional or constitutive genetic deletion by homologous recombination in

embryonic stem cells. LoxP sites do not disrupt processing of the microRNA if they are placed outside of the hairpin. In any case, great care should be taken to avoid conserved elements, however, due to the robust nature of pre-microRNA processing, generation of a conditional allele is less troublesome than typical mRNA conditional alleles.

Of great importance to the study of microRNAs is the use of microRNA inhibitor molecules both in vitro and in vivo. Due to the therapeutic potential of microRNA inhitition in vivo, multiple chemistries have been developed that show efficacy as microRNA inhibitors. The first verified microRNA inhibitors were cholesterol modified complete antisense compounds termed “antagomiRs” (Krutzfeldt et al. 2005; Krutzfeldt et al. 2007). Comparison studies have now shown that a variety of chemically modified small antisense compounds repress microRNA function in an equally efficient manner (Lennox and Behlke 2010; Robertson et al. 2010). These include locked nucleic acid (LNA) modified microRNA antisense inhibitors. This specific class of microRNA inhibitors has been shown to be therapeutically efficacious for the treatment of HCV and therefore displays great clinical potential (Elmen et al. 2008a; Elmen et al. 2008b; Lanford et al. 2010). Typically, inhibitors are transfected in vitro and are injected intravenously in vivo to study the function of microRNA inhibition.

Chapter II

Defective Erythroid Differentiation in miR-451 Mutant Mice Mediated by 14-3-3ζ

ABSTRACT

Erythrocyte formation occurs throughout life in response to cytokine signaling. We show that miR-451 regulates erythropoiesis in vivo. Mice lacking miR-451 display a reduction in hematrocrit, an erythroid differentiation defect, and ineffective erythropoiesis in response to oxidative stress. 14-3-3ζ, an intracellular regulator of cytokine signaling that is repressed by miR-451, is up-regulated in *miR-451*$^{-/-}$ erythroblasts, and inhibition of 14-3-3ζ rescues their differentiation defect. These findings reveal an essential role of 14-3-3ζ as a mediator of the pro-erythroid differentiation actions of miR-451 and highlight the therapeutic potential of miR-451 inhibitors.

INTRODUCTION

Erythropoiesis

In mammals, there are two phases of hematopoiesis during embryogenesis, primitive and definitive. Primitive hematopoiesis occurs in the yolk sac during early embryogenesis. The function of primitive hematopoiesis is to provide the first circulating cells and capillary networks to the yolk. These cells are transient and do not contribute to the adult hematopoietic cell population. Definitive hematopoiesis begins in the aorta-gonad mesonephros region near the aorta. These cells then migrate to the fetal liver during late embryogenesis and then to the bone marrow shortly before birth. Definitive hematopoiesis is responsible for the generation of the adult hematopoietic stem cell population (Gilbert 2000).

The process of erythropoiesis is highly specialized. In mammals, mature erythrocytes develop from a series of progenitors including the hematopoietic stem cell, the common myeloid progenitor, and the megakaryocyte/erythrocyte precursor cells (MEP). Committed erythrocyte precursors undergo a series of dramatic morphological changes including establishment of a biconcave shape and the loss of the nucleus in a process termed enucleation (Prchal 2006). Throughout these stages, erythrocyte precursors express a variety of surface markers. Immature erythrocytes express CD71 antigen, the transferrin receptor essential for iron uptake, whereas mature erythrocytes lose CD71 expression and gain expression of the glycoprotein TER119 (Fig. 2.1) (Socolovsky et al. 2001). The developmentally regulated expression of these surface markers allows for the analysis of erythrocyte differentiation by flow cytometry. Due to the highly characterized process of embryonic erythrocyte maturation, analysis of this process is

most commonly performed on fetal liver cells, however, analyses of adult hematopoietic tissues are also informative.

Essential to the development of erythrocytes is the pro-differentiation cytokine erythropoietin (EPO). EPO is secreted by renal tubular cells in response to hypoxia. Once EPO binds to the EPO receptor on the burst-forming-unit-erythroid (BFU-E) cells a series of signaling events occur that result in the stimulation of the differentiation process (Prchal 2006). These signaling events are primarily generated by the activation of Janus kinase 2 (JAK2) by the EPO receptor. JAK2 is a member of a large scaffolding complex localized to the EPO receptor. This complex includes phosphatidylinositol 3-kinase (PI3K), mitogen activated protein kinases (MAPK), and signal transducer and activator of transcription 5 (STAT5). Upon EPO binding to the receptor, JAK2 is activated. Once active, JAK2 phosphorylates a variety of downstream signaling molecules including members of the PI3K/AKT pathway, MAP-kinase pathways, and most importantly, the STAT5 transcriptional network (Constantinescu et al. 1999; Ghaffari et al. 2001; Zhang et al. 2007).

Perturbation of these pathways specifically in erythrocytes results in attenuation of erythrocyte maturation. Targeted deletion of the STAT5 transcription factor in mice results in fetal anemia, an observable disruption of erythrocyte maturation, and a reduced ability to increase erythropoiesis in response to hypoxic stress. Despite these abnormalities, these animals are viable and fertile, highlighting the reserve capacity of erythroid precursors to compensate for disruptions in differentiation (Socolovsky et al. 1999; Socolovsky et al. 2001). Reduction of MAP-kinase and PI3K signaling by deletion of Ras kinase results in a similar erythroid differentiation defect. Interestingly, overexpression of constitutively active Ras kinase results in a similar defect (Zhang et al. 2003; Zhang and Lodish 2005; Zhang et al. 2007; Zhang and

Lodish 2007). Taken together, these data suggest that a balance of these signaling cascades is required for accurate erythrocyte maturation. Due to the role of microRNAs as fine tuners of gene expression, it is not surprising that they play an important role in this process.

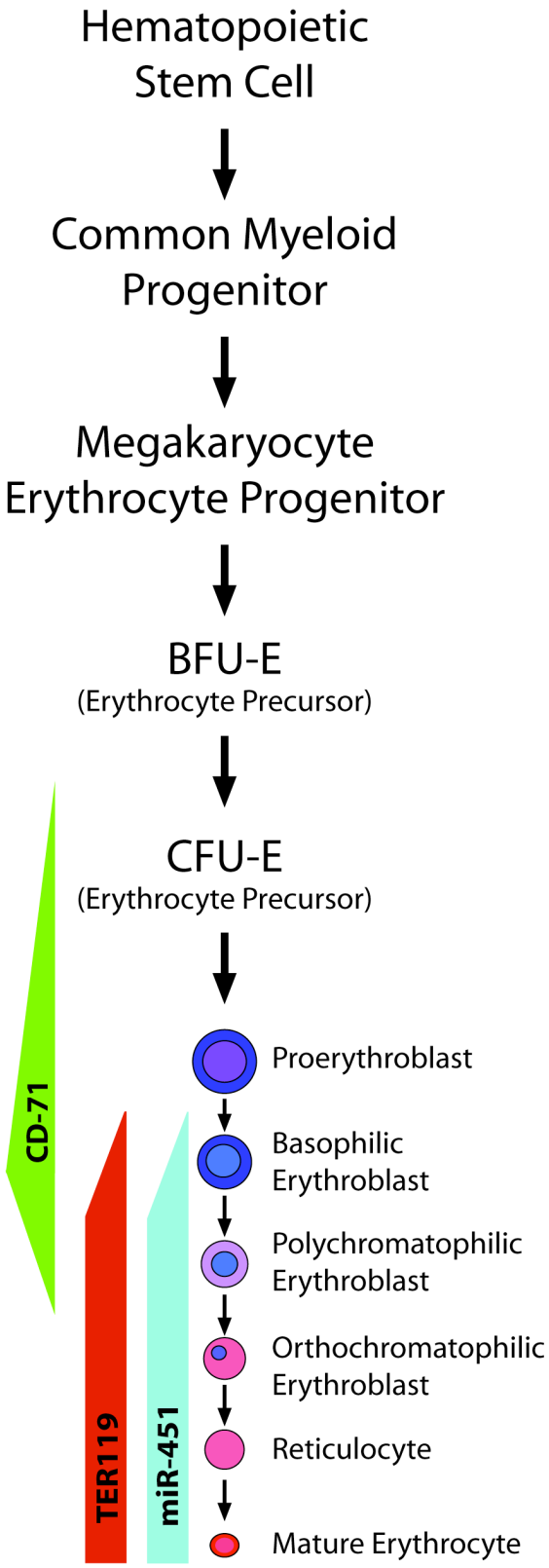

Figure 2.1. Schematic of erythrocyte maturation. Mature erythrocytes develop from hematopoietic stem cells through a series of specific precursors including the common meloid progenitor, the megakaryocyte erythrocyte precursor, the burst forming unit erythroid (BFU-E), and the colony forming unit erythroid (CFU-E). Cell division ceases after CFU-E and erythroblasts progress through a series of morphological changes including nuclear exclusion. The surface markers CD-71 and TER119 are expressed on specific populations of erythrocyte precursors. miR-451 expression is restricted to TER119^{+} erythroblasts and erythrocytes.

MicroRNAs and erythropoiesis

Early studies investigating the role of Ago2 as a regulator of hematopoiesis revealed its central role in erythropoiesis. Ago2 global mutant mice die embryonically due to implantation defects. However, upon targeted conditional deletion of Ago2 with MX1-Cre (a hematopoietic-cell specific inducible cre) in adult mice, a specific erythrocyte differentiation defect similar to that of the STAT5 mutant mice was observed (O'Carroll et al. 2007). Due to the redundancy of Ago1-4 as mediators of microRNA-mediated target repression, it is not surprising that these animals displayed appropriate differentiation patterns and populations of other hematopoietic lineages. Due to the established role of Ago2 as a member of the microRNA-RISC, these data suggest a possible role for microRNAs in erythropoiesis. However, the highly specific erythropoietic defect suggests a specific role for Ago2.

Several specific microRNAs have been implicated as regulators of erythropoiesis (Zhao et al. 2010). MiRs -221 and -222 are downreglated during erythroid differentiation. These two microRNAs are members of the same family and have been shown to directly target KIT, a receptor essential for the expansion of immature erythroid precursors (Felli et al. 2005). MiRs -24, 150, 223, and 15 are all similarly downregulated during erythropoiesis and have been shown to directly target pro-erythropoietic molecules such as ACVR1B, MYB, LMO2, and GATA1 (Lu et al. 2008; Wang et al. 2008a; Yuan et al. 2009). In each of these cases, the microRNA targets pro-differentiation factors and is downregulated during differentiation. Interestingly, only a single microRNA locus, *miR-451/144* has been described as pro-erythroid and is dramatically upregulated during erythroid differentiation.

miRs -144 and -451 as modifiers of erythropoiesis

The *miR-144/451* cluster is an intergenic bicistronic microRNA locus that is conserved in verterbrates. The function of this locus was originally suggested in a study describing an *N*-ethyl-*N*-nitrosourea (ENU) generated zebrafish mutant termed *Meunier*. *Meunier* fish developed normally, however circulating erythrocytes in these animals appeared immature as measured by their nuclear/cytoplasmic ratio. Analysis of erythrocyte development in these fish revealed an erythrocyte developmental delay. Mapping of the *Meunier* mutation revealed a loss-of-function allele of *miR-144/451*. Microinjection of miR-451 into the embryo rescued this defect, whereas injection of miR-144 had no effect (Pase et al. 2009). These experiments strongly suggested a role for miR-451 and not miR-144 in the process of erythroid differentiation.

Expression analyses and transcriptional profiling of *miR-144/451* also suggested its role in erythropoiesis. Both miR-144 and -451 are restricted to TER119-positive erythrocytes, suggesting its role in terminal erythroid differentiation (Figure 2.1). The role of this locus in terminal erythroid differentiation is also supported by chromatin immunoprecipitation studies which revealed the presence of the RNA Polymerase II complex at a site approximately 1.1 kbp upstream of pre-miR-144. Detailed analysis of this site revealed active binding of the pro-erythroid differentiation transcription factor GATA-binding factor 1 (GATA1) to this site (Zhan et al. 2007; Dore et al. 2008).

GATA1 is essential for erythropoiesis and mice mutant for GATA1 die embryonically due to inefficient primitive erythropoiesis (Pevny et al. 1991). Interestingly, an erythroid specific cell line that expresses an inducible form of GATA1 dramatically upregulates the *miR-144/451* cluster upon GATA1 induction. These data establish a mechanism for miR-451 upregulation during terminal erythroid differentiation, however, it is apparent in these assays that the absolute

levels of miR-144 are significantly lower than that of miR-451 (Dore et al. 2008). This is congruent with profiling studies that describe miR-451 as the most abundant microRNA in erythrocytes with signal intensities that are orders of magnitude higher than miR-144 (Merkerova et al. 2008). It is also apparent in this report, that miR-451 appears as multiple species when analyzed by northern blot, suggesting unique processing of miR-451 and not miR-144.

Processing of miR-451

As sated above, the microRNA-microRNA* duplex is generated by cleavage of the pre-microRNA hairpin by Dicer. Interestingly, the mature microRNA-451 extends into the hairpin which contains no recognizable microRNA* strand. This hairpin structure is unique among all microRNAs. Early analyses of microRNA species associated with Ago2 in hematopoietic cells revealed the dramatic predominance of miR-451. Interestingly, all species retained identical 5' ends, however, multiple 3' cleavage sites were discovered (Nelson et al. 2007). These studies revealed the presence of multiple miR-451 species with identical seed regions, but varying in the final 3' nucleotide.

Studies investigating the specific role of Ago2 in erythropoiesis revealed its unique role as the miR-451 processing enzyme. To examine the function of Ago2 slicer activity, these groups generated mice with a point mutation in the Ago2 slicer active site. This rendered Ago2 "slicer-dead", but allowed it to function similarly to other Argonaute family members (Cheloufi et al. 2010; Cifuentes et al. 2010). Unlike the *Ago2*$^{-/-}$ animals which die embryonically, these animals die post-natally. Analysis of microRNA expression levels in fetal liver, the primary hematopoietic organ of late embryogenesis, revealed normal expression of all microRNAs and an absence of miR-451. Further analyses have revealed that Ago2 is solely responsible for

processing of the pre-miR-451 hairpin (Cheloufi et al. 2010; Cifuentes et al. 2010). This unique processing event has been conserved across vertebrates and is responsible for the variation in 3' cleavage of the hairpin, the ladder-like appearance of miR-451 species when probed by northern blotting, and its predominant abundance over miR-144 despite a shared transcript. Several applications of this novel microRNA biosynthetic mechanism have been proposed, including the use of engineered microRNA hairpins containing the seed of alternate microRNAs while retaining the microRNA-451 hairpin (Yang et al. 2010). This allows for Dicer independent processing of microRNAs and thus the rescue of Dicer deletion phenotypes with individual or specified groups of microRNAs. Despite the evidence suggesting a role of miR-451 in erythropoiesis, the exact function of miR-451 was unclear, and the mechanism of action of miR-451 was equally unclear.

Role of 14-3-3 molecules in hematopoiesis

14-3-3 molecules have been shown to play an important role in the assembly of signaling complexes required for the coordinate activation of pathways downstream of growth factor receptors. These proteins are classified as a family of phosphoserine/threonine binding molecules that dimerize and modulate protein-protein interactions and subcellular localization (Aitken 2006). The specialized roles of 14-3-3 isoforms in the regulation of receptor signaling highlight the importance of defining isoform-specific mechanisms (Rosenquist et al. 2000). 14-3-3 proteins have been implicated to play a role in the process of hematopoiesis (Ghaffari et al. 2001). Specifically 14-3-3ζ has been shown to play a nodal role in tyrosine kinase signaling networks. 14-3-3ζ was shown to interact with the common signaling subunit of the GM-CSF, IL-3, and IL-5 receptors, suggesting a role specifically for 14-3-3ζ in the transduction of signals

downstream of growth factor receptors (Stomski et al. 1999). Recently, 14-3-3ζ was described as a critical mediator in the activation of PI3K signaling downstream of GM-CSF suggesting that 14-3-3ζ plays a critical role in signal transduction in hematopoietic cells (Barry et al. 2009). Similarly, 14-3-3 association with Gab2, a docking protein essential for hematopoiesis, terminates Gab2 function (Brummer et al. 2008). This interaction suggests that the stoichiometry of 14-3-3ζ likely impacts tyrosine kinase signaling, specifically in hematopoietic cells types. 14-3-3ζ has been shown to interact with the IL-9 receptor, implicating a direct role for 14-3-3ζ in erythropoiesis (Sliva et al. 2000). Finally, *ywhaz*, the transcript encoding 14-3-3ζ contains a conserved miR-451 binding site.

RESULTS AND DISCUSSION

MicroRNA-451 expression is restricted to erythrocytes

miRs -144 and -451 are transcribed as a bicistronic transcript that is processed to give rise to the two mature microRNAs (Fig. 2.2A) (Dore et al. 2008). We confirmed that miR-451 expression overlaps with that of miR-144 across multiple tissues, with highest expression in bone marrow and spleen (Fig. 2.2B). Despite being generated from a common pri-microRNA, it is apparent that miR-451 is expressed at a markedly higher level than miR-144, which likely reflects differences in microRNA stability or processing. The absence of a detectable pre-miR-451 suggests that miR-451 processing may differ from that of other miRs. In this regard, miR-451 migrates as a ladder upon gel electrophoresis, due to multiple 3' termini (Nelson et al. 2007).

To further characterize the expression of the miR-144/451 locus in vivo, we generated transgenic mice in which β-Galactosidase (β-Gal) was expressed under the control of a highly conserved 5kb promoter/enhancer region containing the previously characterized GATA binding sites (Fig. 2.3) (Dore et al. 2008). Whole-mount analysis at late embryonic stages revealed β-Gal reporter expression throughout the circulatory system (Fig. 2.2C). Sections through the intersomitic veins indicate that this expression is primarily due to β-Gal positivity in circulating erythrocytes (Fig. 2.2D).

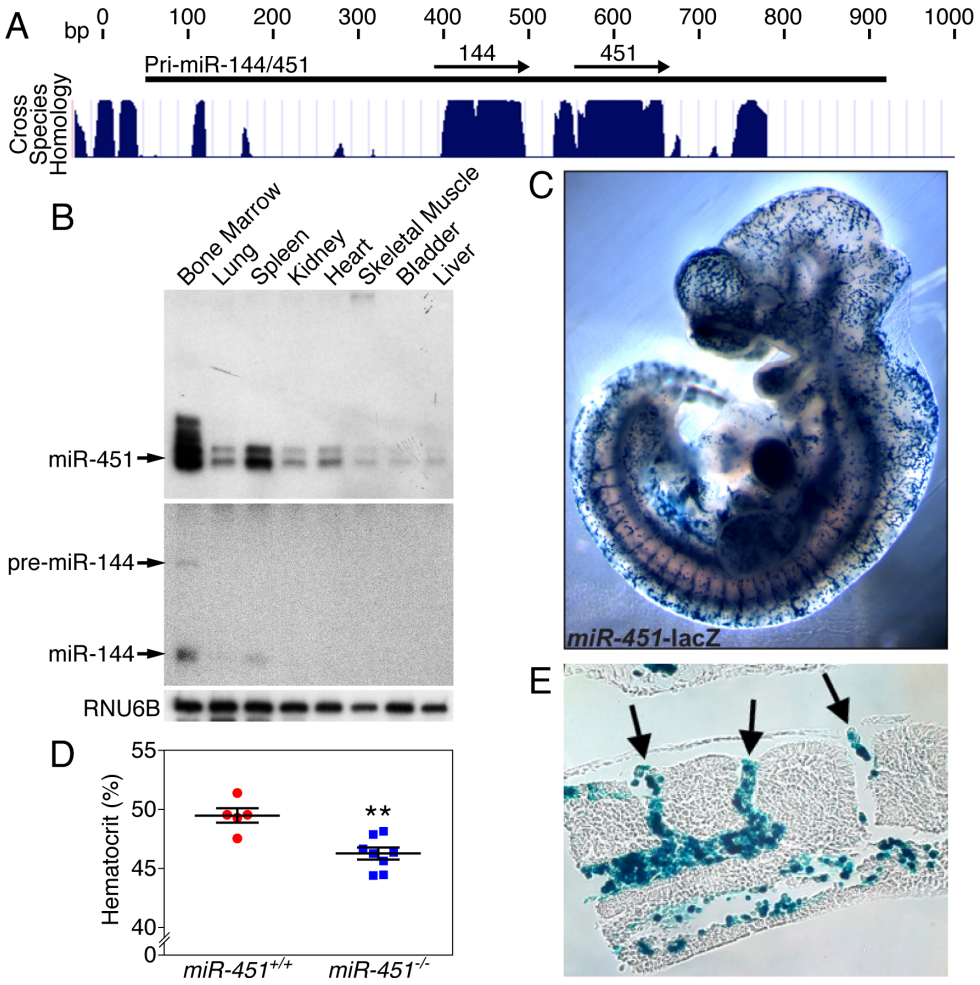

Figure 2.2. MiR-451 is expressed in Erythrocytes and *miR-451*$^{-/-}$ mice display a reduction in hematocrit. (*A*) A schematic showing the genomic location of the *miR-144/451* transcription unit. Mammalian conservation is represented as a histogram. (*B*) Northern blot analysis of miR-451 and miR-144 expression across multiple tissues. Pre-miR-144 is denoted with an arrow. Pre-miR-451 is not detected. (*C*) Expression of β-Gal driven by the miR-451 enhancer is restricted to the circulatory system at 13.5 d.p.c. (*D*) Hematocrit measurements represented as a dot-plot. Data from n=5 (*miR-451*$^{+/+}$) and n=8 (*miR-451*$^{-/-}$) animals are shown as means ± SEM. (**) $P < 0.01$. (*E*) Cross-section through the intersomitic veins reveals β-Gal positivity of circulating erythrocytes.

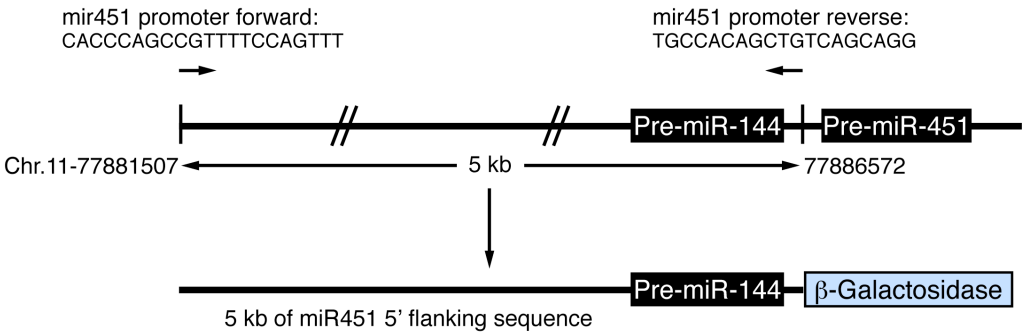

Figure 2.3. MiR-451-LacZ gene structure. Diagram schematizing the cloning strategy for the generation of the miR-451-LacZ transgenic animals. Primers are indicated and the chromosomal coordinates of the 5' and 3' ends of the fragment are also indicated.

Generation of miR-451 knockout mice

To generate miR-451 mutant mice, loxP sites for Cre-mediated recombination were introduced at both ends of the pre-miR-451 coding region by homologous recombination in ES cells, leaving the complete hairpin structure for the pre-miR-144 unmodified. The deletion mutation removed 76 base-pairs (bp) of genomic DNA encompassing the hairpin structure of pre-miR-451 (Fig. 2.4A). Cells displaying proper targeting of the *miR-451* locus were injected into blastocysts to generate chimeric mice. Germline transmission was determined by Southern blot analysis (Fig. 2.4B). Mice heterozygous for the targeted allele were bred to C57BL/6 mice harboring the FlpE transgene for deletion of the neomycin cassette. The resultant *miR-451*$^{fl/+}$ mice were bred to C57BL/6 mice harboring the ubiquitously expressed CAG-cre transgene for deletion of miR-451 in all tissues and generation of *miR-451*$^{+/-}$ mice. Deletion of miR-451 was confirmed by genomic PCR analysis (Fig. 2.5).

Northern blot analysis of RNA extracted from bone marrow of 8-week old mice showed a 50% reduction in *miR-451*$^{+/-}$ animals and the absence of miR-451 in *miR-451*$^{-/-}$ animals. miR-144 levels were unchanged across all genotypes (Fig. 2.4C). Real time RT-PCR on fetal liver cells positive for the mature erythrocyte marker, TER119, confirmed these results, showing the absence of miR-451 in *miR-451*$^{-/-}$ animals and intermediate expression in *miR-451*$^{+/-}$ animals with no change in miR-144 (Fig. 2.4D). *miR-451*$^{-/-}$ animals were obtained at predicted Mendelian ratios from heterozygous intercrosses and displayed no overt abnormalities up to 8-months of age (Table 2.1). However, we found a mild but reproducible reduction in hematocrit of adult *miR-451*$^{-/-}$ mice compared to *miR-451*$^{+/+}$ littermates, suggesting an erythrocyte defect (Fig. 2.2E).

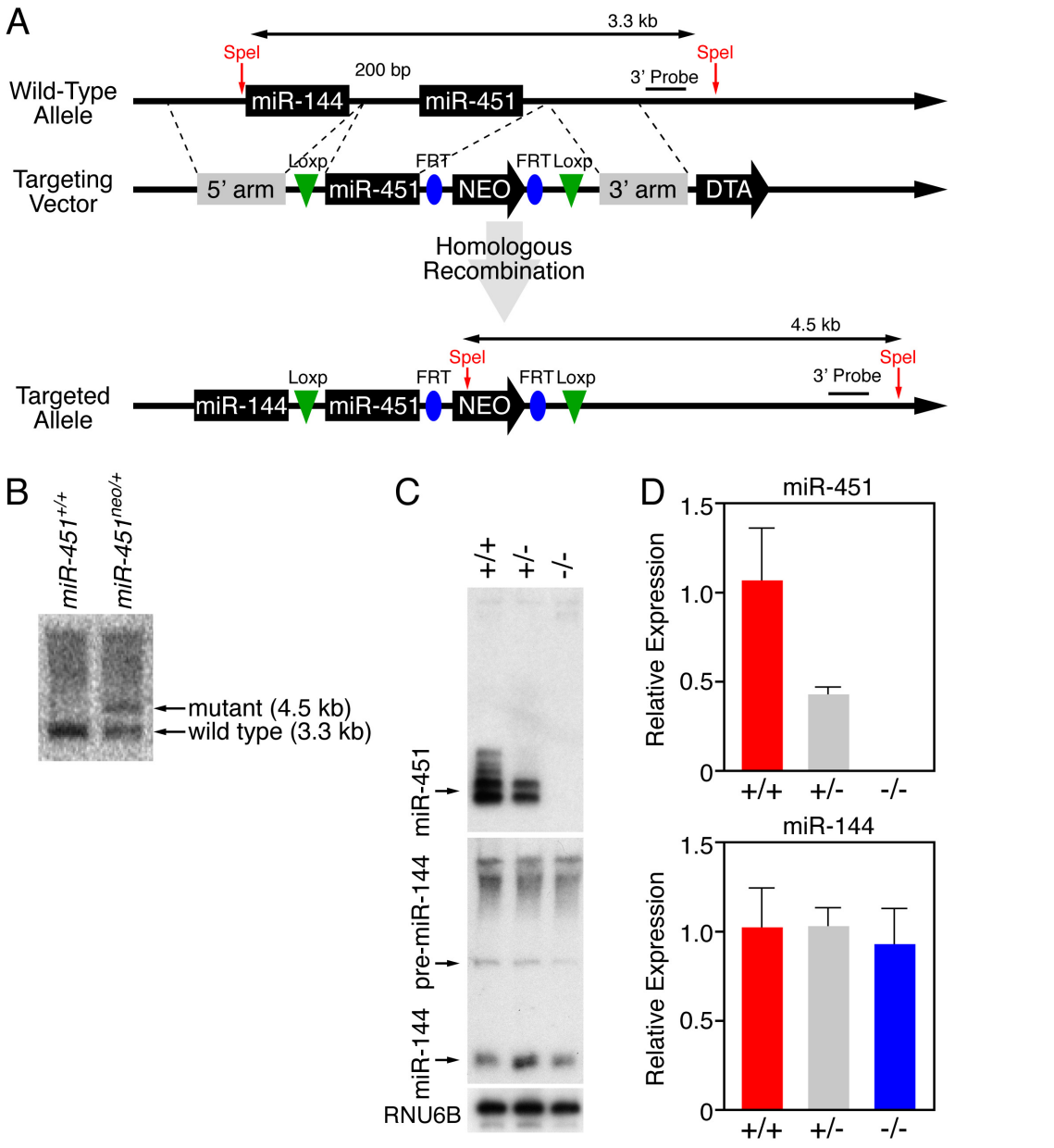

Figure 2.4. Targeting strategy and confirmation of targeting in *miR-451* conditional knockout mice. (*A*) Conditional knockout strategy to specifically target miR-451. Upon Cre-mediated recombination, miR-451 is deleted leaving miR-144 unaffected. (*B*) Southern blot analysis using a 3'-probe. Efficient targeting of the miR-451 locus is determined by the presence of the 4.5 Kb mutant band. (*C*) Northern blot analysis of miR-451 and miR-144 on RNA harvested from bone marrow of 8-week old adult male littermates. Pre-miR-144 is denoted with an arrow, whereas pre-miR-451 is not detected. (*D*) Real-time RT-PCR from TER119^{+} erythroblasts from 14.5 d.p.c. littermates. Data from a representative litter n=3 (*miR-451*$^{+/+}$), n=5 (*miR-451*$^{+/-}$), and n=2 (*miR-451*$^{-/-}$) animals are shown as means ± SEM. (**) $P < 0.01$.

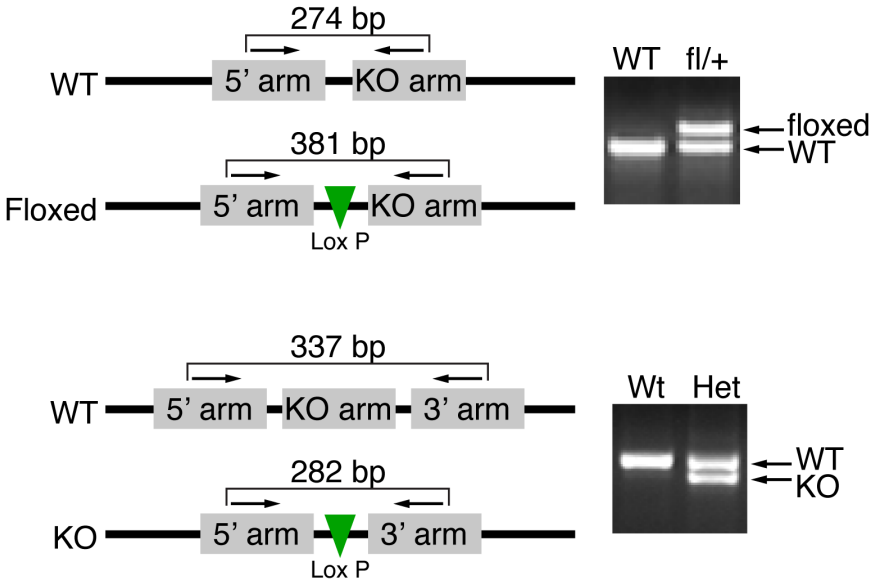

Figure 2.5. miR-451 genotyping strategy. Diagrams schematizing the genotyping strategies for both the conditional and global miR-mutant animals. For the conditional allele, primers flanking the LoxP site distinguish between the conditional and wild-type alleles. An ethidium bromide stained agarose gel of the products are shown. For the mutant allele, primers flanking the LoxP site that replaces the KO arm upon homologous recombination distinguish between the WT and the KO alleles. An ethidium bromide stained agarose gel of the products is shown.

miR-451 Genotype: (30 animals)	+/+	+/-	-/-
Expected	7.5 (25%)	15 (50%)	7.5 (25%)
Observed	6 (20%)	17 (57%)	7 (23%)

Table 2.1. . ***miR-451*** $^{-/-}$ **animals are born at expected Mendelian ratios.** Total number of animals both expected and observed from a total of 30 are represented with the percentage in parentheses.

$MiR\text{-}451^{-/-}$ mice display an erythrocyte autonomous embryonic erythroid differentiation defect

To examine the effect of miR-451 loss-of-function on erythroid differentiation, livers were isolated from embryos at 14.5 and 16.5 days post coitus (d.p.c). from $miR\text{-}451^{+/-}$ intercrosses. Erythrocyte development was assayed by flow cytometry analysis based upon the expression of CD71 and TER119 as previously described (Socolovsky et al. 2001). Fetal liver cells isolated from $miR\text{-}451^{-/-}$ embryos showed a significant decrease in the region IV $CD71^{-}$ /$TER119^{+}$ cell population, representing the most mature erythrocytes (Fig. 2.6A and Fig. 2.7). $miR\text{-}451^{+/-}$ embryos displayed a haploinsufficient phenotype, with approximately 50% of wild-type levels of region IV $CD71^{-}/TER119^{+}$ cells (Fig. 2.6B). Haploinsufficient phenotypes are not typically observed in mice heterozygous for other microRNA null alleles, highlighting the dependence of erythroid differentiation on miR-451 levels.

To determine whether the differentiation defect observed in $miR\text{-}451^{-/-}$ mice reflected an erythroid cell-autonomous function of miR-451 versus a disruption of microenvironmental cues within the hematopoietic niche, in vitro differentiation assays were performed on 14.5 d.p.c. fetal liver cells. This assay removes erythroid precursors from the hematopoietic microenvironment and replaces endogenous cues with exogenously supplied growth factors, thus allowing for standardization of the microenvironment. To perform this assay, we incubated cells isolated from the livers of $miR\text{-}451^{+/+}$ and $miR\text{-}451^{-/-}$ mice at 14.5 d.p.c. with anti-TER119-biotin-conjugated antibody and then with streptavidin-conjugated magnetic beads. $TER119^{+}$ fetal liver cells were depleted by magnetic cell separation (MACS) and $TER119^{-}$ progenitor-rich fetal liver cells were recovered. These cells were incubated on fibronectin-coated plates and treated with conditioned media as previously described (Zhang et al. 2003). In vitro differentiation,

monitored by flow cytometry, revealed a decrease in the $CD71^{-}/TER119^{+}$ cell population from cell suspensions isolated from *miR-451*$^{-/-}$ mice when compared to wild type littermates, indicating that the differentiation defect observed in vivo is erythrocyte autonomous (Figs. 2.6C, 2.6D). Whether miR-451 has additional functions in other hematopoietic cell types in which it is expressed remains to be determined.

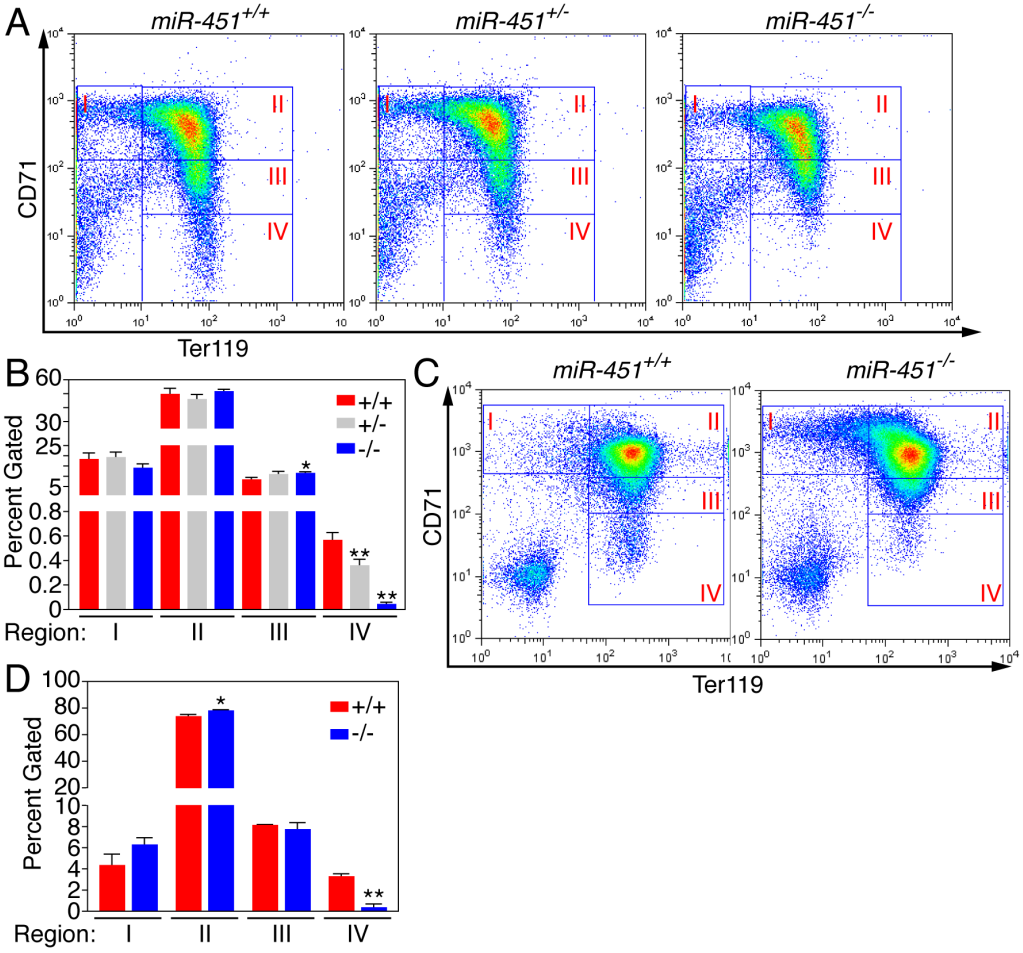

Figure 2.6. *miR-451*$^{-/-}$ animals display an embryonic erythroid differentiation defect. (*A*) FACS analysis of fetal livers harvested from embryos 16.5 days post-coitus (*d.p.c.*) and stained for CD71 and TER119. Erythrocytes progress from Regions I-IV throughout differentiation, with the most mature erythrocytes represented in Region IV. Representative FACS plots from one litter at each time point are shown. (*B*) Quantitation of percent of cells gated within each region. Data from a representative litter n=3 (*miR-451*$^{+/+}$), n=4 (*miR-451*$^{+/-}$), and n=2 (*miR-451*$^{-/-}$) animals are shown as means ± SEM. (*) $P < 0.05$, (**) $P < 0.01$. (*C*) FACS analysis of *in vitro* differentiated TER119 depleted 14.5 d.p.c. fetal liver three days post-induction by erythropoietin. Cells were stained for CD71 and TER119. Representative FACS plots from one litter are shown. (*D*) Quantitation of percent of cells gated within each region. Data from n=2 (*miR-451*$^{+/+}$) and n=3 (*miR-451*$^{-/-}$) animals are shown as means ± SEM. (*) $P < 0.05$, (**) $P < 0.01$.

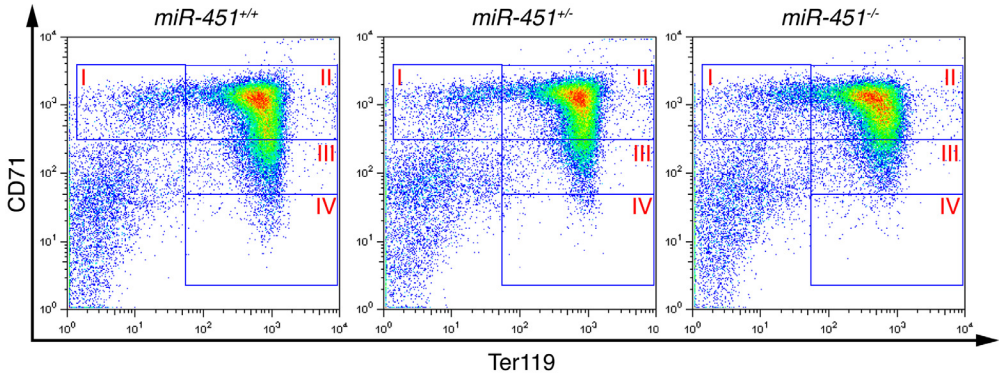

Figure 2.7. *miR-451*$^{-/-}$ and *miR-451*$^{-/+}$ animals display an embryonic erythroid differentiation defect. FACS analysis of fetal livers harvested from embryos 14.5 d.p.c. and stained for CD71 and TER119.

$MiR\text{-}451^{-/-}$ mice display an adult erythrocyte differentiation defect and cannot sustain a high erythropoietic rate

To determine the effect of miR-451 ablation on erythrocyte differentiation in adult hematopoietic tissues, flow cytometry analysis was performed. $miR\text{-}451^{-/-}$ animals displayed a reduction in region IV $CD71^{-}/TER119^{+}$ erythrocytes and a concomitant increase in region II $CD71^{+}/TER119^{+}$ erythroblasts in bone marrow (Figs. 2.8A, 2.8B). This defect likely contributes to the observed reduction in the hematocrit of $miR\text{-}451^{-/-}$ animals compared to $miR\text{-}451^{+/+}$ littermates.

Histologic analysis of spleens isolated from $miR451^{+/+}$ and $miR\text{-}451^{-/-}$ animals revealed an obvious increase in cellularity in the mutants with hypercellular clusters of erythroid colonies (Fig. 2.8C, Fig. 2.9). We measured the number of erythroid progenitors in spleen and bone marrow directly by performing colony forming assays for BFU-E and colony forming unit erythroid (CFU-E) progenitors (Fig. 2.8D). $miR\text{-}451^{-/-}$ animals displayed dramatically increased numbers of CFU-E progenitors in bone marrow and spleen, however, BFU-E progenitors were similar in both $miR\text{-}451^{-/-}$ and $miR\text{-}451^{+/+}$ littermates. Consistent with the expansion of immature erythroid precursors observed by flow cytometry analysis, these data suggest that the erythrocyte differentiation defect results in the expansion of the early erythroblast population. This expansion may be due to the loss of miR-451 or it may reflect a response to increased EPO secretion secondary to an anemic state. Finally, the cell autonomous differentiation defect observed embryonically and the maintenance of this phenotype throughout adulthood suggests a constitutive need for miR-451 specifically in the process of erythroid differentiation.

A low-rate of erythropoiesis is required to maintain a steady-state hematocrit in adult mice compared to embryonic hematopoietic tissue. Therefore, the mild reduction in hematocrit

of adult *miR-451*$^{-/-}$ animals likely reflects the ability of *miR-451*$^{-/-}$ hematopoietic tissues to compensate and achieve a steady-state output of erythrocytes. To examine the ability of adult hematopoietic tissues to increase their erythropoietic rate in the absence of miR-451, we subjected *miR-451*$^{-/-}$ and *miR-451*$^{+/+}$ animals to hemolytic anemia by injecting them with phenylhydrazine hydrochloride (PHZ), which causes hemolysis and triggers an increase in erythropoiesis (Socolovsky et al. 2001; Maeda et al. 2009). Hematocrit and reticulocyte levels were monitored on days 0, 3, 6, and 9 thereafter. The decrease in hematocrit was greater in *miR-451*$^{-/-}$ animals compared to *miR-451*$^{+/+}$ littermates, reflecting a hypersensitivity of mutant erythrocytes to PHZ-induced damage. *miR-451*$^{-/-}$ animals displayed a delay in recovery (Fig. 2.8E), indicative of a defect in generating a high erythropoietic rate. These data are consistent with results indicating that miR-451 regulates the erythrocyte response to oxidative stress (Yu et al. 2010). These findings also indicate a constitutive requirement for miR-451 in the process of erythroid differentiation.

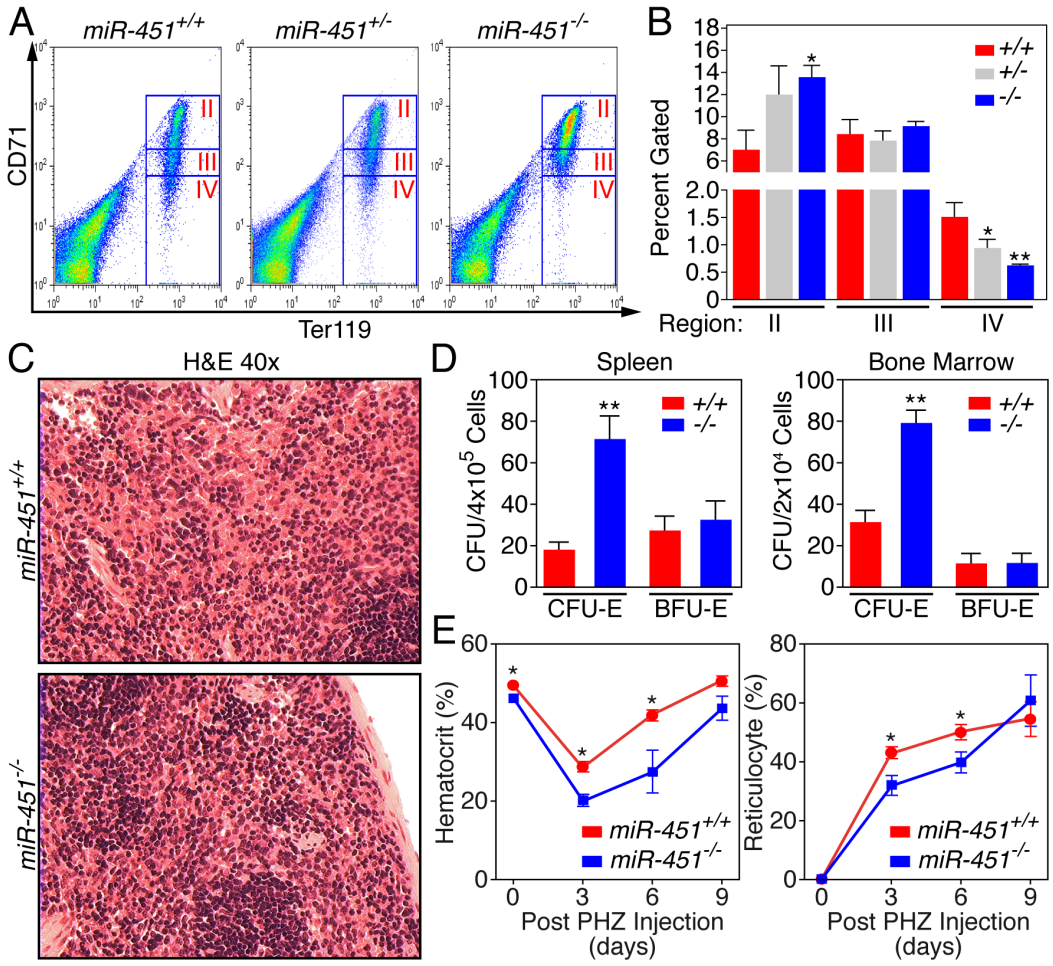

Figure 2.8. *miR-451*$^{-/-}$ mice display an erythroid differentiation defect in adulthood and cannot sustain a high rate of erythropoiesis. (*A*) FACS analysis of bone marrow harvested from 8-week old male littermates stained for CD71 and TER119. Representative FACS plots from one litter are shown. (*B*) Quantitation of percent of cells gated within each region. Data from n=3 (*miR-451*$^{+/+}$), n=5 (*miR-451*$^{+/-}$), and n=3 (*miR-451*$^{-/-}$) animals are shown as means ± SEM. (*) $P < 0.05$, (**) $P < 0.01$. (*C*) Hematoxylin and eosin stained sections of spleens harvested from 8-week-old male littermate *miR-451*$^{+/+}$ and *miR-451*$^{-/-}$ animals. Increased cellularity is observed at 40X magnification. (*D*) Colony formation assays for CFU-E and BFU-E were performed on three independent sets of miR-451$^{+/+}$ and miR-451$^{-/-}$ littermates. Data from a representative set of littermates is displayed with n=2 assays for each animal. Data is shown as means ± SEM. (**) $P < 0.01$. (*E*) Phenylhydrazine hydrochloride was injected in *miR-451*$^{-/-}$ and *miR-451*$^{+/+}$ animals on days 0, 1, and 3. Hematocrit values and reticulocyte counts were obtained on days 0, 3, 6, and 9. Data from n=5 (*miR-451*$^{+/+}$) and n=8 (*miR-451*$^{-/-}$) animals are shown as means ± SEM. (*) $P < 0.05$.

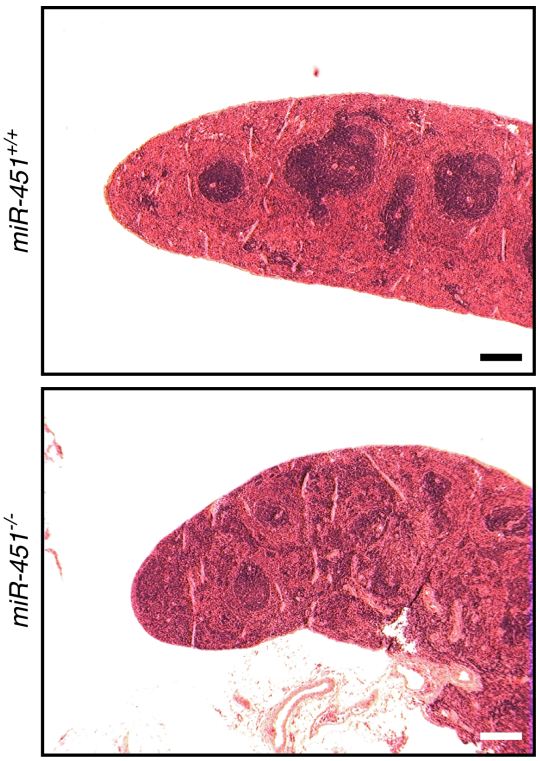

Figure 2.9. *miR-451*$^{-/-}$ animals display increased splenic cellularity. (*A*) Hematoxylin and eosin stained sections of spleens from 8-week-old male littermate *miR-451*$^{+/+}$ and *miR-451*$^{-/-}$ animals. Increased cellularity can be observed at 5X magnification. Bar = 100 μm.

Transient inhibition of miR-451 with antagomir-451 induces an adult erythroid differentiation defect

The erythroid differentiation defect observed in *miR-451*$^{-/-}$ animals could, in principle, result from a developmental insult or the chronic absence of miR-451. To test whether acute inhibition of miR-451 was also sufficient to impede erythroid differentiation, we performed injections of wild-type animals with a cholesterol-modified miR-451 antagomir, which inhibits microRNA function by Watson-Crick base-pairing to the mature microRNA (Krutzfeldt et al. 2005; Krutzfeldt et al. 2007). C57BL/6 animals were injected with 80 mg/kg of either antagomir-451 or a mismatch control antagomir on consecutive days (Fig. 2.10A). Animals were sacrificed on day 4 and erythrocyte differentiation was analyzed by Northern blot and flow cytometry analysis. miR-451 antagomir-treated animals displayed a 90% reduction of miR-451 in bone marrow and complete loss in other tissues (Fig. 2.10B, Fig. 2.11). Antagomir-451 injected animals also displayed an increase in region II CD71^{+}/TER119^{+} erythroblasts with a concomitant decrease in region IV CD71^{-}/TER119^{+} erythrocytes, suggesting that acute inhibition of miR-451 function results in the rapid block of erythrocyte differentiation as observed in the *miR-451*$^{-/-}$ animals (Fig. 2.10C). These data suggest that miR-451 plays a constitutive role in the differentiation of erythrocytes and that *miR-451*$^{-/-}$ erythrocytes display this defect due to the chronic requirement for miR-451 rather than an embryonic insult. These findings are also important because they demonstrate that chronic *versus* transient loss of microRNA function has similar consequences. This is the first report concomitantly describing the same phenotype in both microRNA-genetic null animals and animals injected with microRNA inhibitors.

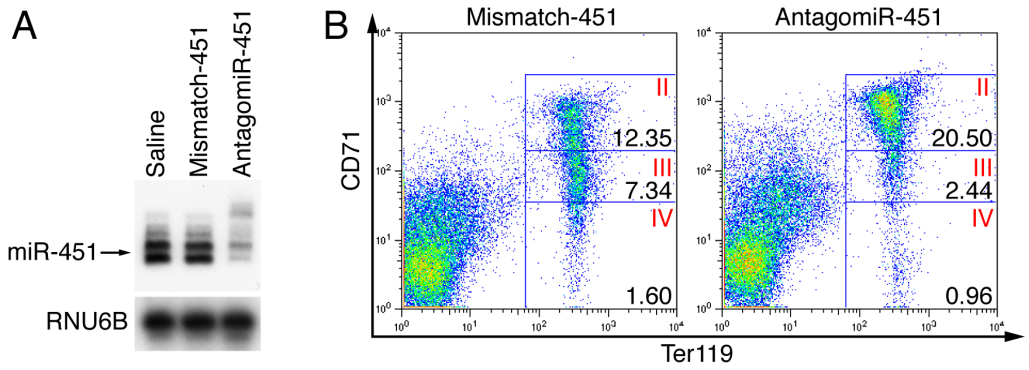

Figure 2.10. miR-451 inhibition with antagomir-451 rapidly induces a defect in erythroid differentiation. (*A*) Northern blot analysis of miR-451 in bone marrow of animals injected with either saline, mismatch, or antagomir-451 shows 90% knockdown of miR-451. (*B*) FACS analysis was performed on bone marrow stained with CD71 and TER119. Percentage of cells gated are displayed within the respective gate

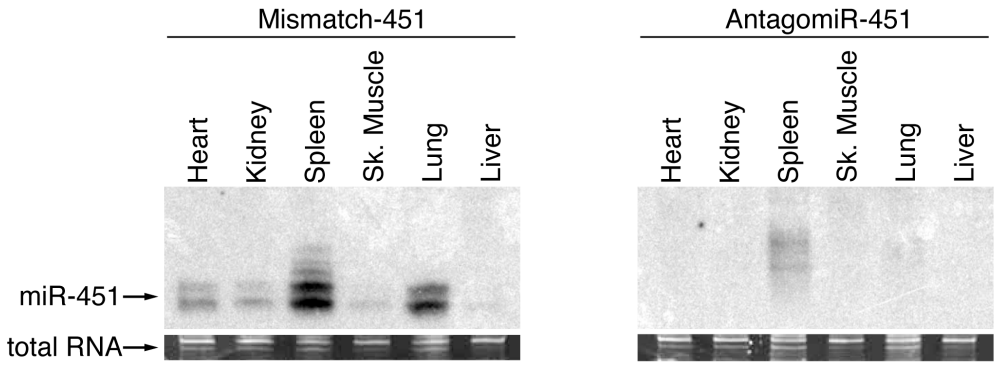

Figure 2.11. AntagomiR-451 reduces expression of miR-451 in multiple tissues. Northern blot analysis from animals injected with either antagomiR-451 or a mismatch-451 control. AntagomiR-451 abolishes miR-451 levels in all tissues shown.

MiR-451 target gene *ywhaz* is upreglated in *miR-451*$^{-/-}$ erythroblasts

It has been suggested that miR-451 regulates zebrafish hematopoiesis by targeting the pro-stem cell factor GATA2 (Pase et al. 2009). However, due to the lack of a conserved miR-451 binding site in the GATA2 3'-UTR in mammals, it is unlikely that this mechanism is conserved. To determine the mechanism of miR-451 mediated erythroid differentiation, we compared gene expression profiles of CD71^{+}/TER119^{+} erythroblasts from miR451$^{-/-}$ and *miR-451*$^{+/+}$ fetal liver cells at 14.5 d.p.c. It has been previously shown that miR-451 expression is low in TER119^{-} erythroblasts (Dore et al. 2008). Therefore the CD71^{+}/TER119^{+} (Region II) population was chosen for analysis due its high expression of miR-451 and its relative uniformity across genotypes at 14.5 d.p.c.

By microarray analysis, we found a total of 130 probe sets that were up-regulated ≥2-fold and 26 probe sets that were up-regulated ≥3-fold in *miR-451*$^{-/-}$ cells compared with *miR-451*$^{+/+}$ cells (Table 2.2). From this list, 13 genes are predicted to be targeted by miR-451 by the target prediction algorithm microcosm (www.ebi.ac.uk/enright-srv/microcosm/htdocs/targets/), whereas only three of these genes are predicted miR-451 targets by the targetscan algorithm (www.targetscan.org), which more stringently considers cross-species conservation. These three genes (*ywhaz*, *cab39*, and *vapa*) contain miR-451 binding sites conserved in mammals. Of these genes, *ywhaz*, which encodes the chaperone protein 14-3-3ζ, was most dramatically up-regulated. Conservation of the miR-451 target sequence in *ywhaz* 3' unstranslated regions (UTRs) across species is shown (Fig. 2.12A).

To directly test for possible regulation of *ywhaz* by miR-451, TER119^{+} enriched E14.5 fetal liver cells were harvested from *miR-451*$^{-/-}$ and *miR-451*$^{+/+}$ animals by MACS, and quantitative real time RT-PCR was performed for six transcripts encoding multiple 14-3-3

isoforms. Of these transcripts, only *ywhaz* was up-regulated in *miR-451*$^{-/-}$ cells compared to *miR-451*$^{+/+}$ cells (Fig. 2.12B). Immunoblot analysis revealed ~1.5-fold up-regulation of 14-3-3ζ protein levels in *miR-451*$^{+/-}$ cells and 2-fold upregulation in *miR-451*$^{-/-}$ cells (Figs. 2.13A and 2.13B). A luciferase reporter fused to the *ywhaz* 3'-UTR was repressed by miR-451 in COS-1 cells, and mutation of the miR-451 binding site within this UTR abolished repression by miR-451 (Fig. 2.13C).

Gene ID	Relative Expression KO/WT	Targetscan	microCosm
Pitpnd	20.4		
Wasf1	14.1		yes
Chga	10.1		
Spry1	9.1		
Ywhaz	8.6	yes	yes
Tac2	7.0		
Ppp1r11	6.9		
Pdcd4	6.6		
Padi2	6.4		
Deadc1	4.9		
Fkbp8	4.8		
1110002B05	4.6		yes
Rbmx	4.3		
Tmem85	4.2		yes
Dusp16	4.1		
Dhodh	4.1		
Igf2bp3	3.9		yes
Rnf103	3.8		
Cap1	3.6		
Hmga1	3.5		
MGC7482	3.3		
Dtx3	3.2		
Adcy7	3.1		
Limd1	3.1		
Cntnap2	3.0		
Drg2	3.0		
Gmfb	3.0		yes
Ccnd2	2.9		
Asc-pending	2.9		
Slc6a3	2.9		
mdn1	2.8		
Tjp1	2.8		
Vps72	2.7		
Vapa	2.7	yes	yes
X83328	2.7		yes
Zfr	2.7		
Tmem115	2.7		
Hk1	2.6		
Btn1a1	2.6		
Pklr	2.6		
Arhgdig	2.5		
Snrpa	2.5		
3110023E09Rik	2.5		
Aldo1	2.5		
Pfkl	2.5		
Surf4	2.5		
Cab39	2.5	yes	yes
Elf1	2.5		
Dscr2	2.5		
Nsmaf	2.4		yes
Nek2	2.4		
Cyfip1	2.4		
sdhc	2.4		
Nphp1	2.3		
Rab7	2.3		
2410002O22Rik	2.3		
Plscr3	2.3		
Ccng	2.3		
Aig1	2.3		yes
Ruvbl2	2.3		
Rpn1	2.2		
Mif	2.2		yes
Hmg20a	2.2		
Letmd1	2.2		
Rpn1	2.2		
Pigm	2.2		
Gmppa	2.2		
Gmppa	2.2		
2810470K21Rik	2.2		
Rer1	2.2		yes
Stard10	2.1		
Ct7	2.1		
Upf1	2.1		
Phtf	2.1		
Fto	2.1		
Nr1h2	2.1		
Tox4	2.1		
Sec61a2-pending	2.1		
AL033314	2.1		
Gpsn2	2.1		
St3gal2	2.0		
Clptm1	2.0		
Myo15	2.0		
Atpv0a1	2.0		
Trp53inp1	2.0		
Akr1b3	2.0		
Arf1	2.0		
Grap2	2.0		
Gpr56	2.0		
Klhdc3	2.0		
Tspan31	2.0		
Nat6	2.0		
Hspa14	2.0		
IMMP2L	2.0		
0610010E05Rik	2.0		
Gata2	1.0		

Table 2.2. Microarray analysis of transcripts enriched 2-fold or more *miR-451*$^{-/-}$ erythroblasts. Analysis was performed on RNA harvested from 14.5 d.p.c. fetal liver cells represented in Region II. Of the upregulated transcripts, thirteen are predicted miR-451 targets by the Microosm target prediction algorithm and three are predicted by the Targetscan algorithm. Y*whaz*, the transcript encoding 14-3-3ζ, is the most highly upregulated, conserved miR-451 target transcript. GATA2 expression was unmodified.

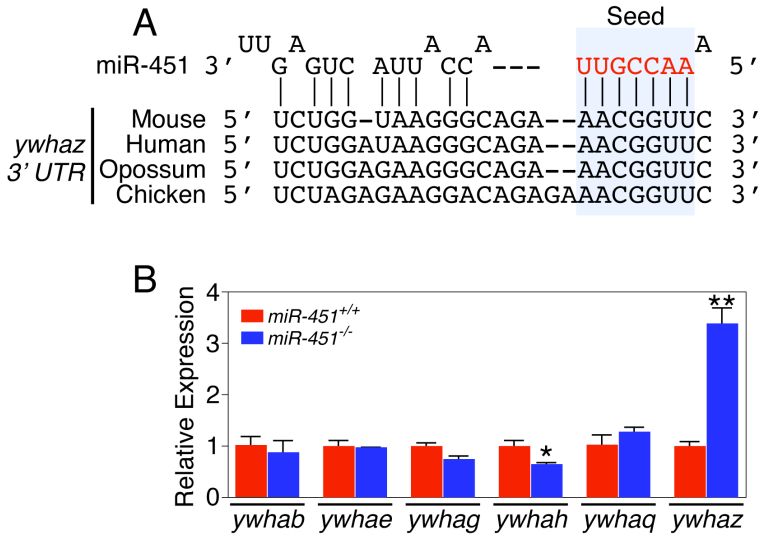

Figure 2.12 *Ywhaz* is a miR-451 target gene. (*A*) Schematic representing miR-451 binding and seed region conservation across multiple species. (*B*) Real-time RT-PCR on cDNA generated from RNA harvested from 14.5 d.p.c. fetal liver TER119^{+} erythrocytes for transcripts encoding 6 14-3-3 isoforms. Data from n=3 (*miR-451*$^{+/+}$) and n=4 (*miR-451*$^{-/-}$) animals are shown as means ± SEM. (*) $P < 0.05$, (**) $P < 0.01$.

Knockdown of 14-3-3ζ in *miR-451*$^{-/-}$ attenuates the erythroid differentiation effect

14-3-3 chaperone proteins play important roles in the assembly of signaling complexes required for the coordinate activation of pathways downstream of growth factor receptors. These proteins bind phosphoserine/threonine containing sequences and thereby modulate protein-protein interactions and subcellular localization of their targets (Aitken 2006). Numerous studies have implicated 14-3-3ζ in signaling and transcriptional events involved in hematopoiesis (Stomski et al. 1999; Barry et al. 2009). 14-3-3ζ coordinates signal transduction downstream of hematopoietic growth factor receptors by interacting with the common signaling subunit of the GM-CSF, IL-3, and IL-5 receptors and interacts directly with the IL-9 receptor (Sliva et al. 2000). 14-3-3ζ also governs PI3K signaling downstream of GM-CSF, a key regulator of erythropoiesis, and association of 14-3-3 with Gab2, a docking protein required for hematopoiesis, terminates Gab2 function (Brummer et al. 2008; Barry et al. 2009).

Due to the role of 14-3-3ζ as a regulatory molecule in hematopoiesis, we hypothesized that repression of 14-3-3ζ expression in *miR-451*$^{-/-}$ erythrocytes would relieve the erythroid differentiation defect. To test this hypothesis, we infected 14.5 d.p.c. TER119^{-} progenitor rich fetal liver cells with short hairpin RNAs (shRNAs) targeting two separate regions of the *ywhaz* transcript, abbreviated sh-1 and sh-2, using retroviral vectors. A retrovirus expressing a shRNA directed against luciferase (sh-Luc) was used as a control. Due to the reproducible differentiation defect observed ex vivo, we utilized our in vitro differentiation system and FACS analysis to assay for functional rescue of the erythroid differentiation defect observed in *miR-451*$^{-/-}$ animals. Expression of green fluorescent protein (GFP) from an internal ribosomal entry site (IRES) allowed for the identification of viable infected cells throughout differentiation. Each shRNA directed against 14-3-3ζ efficiently reduced its expression (Fig. 2.14). Pooled fetal liver

cells from 14.5 d.p.c. embryos isolated from *miR-451*$^{-/-}$ intercrosses were first depleted of TER119^{+} cells by MACS, separated into individual wells, and then infected with retrovirus expressing either sh-1, sh-2, or sh-Luc. Cells were then resuspended in medium containing EPO, plated on fibronectin-coated wells, and induced to differentiate as previously described (Zhang et al. 2003). Knockdown of *ywhaz* was confirmed from total cell suspensions (GFP-positive and negative cells) isolated at the time of flow cytometry analysis (Fig. 2.13F). Due to contaminating uninfected GFP-negative cells, this knockdown efficiency is likely an underestimation of functional 14-3-3ζ knockdown in GFP-positive cells. On day 3, a differentiation defect was clearly observed in *miR-451*$^{-/-}$ GFP-positive cells infected with sh-Luc, however cells infected with sh-1 or sh-2 displayed an increase in CD71^{-}/TER119^{+} cells (Fig. 2.13D, 2.13E). This shift was observed in both shRNA treated groups and not in the sh-Luc infected groud, indicating an increase in erythroid differentiation due to the specific repression of 14-3-3ζ. These data demonstrate that repression of 14-3-3ζ enhances erythroid differentiation in the absence of miR-451 and strongly supports the conclusion that miR-451 mediated repression of 14-3-3ζ functions to enhance erythroid differentiation.

Loss-of-function and gain-of-function of specific effectors downstream of the EPO receptor typically result in erythrocyte defects (Zhang and Lodish 2007). Loss of K-Ras results in diminished AKT activation and thereby results in a mild erythroid differentiation defect (Zhang and Lodish 2005; Zhang et al. 2007). Conversely, overexpression of factors that exaggerate intracellular signals similarly induce erythroid differentiation defects. Chronic activation of STAT5, AKT, and p44/42 MAP-kinase in erythroid progenitors by K-ras expression leads to a mild block in terminal erythroid differentiation and expansion of erythroid progenitors (Zhang and Lodish 2007). Hyperactivation of these pathways blocks terminal

erythroid differentiation and leads to cytokine independent growth of erythroid progenitors (Braun et al. 2004). Due to the essential function of 14-3-3ζ as an effector of PI-3K/AKT pathways, it is likely that its misregulation in erythroid progenitors affects the differentiation process. Finally, our finding that inhibition of 14-3-3ζ in *miR-451*$^{-/-}$ animals restores erythroid differentiation suggests that 14-3-3ζ is a key downstream effector of the pro-erythroid actions of this microRNA.

Our results indicating the sensitization of *miR-451*$^{-/-}$ erythrocytes to oxidative stress are consistent with work indicating a similar phenotype in *miR-144*$^{-/-}$*/miR-451*$^{-/-}$ animals, and suggest that miR-451 rather than miR-144 regulates this process (Yu et al. 2010). Also, our findings that red blood cell production shows a stoichiometric dependency on miR-451 levels and that acute inhibition of miR-451 with an antagomir induces an erythroid differentiation defect suggest that miR-451 oligonucleotide inhibitors may be efficacious in the treatment of red cell dyscrasias such as polycythemia vera or other hematopoietic malignancies. Finally, miR-451 has been reported to participate in other disorders, including glioma tumorigenesis and pulmonary hypertension (Caruso et al. 2010; Godlewski et al. 2010). Thus, it will be of interest to determine whether miR-451 inhibitors demonstrate therapeutic efficacy in these disorders.

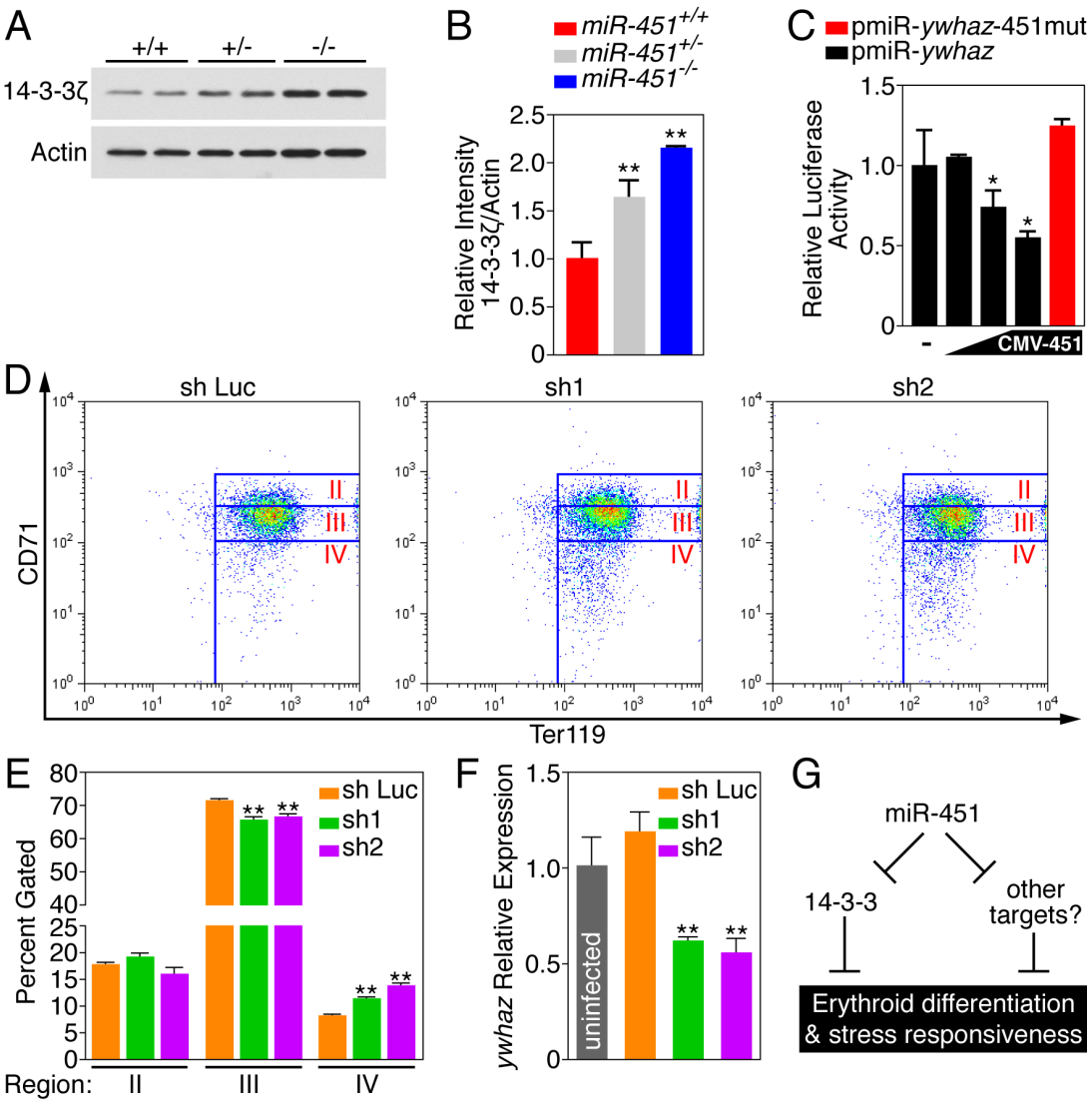

Figure 2.13. *(legend continued on next page)*

Figure 2.13. 14-3-3ζ expression is increased in response to miR-451 inhibition. *(A)* Immunoblot analysis for 14-3-3ζ on protein harvested from E14.5 fetal liver TER119^{+} erythrocytes. Two individual animals from each genotype were run in adjacent lanes. *(B)* Densitometry analysis of the immunoblot shown in *(A)*. Data is shown as means ± SEM. (*) $P < 0.05$, (**) $P < 0.01$. *(C)* A luciferase reporter construct fused the *ywhaz* 3'-UTR is repressed by miR-451 in a dose dependent manner. Mutation of this binding site abolishes miR-451 mediated repression. Data from n=2 per condition is shown as means ± SEM. (*) $P < 0.05$, (**) $P < 0.01$. *(D)* FACS analysis of in vitro differentiated TER119 depleted 14.5 d.p.c. *miR-451*$^{-/-}$ fetal liver cells three days post-induction by erythropoietin. Cells shown are GFP positive, representing viability and expression of one of two shRNAs targeted against 14-3-3ζ (sh-1, sh-2) or against Luciferase (sh-Luc) as a control. Cells were stained for CD71 and TER119. Representative FACS plots from each condition are shown. *(E)* Quantitation of percent of cells gated within each individual region. Data from n=3 per condition are shown as means ± SEM. (*) $P < 0.05$, (**) $P < 0.01$. *(F)* Real-time RT-PCR analysis of *ywhaz* expression from in vitro differentiation assays represented in *(D)*. Reactions were performed on cDNA reverse transcribed from RNA harvested from whole cell suspensions (GFP- and GFP+ cells). *(G)* Schematic representation of the role of miR-451 as a regulator of 14-3-3ζ, erythroid differentiation and the response of erythrocytes to stress.

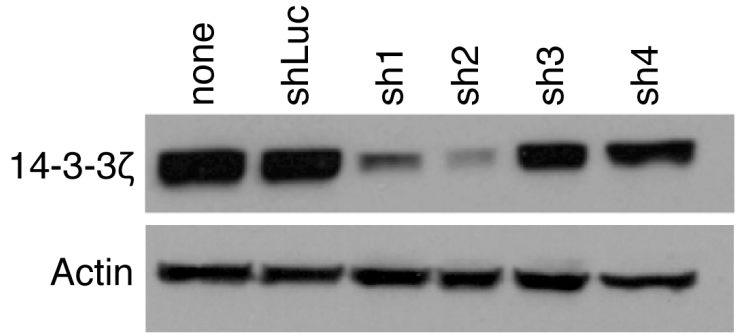

Figure 2.14. Western blot analysis for 14-3-3ζ displays efficient repression by sh1 and sh2. NIH-3T3 cells were infected with retrovirus expressing one of four shRNAs against *ywhaz* (sh1-4) or with a control shRNA against luciferase (shLuc). Only sh1 and sh2 significant repression of 14-3-3ζ expression by Western blot.

MATERIALS AND METHODS

Generation of miR-451 mutant mice

To generate the miR-451 targeting vector, a 4.3 kb fragment (5' arm) extending upstream of a poorly conserved DNA element located between the miR-144 and 451 pre-miR sequences was digested with SacII and NotI and ligated into the pGKneoF2L2dta targeting plasmid upstream of the loxP sites and the Frt-flanked neomycin cassette. A 3.2 kb fragment (3' arm) extending downstream from a poorly conserved region outside of the miR-451 pre-miR was digested with SalI and HindIII and ligated into the vector between the neomycin resistance and Dta negative selection cassettes. Targeted ES-cells carrying the discrupted allele were identified by Southern blot analysis with 5' and 3' probes. Three miR-451 targeted ES clones were identified and used for blastocyst injection. The resulting chimeric mice were bred to C57BL/6 to obtain germline transmission of the mutant allele. PCR primer sequences are available upon request. miR-451 global mutant mice were generated by breeding miR-451neo/neo mice to C57BL/6 mice harboring the ubiquitously expressed Flp-transgene. The resultant *miR-451*$^{fl/+}$ animals were crossed to mice harboring the ubiquitously expressed CAG-cre transgene to generate the global miR-451 mutant allele.

Hematocrit and reticulocyte measurements

Blood from adult animals (8 weeks old) was obtained from the periorbital vascular plexus directly into microhematocrit tubes (70uL Fisher Scientific, Pittsburgh PA). Hematocrit was measured manually after centrifugation of the microhematocrit tube on a hematocrit centrifuge.

Reticulocyte counts were measured manually using the Miller Disc method by Antech Labs inc. (Dallas, TX).

Flow Cytometry, Cell Purification, and in vitro Differentiation Assays

Spleens were mechanically dissociated by crushing the tissue between sterile frosted microscope slides and the lysates were suspended in DMEM/10% FBS. Bone marrow and fetal liver cells were resuspended in DMEM/10% FBS. Freshly isolated spleen, bone marrow, and fetal liver cells were immunostained at 4°C in PBS/2%FBS in the presence of mouse IgG (200μg/mL, BD Pharmingen) to block Fc receptors. Cells were incubated with PE-conjugated anti-TER119 (1μg/mL, BD Pharmingen), FITC-conjugated anti-CD71 (EBiosciences, 1μg/mL) antibodies for 15 minutes. FLOW CYTOMETRY analysis peformed on *ywhaz* knockdown cells supplemented a bioting conjugated CD-71 antibody (Ebiosciences) for CD-71 FITC. For this assay, cells were incubated with Avidin-APC (EBiosciences, 1:1000) in an extra step. Flow cytometry was carried out on a Becton Dickinson FLOW CYTOMETRYCalibur (Franklin Lakes, NJ). Cell sorting was performed by the Flow Cytometry Core Facility (UT Southwestern). For in vitro differentiation, fetal livers were collected at E14.5. Cells were incubated with anti-TER119 biotin conjugated antibody (BD Pharmingen) followed by incubation with streptavidin microbeads (BD Pharmingen). $TER119^-$ cells were purified through MACS separation columns (Miltenyi Biotec). $TER119^-$ progenitor-rich fetal liver cells were plated on fibronectin coated coverslips and induced to differentiation as previously described (Zhang et al. 2003). ShRNA infections were peformed on $TER119^-$ progenitor-rich fetal liver cells by spin infection. Briefly, in medium supplemented with 10 μg/ml polybrene, cells were spun in medium containing ShLuc, Sh1, or Sh2 retroviruses at 1600 RPM at 33 °C in a Sorvall

RT 6000D Centrifuge. Cells were then resuspended in EPO containing medium and plated on fibronectin coated plates.

Phenylhydrazine stress test

Phenylhydrazine was purchased from Sigma and injected subcutaneously and days 0, 1, and 3 at a 40mg/kg dose. Samples for hematocrit and reticulocyte values were collected as previously described (Socolovsky et al. 2001).

Antagomir Injections

80 mg/kg of a miR-451 antagomir or a miR-451 scrambled control antagomiR were injected on days 0 and 1 into the tail vein. Mice were sacrificed on day 3 and analyses were performed.

Microarray, real time RT-PCR analysis

$TER119^{+}/CD71^{+}$ double positive cells were isolated by cell sorting from the fetal liver of *miR-451*$^{+/+}$ and *miR-451*$^{-/-}$ littermates harvested at 14.5 d.p.c. RNA was extracted with Trizol (Invitrogen) reagent according to the manufacturer's instructions. Microarray analysis was performed using Mouse Genome 430A2.0 chips (Affymetrix). Raw expression data was analyzed first by normalization and then by comparison of signal intensity. The genes whose normalized values were greater by more than 2.0 were selected for further evaluation. Reverse transcription was performed with random hexamers (Invitrogen) after which transcript levels were quantitated using realtime PCR Taqman probes purchased from Applied Biosystems.

Colony Formation Assays

Bone marrow cells were harvested from femurs of 6-8 week wild-type or miR-451 knockout littermates, and spleen cells were isolated from spleens of the same animals. After removal of red blood cells, 2×104 bone marrow cells or 4×105 spleen cells were plated in 2 ml IMDM medium containing 80% MethoCult medium (StemCell Technologies, Inc. cat# M3234), mSCF (50 ng/ml, PeproTech), mIL-3 (10ng/ml, PeproTech), mIL-6 (10ng/ml, PeproTech) and Epo (3U/ml, Amgen Inc.). CFU-E colonies were counted after 3 days whereas BFU-E were counted after 5 days of incubation.

Luciferase Assay

The 3'-UTR of *ywhaz* was cloned and inserted into the pmiR-Report vector as the 3'-untranslated region (UTR) of the luciferase product. The miR-451 seed region 5'-AACGGTT-3' was mutated to 5'-ACAAGTT-3'. miR-451 was expressed from pCMV6-miR-451 vector expressing the pre-miR-451 with 50bp of flanking sequence. Constructs were transfected into COS-1 cells using Fugene-6 reagent (Roche).

Northern blot analysis

Tissues were harvested from adult mice (8-weeks) and total RNA was isolated with Trizol reagent (Invitrogen). Northern blots to detect microRNAs were performed as previously described (van Rooij et al. 2006). A U6 probe or total RNA served as a loading control (van Rooij et al. 2007).

Western blotting

Adult whole bone marrow and MACS isolated TER119^{+} fetal liver cells (E14.5) were lysed and then boiled in SDS sample buffer. 14-3-3ζ was resolved by SDS-PAGE and analyzed with antibodies to 14-3-3ζ (Santa Cruz antibody Biotechnology Inc. SC-1019).

Transgenic mice

miR-451 promoter-LacZ transgenic mice were generated by pronuclear microinjection of pHsp68LacZ construct with *miR-451* promoter fragment cloned to the upstream of LacZ using primer sequences shown in figure 2.3.

Chapter III

Stress Dependent Cardiac Remodeling in the Absence of miR-21

ABSTRACT

MicroRNAs inhibit mRNA translation or promote mRNA degradation through binding complementary sequences in 3' untranslated regions of target mRNAs. MicroRNA-21 (miR-21) is up-regulated in response to cardiac stress. Here, we show that miR-21 null mice are normal and, in response to a variety of cardiac stresses, display cardiac hypertrophy, fibrosis, up-regulation of stress-responsive cardiac genes and loss of cardiac contractility comparable to wild-type littermates. Similarly, inhibition of miR-21 through intravenous delivery of a Locked-Nucleic-Acid (LNA)-modified antimiR oligonucleotide also fails to block the remodeling response of the heart to stress. We conclude that miR-21 is not essential for pathological cardiac remodeling.

INTRODUCTION

Cardiac hypertrophy

Heart disease is the leading cause of death for both men and women (Kung et al. 2008). The causes of heart disease include coronary artery disease and hypertension. Coronary artery disease may lead to a variety of syndromes including chronic myocardial ischemia and myocardial infarction (MI) the results of which include cardiac fibrosis, cardiomyocyte hypertrophy, and arrhythmogenesis which contribute to a reduction in cardiac function (Felker et al. 2000). Chronic hypertension results from a variety of conditions, however the most common form of hypertension is idiopathic (Ganau et al. 1992). Hypertension is by definition an increase in cardiac afterload. This increase requires the myocardium to increase contractility parameters in order to maintain cardiac output. This increased demand results in modifications of the myocyte both structurally and genetically. These cells grow in diameter (hypertrophy) and begin to express a gene program that resembles that of the embryonic heart. Pathologic hypertrophy is irreversible and will eventually lead to cardiac failure, which is defined as the inability of the heart to meet the circulatory requirements of the organism (Hill and Olson 2008). Due to the complexity of the myocardial changes that occur during pathologic cardiac hypertrophy, it is likely that microRNAs play a role in this process.

Cardiac microRNAs

Multiple original analyses of microRNA regulation during cardiac hypertrophy have revealed a signature pattern of microRNAs expressed both at baseline and upon stress. Deep sequencing analysis of cardiac microRNAs at baseline has revealed the most abundant cardiac

microRNAs to be miR-1, Let-7/98 family, and the miR-30 family of microRNAs comprising approximately 40%, 15%, and 7% of cardiac microRNAs respectively. The remainder of cardiac microRNAs consist of miRs -26, -378, -143, -133, -126, -125/351, -22, -27, -15/16/195, -23, -208, and -499, totaling 35% of total microRNAs collectively (Figure 3.1) (Rao et al. 2009).

Other studies have identified cardiomyocyte specific microRNAs and have identified their collective function in the maintenance of cardiac structure and function. Deletion of Dicer in mice by Cre-recombinase driven by the cardiomyocyte specific enhancer α-myosin heavy chain (αMHC) results in early postnatal lethality due to cardiac failure (Chen et al. 2008). Interestingly, analysis of the microRNA expression pattern of both Dicer heterozygous hearts and hearts homozygous for the Dicer deletion results in haploinsufficient and deficient levels of specific microRNAs respectively. These microRNAs include miRs -1, -133, Let-7 family, -30 family, -145, -125, -23, -16, -26, -22, -27, -378, -208, -499 and may be considered cardiomyocyte specific. MiR-21 also displayed this pattern of expression, establishing it as a cardiomyocyte specific microRNA at baseline (Chen et al. 2008). Analysis of myocardial microRNA expression upon Dicer deletion by a tamoxifen-inducible cre recombinase driven by the αMHC enhancer (Mer-Cre-Mer) revealed a similar set of microRNAs. These animals displayed rapid onset of cardiac failure and death within 1-week after deletion. Cardiac failure was accompanied by myocyte hypertrophy and cardiac fibrosis. Interestingly, microRNA-21 levels doubled in expression in these failing hearts (da Costa Martins et al. 2008). These two studies taken together suggest that while miR-21 is expressed primarily in cardiomyocytes at baseline, it is upregulated by both cell types upon stress.

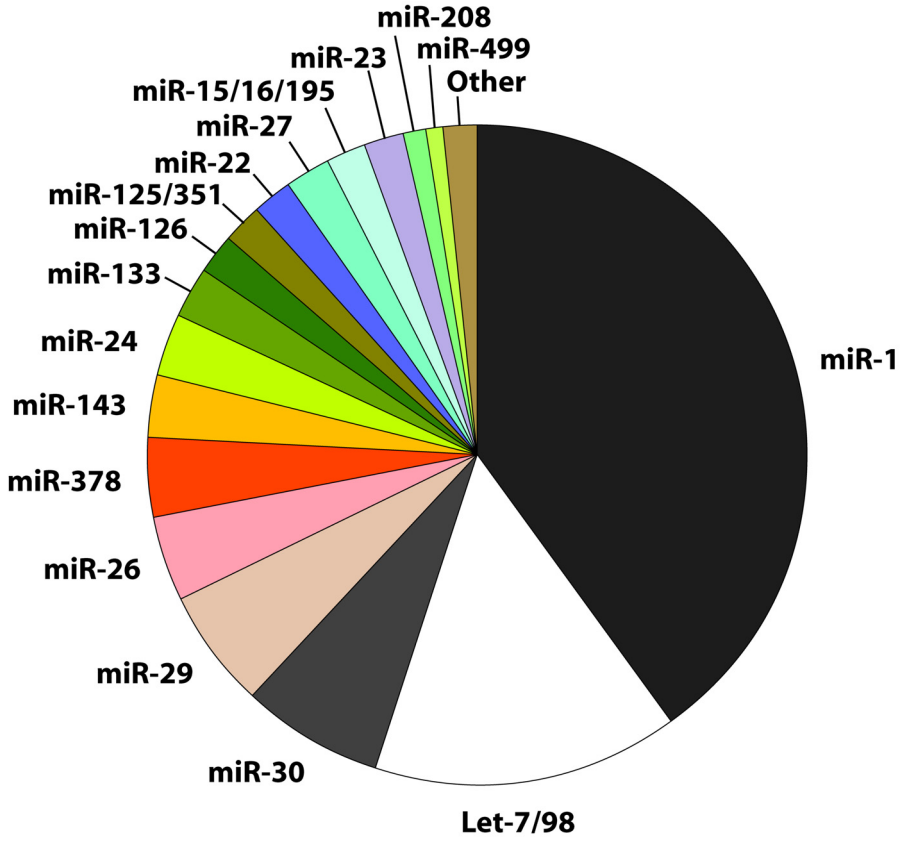

Figure 3.1. MicroRNA abundance in the mouse myocardium. MiRs -1, Let-7 Family, -30 family, and -29 family are the most abundant microRNAs in the heart. Several other microRNAs contribute a smaller percentage. Data adapted from (Rao et al. 2009).

MicroRNAs and pathological cardiac hypertrophy

A signature of microRNA expression during pathological cardiac hypertrophy has been elucidated by independent groups. Profiling of cardiac hypertrophy in mice has employed the use of the thoracic aortic constriction model (TAC) of pressure overload cardiac hypertrophy. TAC is a surgical model whereby a suture is placed around the ascending thoracic aorta and then constricted to a defined diameter (Hill et al. 2000). This increases afterload and results in pressure overload cardiac hypertrophy. MicroRNA profiling studies utilizing this model vary in their findings, however, analysis of these studies as a whole reveals the downregulation of the miR-30 family and miR-150. It also reveals the upregulation of miRs -214, -21, -15 family, -24, -27ab, -210, and 351 (van Rooij et al. 2006; Cheng et al. 2007; Sayed et al. 2007; Tatsuguchi et al. 2007).

Analyses of human tissue has primarily been performed on RNA extracted from the myocardium of patients suffering from heart failure, dilated cardiomyopathy, idiopathic cardiomyopathy, and aortic stenosis. These human disease states are similar to that seen in the mouse TAC model, however, it must be noted that they likely represent the end-point of prolonged pressure overload. With this in mind, microRNA expression analyses of human heart failure reveal a similar signature to that seen in the TAC model with notable differences. Analysis of these studies reveals the upregulation of miRs -214, -21, -15 family, -and 27ab, with the addition of miRs -100, -103, -125, -320 (van Rooij et al. 2006; Ikeda et al. 2007; Thum et al. 2007; Matkovich et al. 2009). These studies did not consistently describe the downregulation of specific microRNAs nor did they imply regulation of miRs -24, -210, or -351 as did the murine pressure overload studies. It can be implied from these studies, that TAC is a medically relevant model for the analysis of specific microRNA function during pathological cardiac hypertrophy.

Specific microRNAs have been described to play a direct role in pathological cardiac hypertrophy. MiR-208a is a member of a family of microRNAs encoded within introns of myosin-heavy-chain genes. This family includes miRs -208b and -499. MiR-208a specifically has been shown to repress repressors of cardiac hypertrophic genes such as β-myosin heavy chain (βMHC) (van Rooij et al. 2007). Mice mutant for microRNA-208a are resistant to TAC induced cardiac hypertrophy. MiR-199b has been shown to target Dyrk1a, a promoter of the pro-hypertrophic phosphatase calcineurin. Knockdown of miR-199b using an antagomir resulted in protection and reversal of cardiac hypertrophy (da Costa Martins et al. 2010). Similarly, inhibition of miR-320 with a cholesterol-modified inhibitor before myocardial infarction, resulted in upregulation of the cardioprotective miR-320 target gene Hsp20 and a reduction in infarct size (Ren et al. 2009).

MiR-21 and cardiac remodeling

Due to the consistent upregulation of miR-21 in both animal models of cardiac remodeling and human cardiac disease, several studies interrogated the role of miR-21 in cardiac disease. These studies vary considerably in their conclusions. Many suggest an anti-apoptotic role for miR-21 in the cardiac myocyte, and thereby support the importance of miR-21 upregulation as cardioprotective (Sayed et al. 2008; Cheng et al. 2009; Dong et al. 2009; Sayed et al. 2010). One study suggests that miR-21 targets Spry2 within cardiomyocytes, a mediator of cellular outgrowths (Sayed et al. 2008). It is proposed in this study that repression of Spry2 allows for increased intercommunication between myocytes during periods of cardiac stress. This increased connectedness may be adaptive, allowing for enhanced conduction velocity. In this case, miR-21 is protective against cardiac remodeling (Sayed et al. 2008). Similarly, miR-21

has been shown to be protective against oxidant-induced cardiomyocyte death by targeting the pro-apoptotic protein programmed cell death 4 (PDCD4) (Cheng et al. 2009). Other reports similarly suggest an anti-apoptotic role of miR-21 in the myocyte (Dong et al. 2009; Sayed et al. 2010). Specifically, overexpression of miR-21 in cardiac myocytes in vivo has been shown to protect cardiomyocytes against ischemia-induced cell death (Dong et al. 2009). Finally, miR-21 has been suggested to reduce the apoptosis of cardiomyocytes by targeting the predicted miR-21 target gene Fasl (Sayed et al. 2010).

Conversely, other studies suggest that miR-21 is a pro-hypertrophic microRNA. An early study described an increase in cardiomyocyte hypertrophy upon miR-21 overexpression in cultured myocytes (Cheng et al. 2007). However, these data are incongruent with previously mentioned study in which overexpression of miR-21 in vivo is cardioprotective. One specific study reported that knockdown of miR-21 through systemic delivery of cholesterol-modified antisense oligonucleotides (antagomirs) prevented cardiac hypertrophy and fibrosis in response to pressure overload induced by transaortic constriction (TAC). These salutary effects were attributed to the derepression of a miR-21 target transcript Spry1, which inhibits MAP kinase signaling specifically in cardiac fibroblasts and not cardiomyocytes (Thum et al. 2008). The incongruity of these studies led us to investigate the role of miR-21 in cardiac remodeling.

RESULTS AND DISCUSSION

Generation of *miR-21*$^{-/-}$ mice

To generate *miR-21*$^{-/-}$ mice, we introduced loxP sites at both ends of pre-miR-21 through homologous recombination (Fig. 3.2A). Deletion of *miR-21* globally was achieved by breeding *miR-21*$^{fl/+}$ mice expressing CAG-Cre. Mice homozygous for *miR-21* deletion were obtained at predicted Mendelian ratios (Table 3.1). Deletion of miR-21 was confirmed by PCR, Southern and Northern blot (Fig. 3.2B-D). Regulatory sequences for the *miR-21* gene are located adjacent to the penultimate intron of the *TMEM49* gene (Fig. 3.2A) (Fujita et al. 2008). *TMEM49* mRNA expression was unaltered in *miR-21*$^{-/-}$ animals (Fig. 3.2A, 3.2E)(Fig. 3.3). Homozygous mutant mice displayed no overt abnormalities. Similarly, mutant mice displayed no abnormalities in heart size, structure, or cardiac contractility and no modification of protein levels of predicted miR-21 target transcripts encoding PDCD4 and Spry1 (Fig. 3.2F, 3.2G).

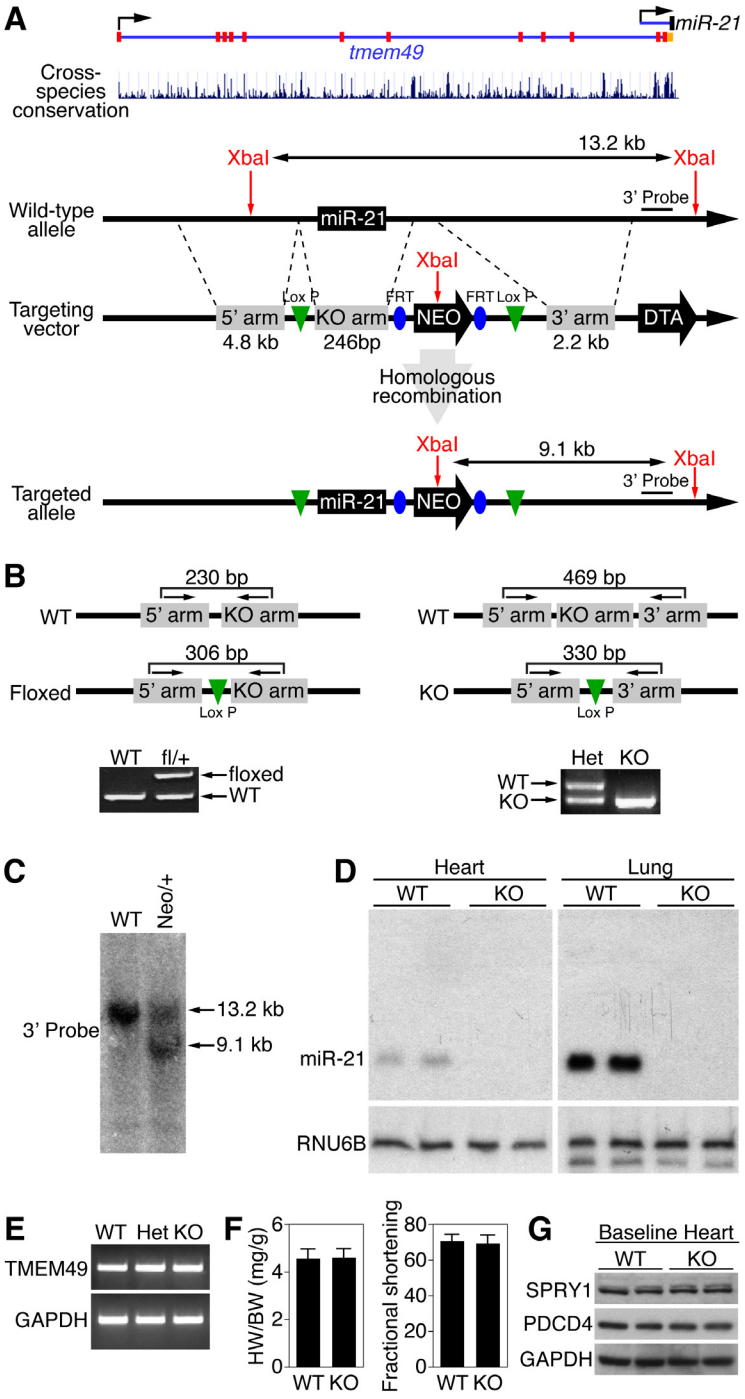

Figure 3.2. *(Figure legend continued on next page)*

Figure. 3.2. Generation of miR-21 mutant mice *(A)* Schematic representation of the mouse *miR-21* locus and targeting strategy. miR-21 is expressed as an overlapping transcript of *Tmem49*. The position of the 3' probe used for Southern blot is shown. Red boxes represent exons of the *Tmem49* gene. DTA represents the selectable marker diptheria toxin A. *(B*) Genotyping PCR approach to confirm targeting and miR-21 deletion. The positions of the PCR primers used for genotyping mutant alleles are marked with arrows and the expected lengths for the PCR products are indicated. *(C)* Southern blot analysis of miR-21 mutant alleles. Genomic DNA was digested with XbaI and hybridized to a 3' probe. WT, wild-type allele; Neo/+, conditional allele. *(D)* Northern blot analysis for miR-21 in hearts and lungs of either wild-type (WT) or knockout (KO) mice indicating efficient deletion of miR-21. RNU6B is used as a loading control. *(E)* RT-PCR of TMEM49 in wild-type (WT), heterozygous mutant (het) and knockout (KO) animals indicates that miR-21 deletion does not interfere with the expression of TMEM49. GAPDH was used as a loading control. *(F)* Morphometric and functional analysis of hearts show that miR-21 deletion has no effect on heart size or function at 1 year of age, as indicated by the ratio between heart weight and body weight (HW/BW) and fractional shortening (FS) respectively. n=4 individuals per group. *(G)* Western blot analysis indicates comparable levels of SPRY1 and PDCD4 in WT and *miR-21*$^{-/-}$ (KO) hearts.

miR-21 Genotype (93 animals)	WT	Het	KO
Expected # (%)	23 (25%)	47 (50%)	23 (25%)
Observed # (%)	19 (20%)	55 (60%)	19 (20%)

Table 3.1. *MiR-21*$^{-/-}$ mice are born at predicted Mendelian ratios.

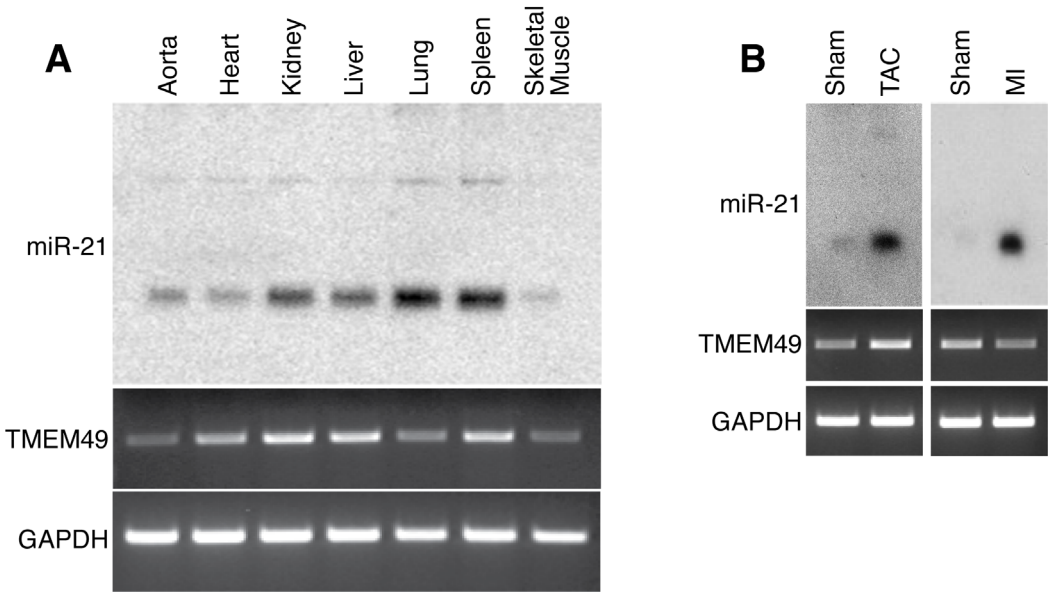

Figure 3.3. Expression of miR-21 and TMEM49. *(A)* miR-21 was detected in the indicated mouse tissues by Northern blot. TMEM49 and GAPDH mRNAs were detected by RT-PCR. *(B)* miR-21 was detected in mouse heart following sham operation or TAC for 21 days. TMEM49 and GAPDH mRNAs were detected by real time PCR.

Cardiac stress responses are unperturbed in *miR-21*$^{-/-}$ mice

To investigate the potential involvement of miR-21 in pathological cardiac remodeling, we subjected *miR-21*$^{-/-}$ mice to four different cardiac stresses: 1) acute pressure overload due to TAC (Hill et al. 2000), 2) chronic calcineurin (CnA) activation (Molkentin et al. 1998), 3) infusion of Angiotensin II (AngII), which induces cardiac remodeling through myocyte autonomous mechanisms and secondary hypertension (Schluter and Wenzel 2008), and 4) MI due to ligation of the proximal left anterior descending (LAD) coronary artery.

Both WT and *miR-21*$^{-/-}$ mice showed comparable pathological remodeling in response to all four stresses (Fig. 3.4A, B). Northern blot analysis for miR-21 revealed upregulation in WT myocardium in response to all stresses and confirmed the absence of miR-21 expression in mutant mice (Fig. 3.4C). Both WT and *miR-21*$^{-/-}$ animals showed a comparable fibrotic response and upregulation of both collagen and fetal cardiac genes (Fig. 3.4D)(Fig. 3.5A). Functional analysis by echocardiography after TAC also indicated no differences between the two genotypes (Fig. 3.6). *miR-21*$^{-/-}$ animals displayed a mildly exaggerated increase in heart weight/body weight (HW/BW) ratio in response to AngII when compared to AngII treated WT animals, suggesting a modest susceptibility to Gq induced cardiac hypertrophy. MI induced by LAD occlusion resulted in pronounced scar formation at the apex and free wall of the left ventricular chamber. The extent of scar formation and remodeling was indistinguishable in mice of the two genotypes (Fig. 3.4A, Fig 3.7A). Quantification of infarct size revealed no significant differences between WT and *miR-21*$^{-/-}$ mice (Fig. 3.7B).

miR-21 was reported to influence cardiac remodeling by regulating MAP kinase signaling, and phosphorylation of ERK (Thum et al. 2008). However, western blot analysis showed a stress-dependent increase in phospho-ERK even in the absence of miR-21 (Fig 3.5B).

Thus, the chronic deletion of miR-21 does not alter myocardial MAP kinase signaling in response to cardiac stress.

Based on prior studies, we anticipated that miR-21 would be required for cardiac hypertrophy and fibrosis. The failure of genetic deletion of miR-21 to diminish these cardiac stress responses might be explained by compensatory mechanisms activated in the persistent absence of miR-21 (van Rooij et al. 2006; Cheng et al. 2007; Ikeda et al. 2007; Tatsuguchi et al. 2007; Thum et al. 2008). To further explore the potential involvement of miR-21 in the responses of the heart to stress, we inhibited miR-21 acutely using an antimiR approach.

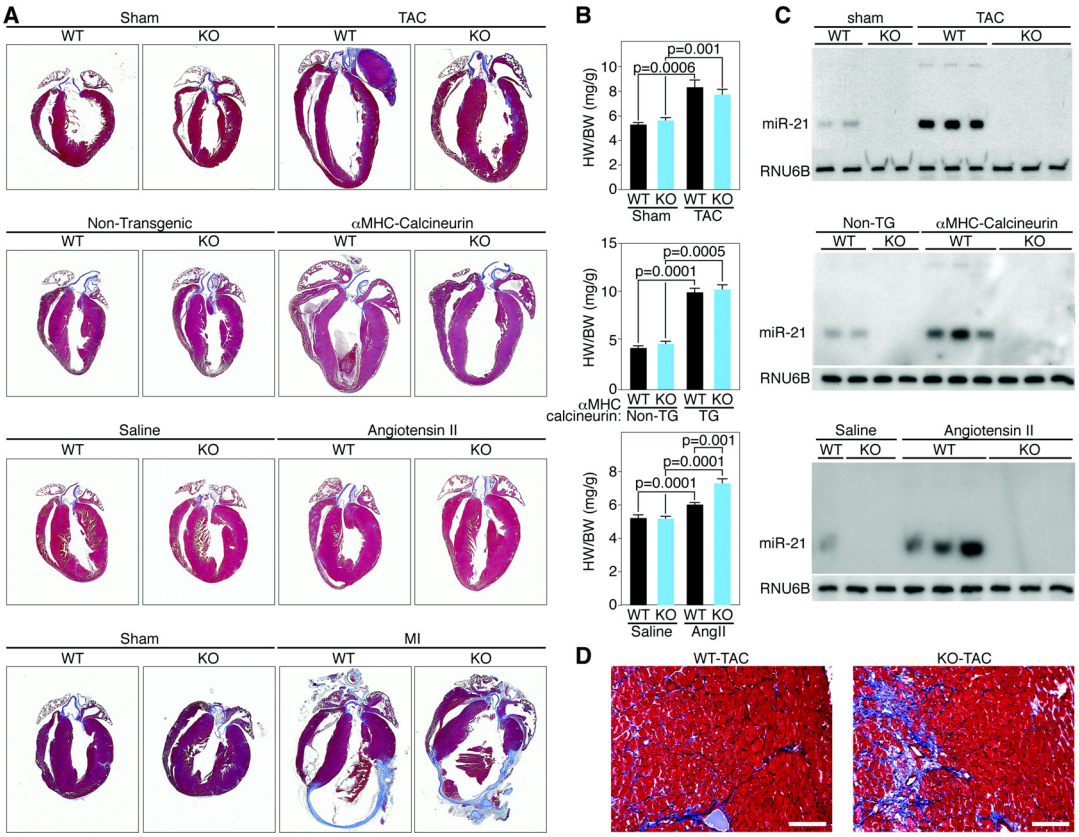

Figure 3.4. miR-21 is not required for cardiac hypertrophy or fibrosis in response to stress *(A)* Trichrome staining on cardiac sections of WT and *miR-21*$^{-/-}$ (KO) animals after TAC, transgenic expression of calcineurin, chronic AngII infusion, or MI, as indicated. Histological analysis shows that miR-21 deletion has no effect on cardiac remodeling in response to stress, based on cardiac hypertrophy and fibrosis. *(B)* HW/BW ratios from mice of the indicated genotypes in response to the indicated stresses. HW/BW data shown for TAC experiments represent n = 9 for WT sham, n = 10 for KO sham, n = 14 for WT TAC, and n = 13 for KO TAC. HW/BW data shown for Calcineurin overexpression represent n = 4 WT non-TG, n = 3 KO non-TG, n = 4 WT TG, and n = 3 KO TG. HW/BW data shown for AngII infusion represent n = 9 WT saline, n = 8 KO saline, n = 11 WT AngII, and n = 7 KO AngII. *(C)* Detection of miR-21 expression in hearts of mice of the indicated genotypes in response to the indicated stresses by northern blot analysis. RNU6B was detected as loading control. *(D)* Trichrome staining of hearts of the indicated genotypes 3 weeks following TAC surgery. Bar = 100 um.

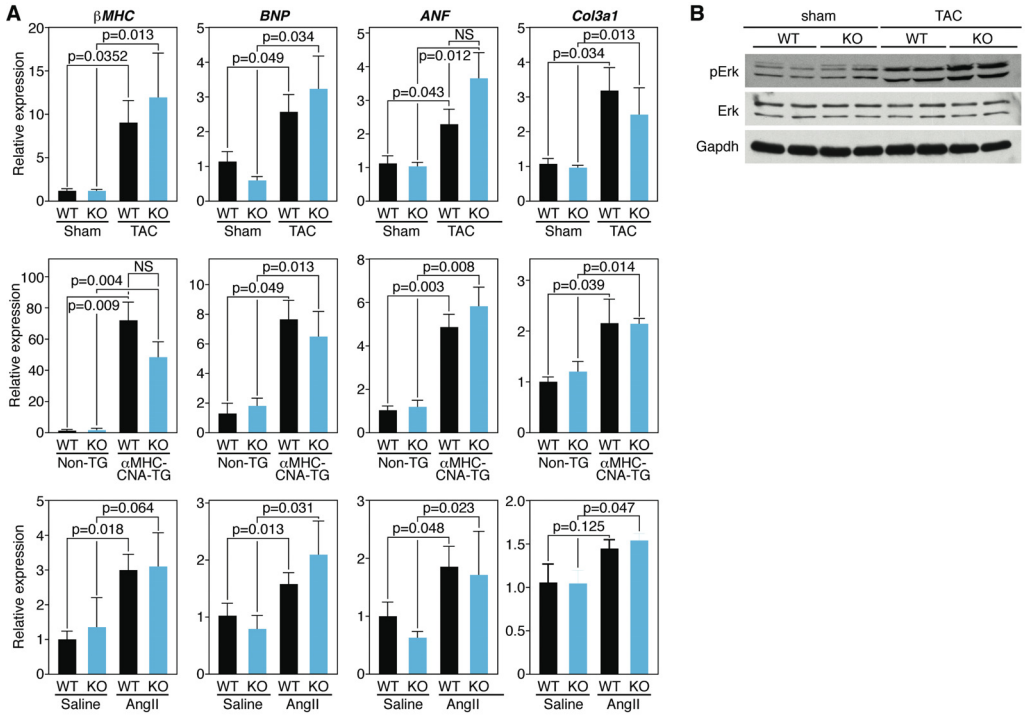

Figure 3.5. **miR-21 deletion does not alter the expression of cardiac stress markers**. *(A)* Quantitative realtime PCR analysis for hearts of the indicated genotypes in response to the indicated stresses shows no effect on cardiac gene expression during stress in the absence of miR-21. Gene expression data shown for TAC experiments represent n = 6 for WT sham, n = 6 for KO sham, n = 10 for WT TAC, and n = 10 for KO TAC. Data shown for Calcineurin overexpression represents n = 3 WT non-TG, n = 3 KO non-TG, n = 3 WT TG, and n = 3 KO TG. Data shown for AngII infusion represent n = 3 WT saline, n = 3 KO saline, n = 4 WT AngII, and n = 3 KO AngII. *(B)* Western blot analysis indicates a comparable stress-induced increase in phospho-ERK for both WT and *miR-21*$^{-/-}$ (KO) hearts in response to TAC.

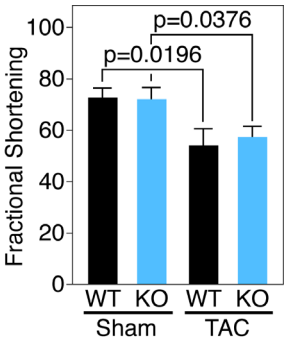

Figure 3.6. Measurement of cardiac function by fractional shortening. Fractional shortening was determined by echocardiography on wild type and miR-21 KO mice following sham operation or TAC for 21 days. Cardiac function is reduced comparably in mice of both genotypes following TAC. Data represent n = 8 for WT sham, n = 8 for KO sham, n = 11 for WT TAC, and n = 10 for KO TAC.

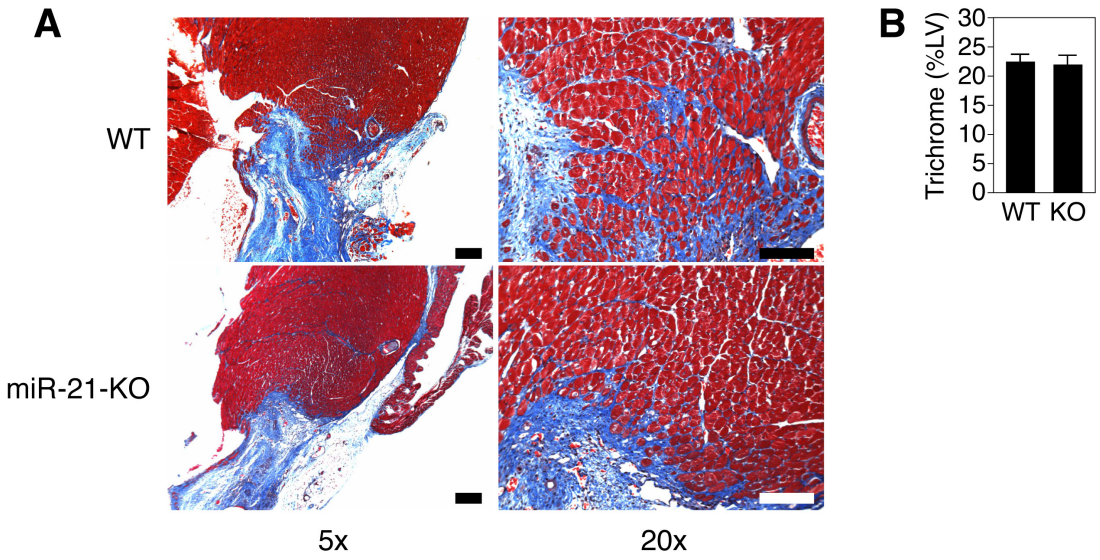

Figure 3.7. Fibrosis and scar formation following myocardial infarction. *(A)* Wild type and miR-21 KO mice were subjected to LAD ligation to induce myocardial infarction (MI). Hearts were isolated 21 days later, sectioned and stained with Masson's trichrome. Bar = 100 um. Comparable fibrosis and scar formation are seen in mice of both genotypes. *(B)* Quantification of fibrosis in WT and KO hearts subjected to LAD. Fibrosis is displayed as the percentage of trichrome positive left ventriclular area. Data represent n=3 per condition.

LNA-mediated knockdown of miR-21

Therapeutic efficacy of LNA-antimiR technology has recently been reported (21, 22) (Elmen et al. 2008a; Lanford et al. 2010). As a consequence of the high binding affinity of LNA-containing antisense oligonucleotides, biological activity is attained with shorter LNA oligonucleotides. We chose to utilize a small LNA-modified antimiR shown to be highly efficacious in vivo (Obad et al. 2011). To test whether miR-21 could be inhibited in the heart with LNA-modified antimiRs, we used an 8 nt fully LNA-modified phosphorothioate oligonucleotide complementary to the seed region of miR-21 (antimiR-21) (Fig. 3.8A). The activity of a luciferase reporter fused to the 3'-UTR of the miR-21 target transcript PDCD4 was repressed by increasing concentrations of miR-21 in Cos cells, whereas co-transfection of this reporter with antimiR-21 derepressed the PDCD4-luciferase reporter, which we attribute to functional inhibition of endogenous miR-21 (Fig. 3.8B) (Cheng et al. 2009).

To examine the ability of antimiR-21 to repress miR-21 levels in vivo, we exposed animals to TAC to induce miR-21 and 6 weeks later injected them intravenously with antimiR-21 or a scrambled control (Fig. 3.9A). While TAC induced cardiac miR-21 expression, systemic administration of antimiR-21 resulted in dose-dependent inhibition of miR-21 expression in the heart, whereas the LNA control had no effect (Fig. 3.8C). Inhibition of miR-21 with antimiR-21 caused an increase in the miR-21 target PDCD4, while a comparable dose of the LNA scramble control had no effect (Fig. 3.8D).

Based on these data, we used antimiR-21 to determine whether inhibition of miR-21 during cardiac stress would influence cardiac remodeling. Animals were dosed with 25mg/kg of antimiR-21 or LNA scramble control as described in the Materials section. Histological examination and measurements of the ratio between HW/BW indicated that cardiac hypertrophy

was comparable between untreated animals and animals treated with antimiR-21 (Fig 3.10A, 3.10B)(Fig. 3.9B). TAC caused a 2.7-fold increase in miR-21 expression 21 days after surgery compared to sham-operated animals. AntimiR-21 effectively antagonized miR-21, whereas treatment with LNA control had no effect on cardiac miR-21 levels (Fig. 3.10C, 3.10D). Notably, Northern blot analysis using a LNA probe complementary to the entire miR-21 sequence revealed a shifted band only in samples harvested from antimiR-21 treated mice. These data indicate that mature miR-21 is sequestered in a slower-migrating heteroduplex with the antimiR-21 that binds to the seed sequence rather than promotes the degradation of miR-21.

Echocardiography showed no difference in cardiac function between groups and there was no difference in βMHC up-regulation (Fig. 3.10E)(Fig. 3.11). Western blot analysis showed miR-21 inhibition to have no effect on Erk phosphorylation in response to stress (Fig. 3.10G). However, western blot analysis showed derepression of the miR-21 target PDCD4 after antimiR-21 treatment, indicating effective antagonism of miR-21 in the heart (Fig. 3.10H)

Similarly, intravenous delivery of antimiR-21 for 3 days prior to chronic AngII administration inhibited the up-regulation of miR-21 (Fig. 3.10K), but did not alter the extent of cardiac hypertrophy or remodeling compared to LNA control or saline-treated animals (Fig. 3.10I-J)(Fig. 3.9C). Expression analysis of bMHC, Col3A1, and Col2A1 also showed no difference between groups (Fig. 3.11).

We conclude that LNA-antimiR oligonucleotides can effectively inhibit cardiac microRNAs upon systemic delivery into mice, but inhibition of miR-21 by this approach does not prevent pathological cardiac remodeling in response to pressure overload or AngII administration.

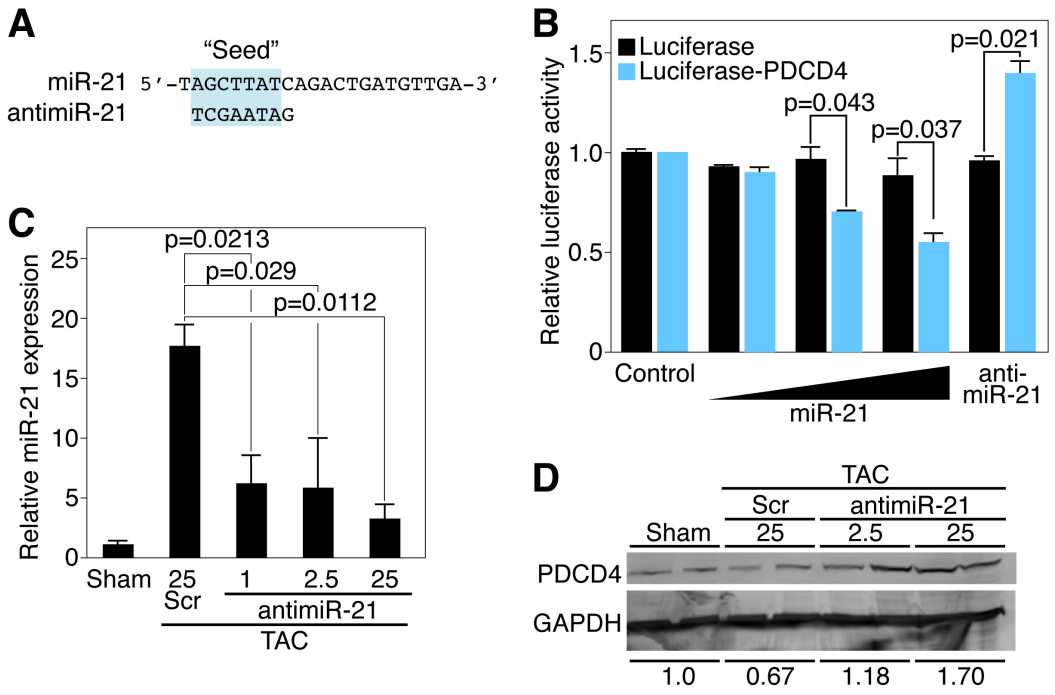

Figure 3.8. Silencing of cardiac miR-21 using an LNA-antimiR. *(A)* antimiR-21 is a fully LNA-modified phosphorothioate oligonucleotide complementary to the seed region of mature miR-21. *(B)* Relative activity of a luciferase reporter fused to the 3′ UTR of PDCD4 displays dose-dependent repression by CMV-driven miR-21, whereas treatment with antimiR-21 derepresses the luciferase reporter in COS-1 cells. Data represents the average of three experiments. *(C)* Real-time RT-PCR analysis of miR-21 was performed on cardiac tissue harvested from animals subjected to either sham or TAC surgeries. Animals subjected to TAC surgeries were injected with either 25 mg/kg LNA scrambled control (scr), 1 mg/kg antimiR-21 (1), 2.5 mg/kg antimiR-21 (2.5), or 25 mg/kg antimiR-21. TAC induces miR-21 expression in the LNA scrambled control treated animals, whereas treatment with antimiR-21 significantly inhibits miR-21 levels. Details of the injection scheme are provided in Supplemental Figure 4. Data shown represent n = 5 per condition. *(D)* Western blotting for PDCD4 on cardiac tissue after antimiR-21 treatment indicates a dose-dependent increase in PDCD4. GAPDH was used as a loading control.

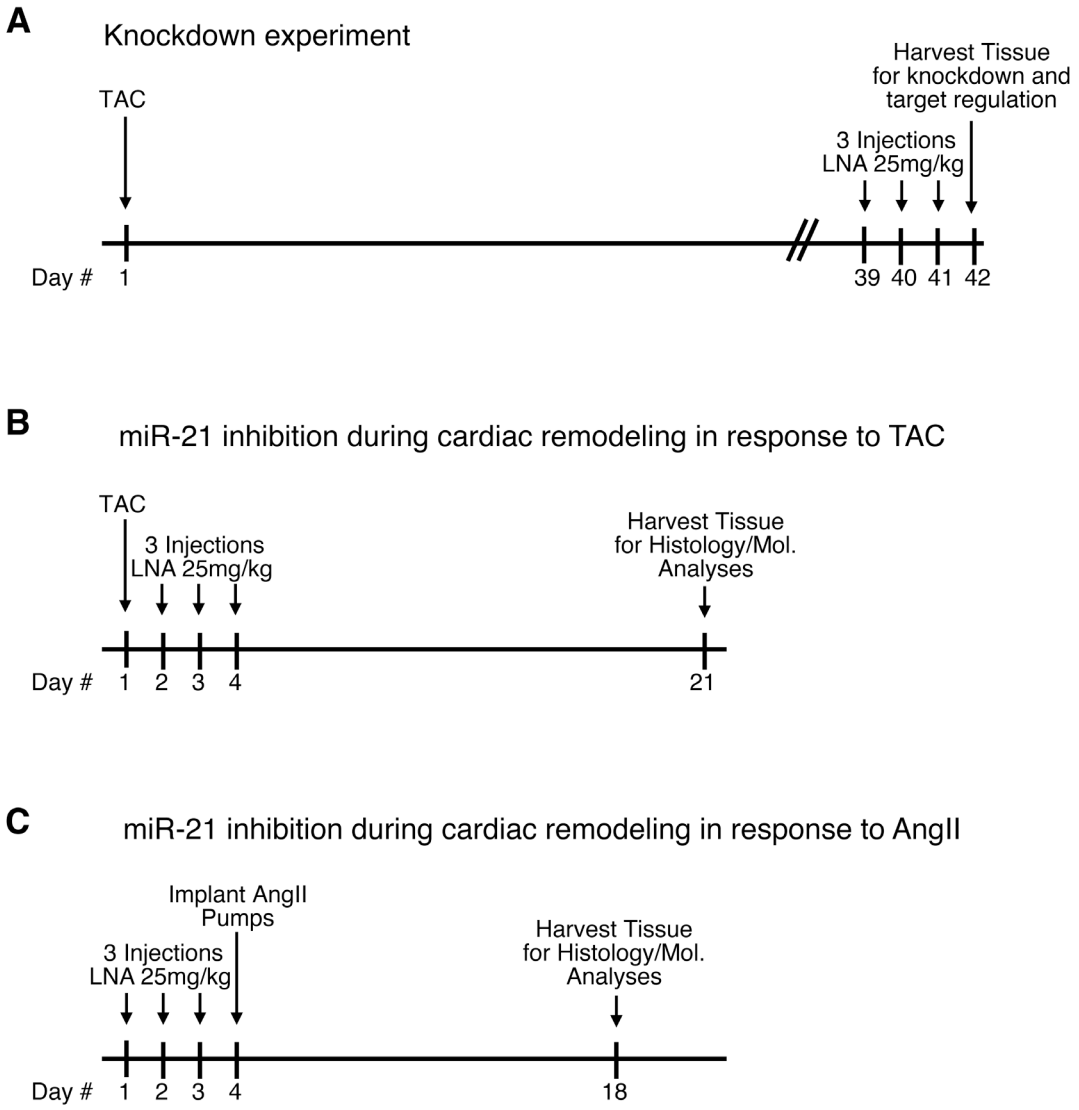

Figure 3.9. Schematic diagrams of anti-miR-21 knockdown experiments. *(A)* TAC was performed to up-regulate miR-21 expression. After 39 days, mice were injected intravenously on three consecutive days with Tiny-21 (25 mg/kg) and hearts were isolated on day 42 and analyzed for miR-21 expression. *(B)* TAC was performed and mice were injected intravenously on three consecutive days with antimiR-21 (25 mg/kg) and hearts were isolated on day 21 and analyzed for histology, miR-21 expression and miR-21 target expression. *(C)* Mice were injected intravenously on three consecutive days with antimiR-21 (25 mg/kg) and on day 4 were implanted with AngII pumps to induce pathological cardiac remodeling. After 18 days, hearts were isolated and analyzed for histology and miR-21 expression.

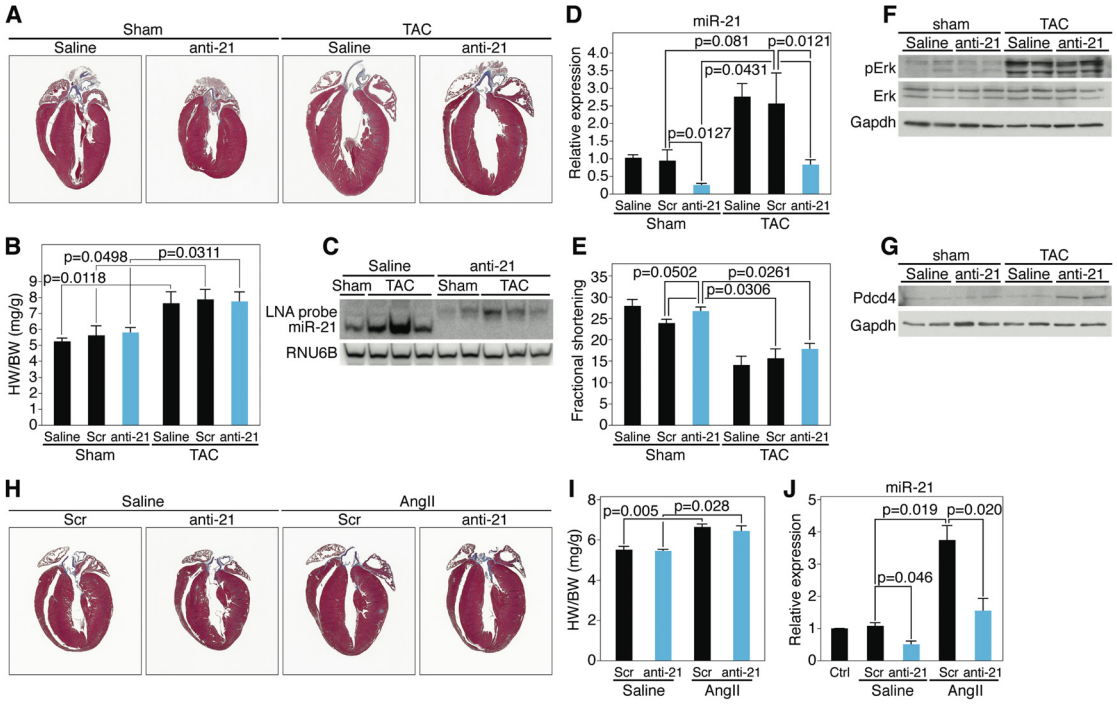

Figure 3.10. Cardiac stress response after antimiR-21 treatment. *(A)* Trichrome stained sections of hearts show that animals treated with both saline and antimiR-21 display induction of cardiac hypertrophy upon TAC. *(B)* HW/BW ratios of mice treated as indicated. HW/BW data represent n=6 for sham conditions and n=12 for TAC conditions. *(C)* Northern blot analysis for miR-21 in cardiac tissue of animals treated as indicated. The upshift reflects a heteroduplex between miR-21 and antimiR-21. RNU6B is a loading control. *(D)* Real-time RT-PCR analysis of miR-21 expression in cardiac tissue after the indicated treatments. Data represent n=5 for sham conditions and n=10 for TAC conditions. *(E)* Functional analysis of the heart represented by fractional shortening. Data represent n=6 for sham conditions and n=12 for TAC conditions. *(F)* Real-time RT-PCR analysis of βMHC expression in cardiac tissue of animals treated as indicated. Data shown represent n=5 for sham conditions and n=10 for TAC conditions. *(G)* Western blot analysis indicates a stress-induced increase in phospho-ERK for saline and antimiR-21 treated mice in response to TAC. *(H)* Western blot analysis shows an increase in PDCD4 in antimiR-21 treated mice in response to TAC. *(I)* Trichrome stained sections of hearts from animals treated as indicated. Animals treated with both LNA scrambled control and antimiR-21 display induction of cardiac hypertrophy upon angiotensin II infusion. *(J)* HW/BW ratios of mice treated as indicated. Ratios represent n=3 for Scr Saline, n=4 for AntimiR-21 Saline, n=3 for AngII Saline, and n=5 for AntimiR-21 AngII. *(K)* Real-time RT-PCR analysis of miR-21 expression in cardiac tissue of animals after the indicated treatments using untreated C57Bl/6 cardiac tissue as control (Ctrl). *(L)* Real-time RT-PCR analysis of the cardiac stress induced genes βMHC, Col3a1, and Col1a2 after the indicated treatment compared to untreated animals. Data represent n=2 for Ctrl, and n=3 for all other conditions.

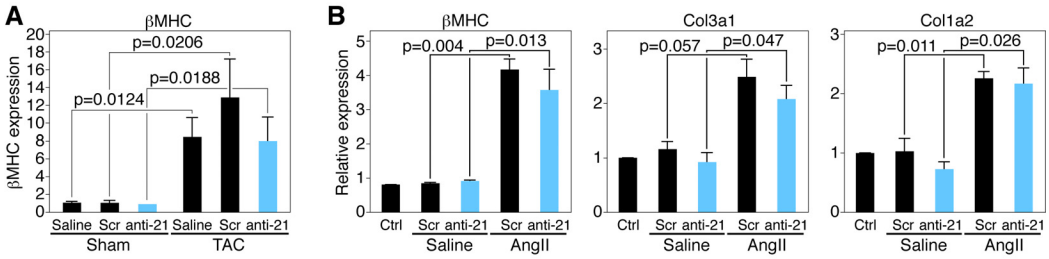

Figure 3.11. Cardiac stress response after antimiR-21 treatment. *(A)* Real-time RT-PCR analysis of βMHC expression in cardiac tissue of animals treated as indicated. Data shown represent n=5 for sham conditions and n=10 for TAC conditions. *(B)* Real-time RT-PCR analysis of the cardiac stress induced genes βMHC, Col3a1, and Col1a2 after the indicated treatment compared to untreated animals. Data represent n=2 for Ctrl, and n=3 for all other conditions.

Transient Genetic Deletion of miR-21

To further determine the effect of transient inhibition of miR-21 on cardiac hypertrophy, *miR-21$^{fl/fl}$* mice were crossed to animals expressing an estrogen-responsive cre recombinase under the control of the ubiquitously expressed CAG enhancer, *CAG-Cre-ESR1* (Danielian et al. 1998). First, to determine the effect of either saline or tamoxifen treatment on the miR-21 allele and miR-21 expression, *miR-21$^{fl/fl}$* and *miR-21$^{fl/fl}$;CAG-Cre-ESR1* animals were treated with either vehicle or tamoxifen for five days and then sacrificed 2-days post the final treatment (Andersson et al. 2010). Both DNA and RNA were generated from heart and lung. Genomic PCR analysis of the *miR-21* locus revealed a low level of baseline recombination of the miR-21 locus in the absence of tamoxifen in heart. Tamoxifen treatment dramatically enhances recombination of the allele (Fig. 3.12A). Northern blot analysis of miR-21 levels in both lung and heart reveals a significant reduction in levels of mature miR-21 and an absence of the pre-miR-21 (Fig. 3.12B, 3.12C). This knockdown is greater than 50%, therefore we can approximate the half-life of miR-21 in cardiac tissue to be between 2 and 7 days. Levels of miR-21 between *miR-21$^{fl/fl}$* and *miR-21$^{fl/fl}$;CAG-Cre-ESR1* animals treated with vehicle were not different. These data suggest that this approach for transient miR-21 deletion is effective.

To determine the effect of transient genetic deletion of miR-21 on cardiac remodeling, we performed vehicle or tamoxifen delivery as described above, and then performed TAC. Histologic analysis of transverse sections revealed significant fibrosis in both groups (Fig. 3.13A). Ventricular weight/tibia length (VW/TL), another measure of cardiac hypertrophy, and HW/BW ratios were identical between *miR-21$^{fl/fl}$* and *miR-21$^{fl/fl}$;CAG-Cre-ESR1*, tamoxifen treated animals (Fig. 3.13B)..

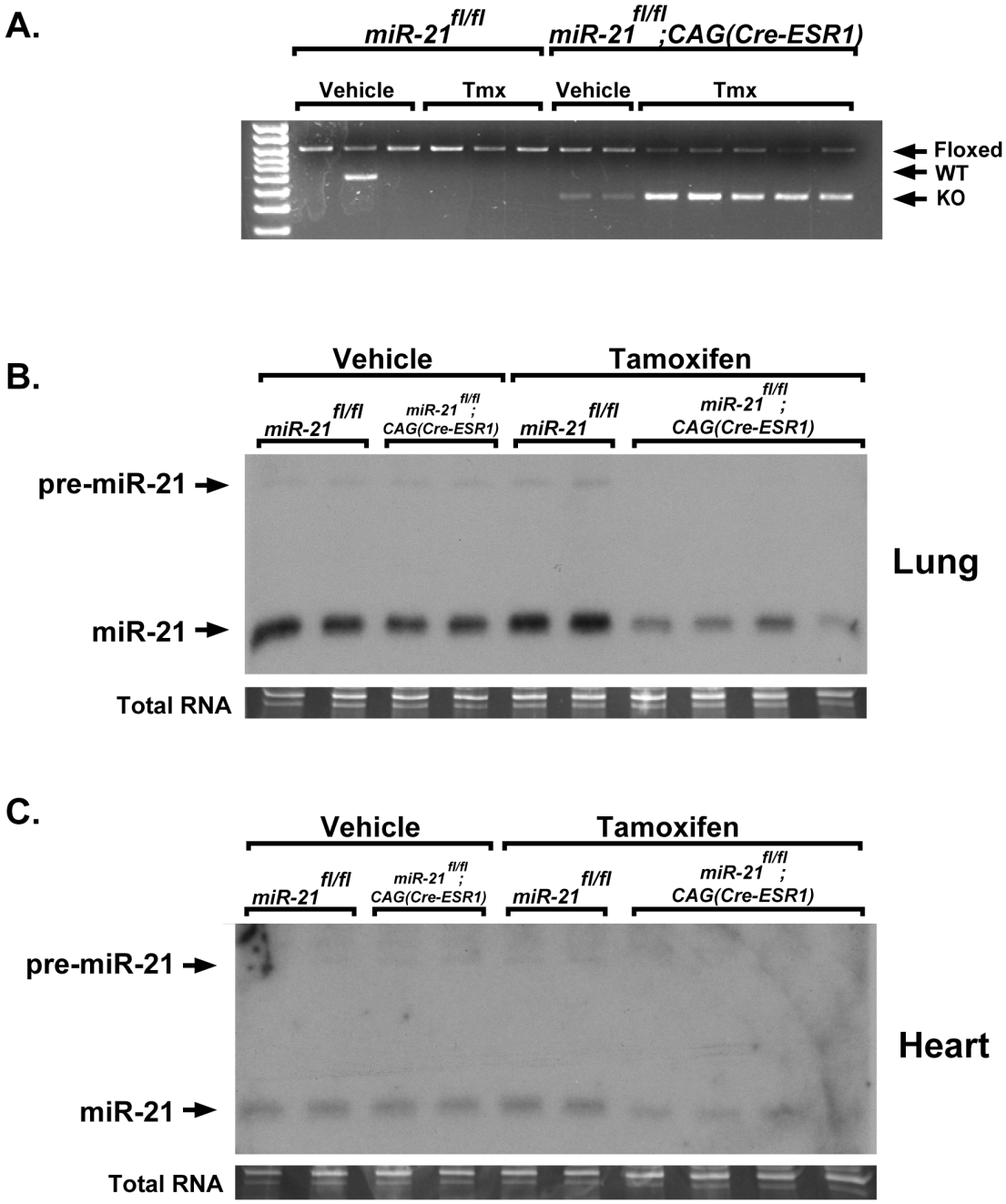

Figure 3.12. Inducible global miR-21 deletion. *(A)* PCR analysis of DNA harvested from hearts of *miR-*$^{21fl/fl}$ or *miR-*$^{21fl/fl}$*;CAG(Cre-ESR1)* animals treated with either vehicle or tamoxifen for 5 days. *miR-21*$^{fl/fl}$*:CAG(Cre-ESR1)* tamoxifen injected animals show significant recombination of the miR-21 mutant allele. *(B)* Northern blot analysis for miR-21 on lungs from animals described in *(A). (C)* Northern blot analysis for miR-21 on hearts from animals described in *(A).*

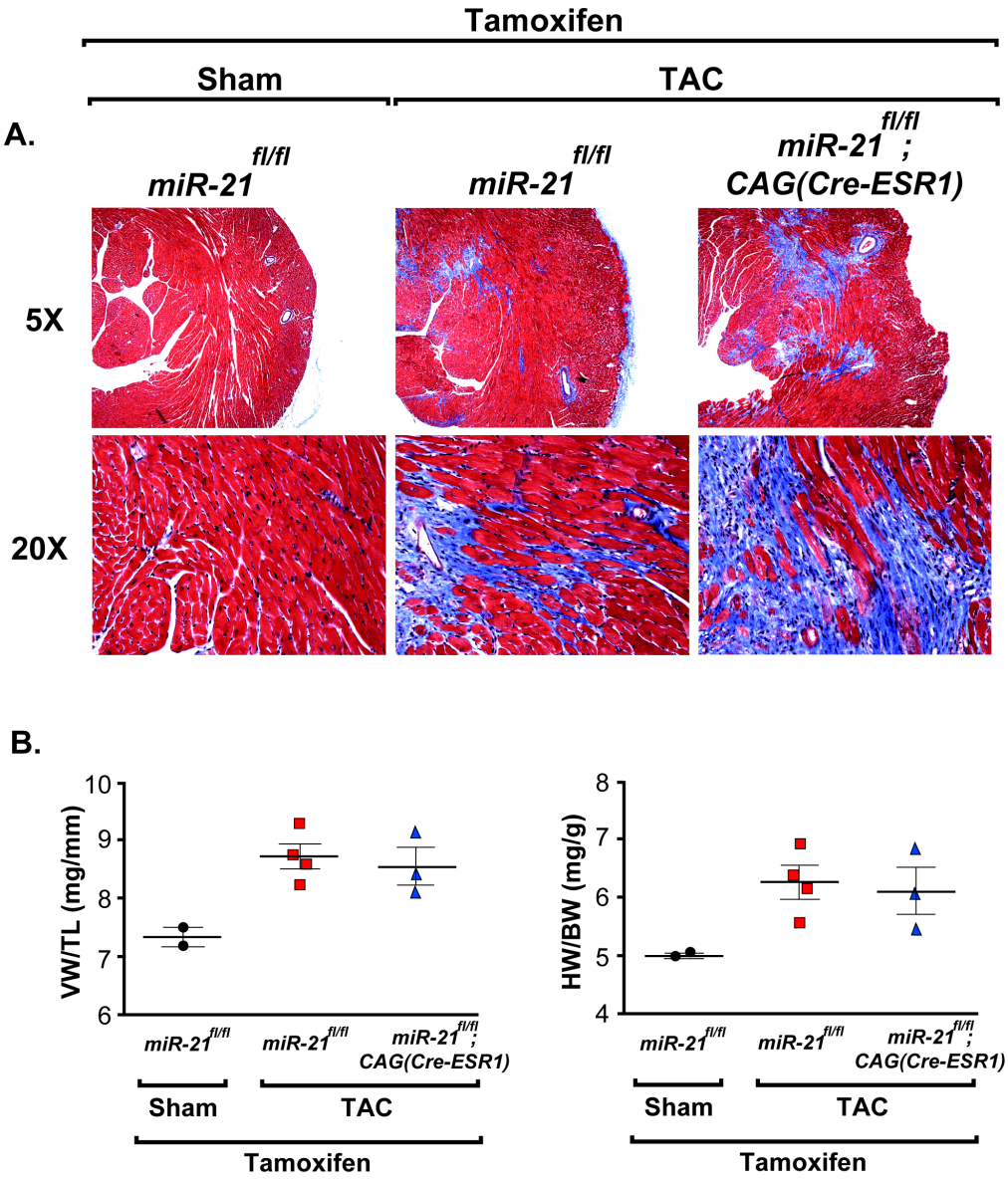

Figure 3.13. Stress-dependent cardiac remodeling upon transient genetic deletion of miR-21. *(A)* Masson's trichrome staining of left-ventricle after TAC reveals significant myocardial fibrosis in *miR-21*$^{fl/fl}$ and *miR-21*$^{fl/fl}$*;CAG(Cre-ESR1)* tamoxifen treated animals. *(B)* Ventricular weight/tibial length (VW/TL) and heart weight/body weight ratios (HW/BW) are equal in both TAC groups suggesting no difference in cardiac remodeling.

This experiment differs significantly from the antimiR study. Theoretically, antimiR-21 reduces miR-21 levels in a uniform manner, knocking down miR-21 to the same level in all cells. However, the level of miR-21 reduction observed in *miR-21*$^{fl/fl}$;CAG-Cre-ESR1 upon tamoxifen treatment most likely represents a proportion of cells that are now null for miR-21. This achieves a complete knockdown of miR-21 in these cells and represents a highly effective "genetic" antimiR. While these data do not rule out the possibility of cre-toxicity or tamoxifen toxicity as confounding variables, when considered together with the *miR-21*$^{-/-}$ and antimiR study, they strongly suggest that miR-21 inhibition does not effect cardiac remodeling. They also strengthen the conclusion that transient inhibition of miR-21 is similar to constitutive inhibition.

It is clear that our results differ from those of Thum et al. who concluded, based on antagomir-21 knockdown studies in mice, that miR-21 was essential for cardiac hypertrophy and fibrosis in response to pressure overload (Thum et al. 2008). How might these differences be reconciled? The failure of constitutive genetic deletion of miR-21 to diminish cardiac hypertrophy or fibrosis in response to stress might be explained by compensatory mechanisms activated in the persistent absence of miR-21. In this regard, and given the chronic nature of heart failure in humans, therapeutic strategies designed to treat this condition should display long-term efficacy, which raises questions as to whether acute inhibition of miR-21 would be therapeutically efficacious in this setting. This conclusion unlikely, however, due to the inefficacy of both an antimiR inhibitor of microRNA-21 and transient genetic deletion of the miR-21 locus on cardiac remodeling.

It is conceivable that variations in the level of cardiac stress imposed by TAC in the two studies could account for differential responsiveness to miR-21 inhibition, although both studies

showed comparable reduction in cardiac contractility and increased phospho-ERK in response to the procedure. Regarding the disparity between the effects of cholesterol-conjugated antagomirs and LNA-modified antimiR-21 on cardiac remodeling, it is worth noting that we injected LNA-antimiRs via the tail vein, whereas Thum et al. injected antagomir via the jugular vein (Thum et al. 2008). There is also a possibility that antagomir-21 acts on targets in addition to miR-21 in vivo or that the cholesterol-conjugated chemistry has a cardioprotective effect through unknown mechanisms. Off-target effects of antagomiR-21 cannot be ruled out as an explanation for these disparities due the absence of a mismatch control antagomiR in the experiments performed by Thum et al. It is conceivable that a mismatch antagomiR may display similar therapeutic properties.

Finally, Thum et al. have attempted to recapitulate these data in a separate study whereby they injected a similar short antimiR against miR-21 and compared its activity to longer classical microRNA ihibitors (Thum et al. 2011). In this report, they show that antagomiR-21 is effective at inhibiting cardiac remodeling whereas the short antimiR is not, thereby implying the ineffectiveness of the LNA-antimiR used in our study. While we take very seriously the conclusions reported, there are several fundamental issues with this study that invalidate their conclusions. Namely, the specific chemistry of their short antimiR is not reported, measurement of miR-21 expression was performed by real-time RT-PCR only, modification of target genes was not reported, they examine miR-21 expression 2-days post injection whereas we measured 30-days post-injection, and they again fail to use a mismatch control oligonucleotide. Most importantly, these data conflict with a technical report describing the efficacy of the LNA-modified antimiR-21 utilized in our studies.

Obad et. al report the half maximal inhibitory concentration (IC_{50}) of the LNA modified antimiR-21 used in our study to be 0.9 nM (Obad et al. 2011). This molecule is cell permeable and induces the upregulation of the miR-21 target gene PDCD4 similar to our study, whereas mismatch control does not. In vivo, they show that antimiR-21 is rapidly distributed to tissues and accumulates in cardiac tissue along with others. Finally, intravenous injection of antimiR-21 into mice harboring a xenograft, which expresses a miR-21-sensitive luciferase reporter, showed a significant increase in luciferase activity, highlighting the in vivo efficacy of antimiR-21 (Obad et al. 2011). Mice injected with a mismatch control did not show a modification in luciferase activity. Irrespective of possible experimental variations between our study and that of Thum et al, our finding that pathological cardiac remodeling in response to four different stresses in vivo is unaffected by genetic deletion of miR-21 seems to rule out an absolute requirement for this microRNA as a driver of heart disease.

Although we were unable to identify an important role for miR-21 in pathological cardiac remodeling, miR-21 knockout mice display a reduced susceptibility to lung tumorigenesis in response to K-ras activation, which reflects the up-regulation of multiple antagonists of the Ras/MAP kinase signaling pathway in these mice (Hatley et al. 2010). Thus, miR-21 clearly possesses modulatory activity for pathogenic signaling pathways in vivo and such mechanisms can be perturbed upon genetic deletion of miR-21. These data will be discussed in chapter IV.

MATERIALS AND METHODS

Generation of miR-21 mutant mice

To generate the miR-21 targeting vector, a 4.8 kb fragment (5' arm) extending upstream of the miR-21 coding region was digested with SacII and NotI and ligated into the pGKneoF2L2dta targeting plasmid upstream of the loxP sites and the Frt-flanked neomycin cassette. A 2.2 kb fragment (3' arm) was digested with SalI and HindIII and ligated into the vector between the neomycin resistance and Dta negative selection cassettes. Targeted ES-cells carrying the disrupted allele were identified by Southern blot analysis. Three miR-21 targeted ES clones were used for blastocyst injection. The resulting chimeric mice were bred to C57BL/6 mice to obtain germline transmission of the mutant allele. PCR primer sequences are as follows: 5prime-arm-Forward- 5'-TACTGTTCTTGGTGTGCCAGAAGA-3' ; 5prime-arm-Forward- 5'-AAAGCAAAGCAAACATCTCTGG-3'. 3prime-arm-Forward- 5'- GAGCCCTTATACC-3' ; 3prime-arm-Reverse- 5'-GCTCGGAGTTTGAC-3' ; KOarm-Forward- 5'-AAACCCTGCCTGAGCACCTCGT-3' ; KOarm-Reverse 5'-CAAGTCTCACAAGACATAAG-3'. Genotyping primer sequences are as follows: miR-21-straightKO-Forward- 5'-CCGGCTTTAACAGGTG-3' ; miR-21-straightKO-Reverse- 5'-GATACTGCTGCTGTTACCAAG-3'. miR-21-conditional-Forward- 5'-GCTTACTTCTCTCTGTGATTTCTGTG-3' ; miR-21-conditional-Reverse- 5'-GGTGGTACAGCCATGCGATGTCACGAC-3'.

Northern blot analysis

Total RNA was isolated from mouse tissue samples by using Trizol reagent (Gibco/BRL). Northern blots to detect microRNAs were performed as previously described (van Rooij et al. 2007). A U6 probe served as a loading control (U6 forward: 5-GTGCTCGCTTCGGCAGC-3, U6 reverse: 5-AAAATATGGAACGCTTCACGAATTTGCG-3). Northern blot analysis for the experiments for which antimiR-21 was used were electrophoresed on non-denaturing gels to show the heteroduplex formation between the antimiR-21 and mature miR-21. Briefly, 12 ug of total heart RNA was loaded unheated on a native 20% acrylamide gel, ran for 1.5 hours at 150V, and transferred to a Zeta-probe blotting membrane (Bio-rad) for 2 hours at 90V. Membranes were probed with a 32P-labelled LNA-modified oligonucleotide probe for miR-21 (Exiqon) and hybridized overnight at 37°C using RapidHyb buffer (GE Healthcare). Blots were visualized using a Storm 860 scanner (Molecular Dynamics).

RT-PCR and real-time RT-PCR analysis

Total RNA from cardiac tissue was isolated using Trizol (Invitrogen). RT-PCR with random hexamer primers (Invitrogen) was performed on RNA samples, after which the expression of a subset of genes was analyzed by either a regular or quantitative real-time RT-PCR using gene specific primers or Taqman probes purchased from ABI. Primers to detect TMEM49 transcript are as follows: TMEM49-Exon10-Forward- 5'-CATCGTGGAGCAGAT-3' ; TMEM49-Exon12-Reverse- 5'-CAAGCGCTGCTGGATTC-3'.

Mouse models of cardiac remodeling

Eight-week-old mice underwent either a sham operation or were subjected to pressure overload induced by TAC as previously described (Hill et al. 2000). Cardiac hypertrophic agonist angiotensin II (2 mg/kg/d) (American Peptide) or saline were administered using osmotic minipumps (model 2002, Alzet) subcutaneously implanted dorsally in 8-week-old male mice. Mice were sacrificed 14 days after AngII administration or 21 days following TAC. miR-21$^{-/-}$ animals were bred to animals harboring the αMHC-Calcineurin transgene as previously described (Molkentin et al. 1998). Male animals heterozygous for miR-21 mutant allele and positive for the transgene were bred to miR-21 heterozygous transgene negative females. Offspring were sacrificed at 16 weeks of age.

To mimic MI adult C57Bl6 male mice were anesthetized with 2.4% isoflurane and placed in a supine position on a heating pad (37°C). Animals were intubated with a 19G stump needle and ventilated with room air, using a MiniVent mouse ventilator (Hugo Sachs Elektronik; stroke volume, 250 ul, respiratory rate, 210 breaths per minute). Via left thoracotomy between the fourth and fifth ribs, the LAD was visualized under a microscope and ligated by using a 6–0 prolene suture. Regional ischemia was confirmed by visual inspection under a dissecting microscope (Leica) by discoloration of the occluded distal myocardium. Sham operated animals underwent the same procedure without occlusion of the LCA. Mice were sacrificed 21 days following MI.

Tamoxifen administration

Animals were injected with 5 mg of 5-hydroxy-tamoxifen (Sigma) dissolved in Peanut Oil (Sigma) in the peritoneum. Injections were performed once a day for 5 days as previously described (Andersson et al. 2010). Animals for baseline analysis were sacrificed two days after the final tamoxifen injection. Animals subjected to either TAC or sham surgery were anesthetized as and operated upon two days after the final tamoxifen injection.

Histological analysis and fibrosis quantitation

Tissues used for histology were incubated in Krebs-Henselheit solution, fixed in 4% paraformaldehyde, sectioned, and processed for Masson's Trichrome staining. Fibrosis was quantitated using Adobe Photoshop. Fibrosis is represented as the area of trichrome positivity as a percentage of total left ventriclular area.

Western blotting

Total heart lysate was prepared by homogenizing tissue in RIPA lysis buffer (50 mM Tris–HCl pH 7.4, 150 mM NaCl, 1 mM EDTA, 1% Triton X-100, 0.1% SDS, 1% sodium deoxycholate) and was resolved by SDS-PAGE, and analyzed to detect PDCD4, ERK1/2, phospho-ERK1/2, and GAPDH using 10 μg protein per sample. The proteins were transferred to PVDF membrane. Santa Cruz Western Blotting Luminol Reagent (Santa Cruz) was used for detection following the manufacturer's instructions. Primary antibodies used include rabbit polyclonal PDCD4 antibody (600-401-956, Rockland) at a dilution of 1:2000, rabbit polyclonal ERK1/2 (9102, Cell Signaling) at a dilution of 1:1000, rabbit polyclonal phospho-ERK1/2 (9101, Cell Signaling) at a dilution of 1:1000, rabbit polyclonal SPRY1 (ab21020, Abcam), and mouse

monoclonal GAPDH (MAB374, Millipore) at a dilution of 1:10,000. HRP-conjugated secondary antibodies were used according to the manufacturer's instructions.

LNA-based knockdown of miR-21

The LNA-antimiR and LNA scramble control oligonucleotides were synthesized as unconjugated and fully phosphorothiolated oligonucleotides (Santaris Pharma, Denmark). The perfectly matching LNA-antimiR oligonucleotide was complementary to nucleotides 2–9 in the mature miR-21 sequence. A 8 nt LNA scramble sequence oligonucleotide was used as a control. For Cos cell transfection, cells were transfected with either a miR-21 expression vector or LNA-antimiR with Lipofectamie 2000 (Invitrogen) at a concentration of 10 nM. C57BL/6 mice were injected intravenously at the indicated timepoints with the indicated doses of antimiR-21, LNA control or a comparable volume of saline, after which the tissues were collected at the days indicated (Fig. 3.9).

Transthoracic echocardiography

Evaluation of animals represented in Figure 3 was performed on mice sedated with 5% isoflurane. All other animals were not sedated for evaluation. Cardiac function and heart dimensions were evaluated by two-dimensional echocardiography using a Visual Sonics Vevo 770 Ultrasound (Visual Sonics, Canada) and a 30-MHz linear array transducer. M-mode tracings were used to measure anterior and posterior wall thicknesses at end diastole and end systole. Left ventricular (LV) internal diameter (LVID) was measured as the largest anteroposterior diameter in either diastole (LVIDd) or systole (LVIDs). The data were analyzed by a single observer

blinded to mouse genotype. LV fractional shortening (FS) was calculated according to the following formula: FS (%) = [(LVIDd - LVIDs)/LVIDd] x 100.

Chapter IV

Conclusions, Future Directions, and Therapeutic Applications

MIR-21

Despite the absence of a role for miR-21 in cardiac remodeling, the evidence for the role of miR-21 in tumorigenesis has been substantiated in greater depth in vivo. As described above, profiling of microRNAs in tumor samples and tumor cell lines have clearly identified the dysregulation of miR-21 as a feature of tumorigenesis (Chan et al. 2005; Ciafre et al. 2005; Volinia et al. 2006; Meng et al. 2007). Specifically, the overexpression of miR-21 has been determined to pro-oncogenic whereas miR-21 inhibition supresses tumorigenesis.

Numerous studies describe an anti-apoptotic role for miR-21 in tumorigenesis. Specifically, as described above, miR-21 has been shown to regulate the proapoptotic tumor suppressor PDCD4 in human colorectal and breast cancer cell lines (Afonja et al. 2004; Asangani et al. 2008; Bitomsky et al. 2008; Frankel et al. 2008). miR-21 has also been shown to regulate the proapoptotic molecule Fas-ligand (Fasl) (Sayed et al. 2010). It has also been shown that miR-21 targets multiple repressors of the Ras/MEK/ERK pathway in cancer cells. These targets include Spry2 and Btg2 (Sayed et al. 2008; Liu et al. 2009).

Recently, in vivo studies conducted by our laboratory and others have confirmed the importance of miR-21 in tumorigenesis. Medina et al. show that activation of miR-21 in B-cells in vivo drives the development of a pre-B malignancy. Interestingly, spontaneous removal of miR-21 overexpression using a doxycycline responsive tetracycline responsive transactivator (tTA) repressive element results in spontaneous regression of the malignancy characterized by a significant increase in apoptosis (Medina et al. 2010). These data describe a form of oncogene addiction whereby the malignancy is dependent on the overexpression of miR-21.

Recent work from our laboratory examined the effects of miR-21 modulation on the progression of non-small-cell lung cancer (NSCLC). The Ras/MEK/ERK pathway has been established as an important driver of NSCLC tumorigenesis (Johnson et al. 2001). Due to the previously described role of miR-21 as a regulator of the Ras/MEK/ERK pathway, the role of miR-21 in NSCLC tumorigenesis was interrogated in vivo. In this report, animals that globally overexpressed miR-21 and *miR-21*$^{-/-}$ animals were crossed to a model of spontaneous NSCLC (Johnson et al. 2001). Interestingly, animals that overexpress miR-21 displayed enhanced tumorigenesis, whereas *miR-21*$^{-/-}$ animals displayed protection against tumorigenesis (Figure 4.1). Further analyses in this study showed that *miR-21*$^{-/-}$ cells display an increased sensitivity to doxorubicin induced apopotosis, supporting an antiapoptotic role for miR-21 in tumorigenesis (Hatley et al. 2010).

Taken together , these studies strongly suggest that miR-21 inhibition may be therapeutically beneficial in the treatment of certain human malignancies. In each case, genetic inhibition of miR-21 results in the sensitization of tumor cells to apoptosis. Interestingly, in the studies performed on *miR-21*$^{-/-}$ animals, no other abnormalities were observed in these mice. Similarly, global overexpression of miR-21 in all tissues did not result in any obvious abnormalities. These observations support our work on miR-21 in cardiac remodeling by suggesting that modification of miR-21 levels in normal tissue does not affect tissue growth or remodeling, but that the effects of miR-21 inhibition may be specific to oncogenic processes. Therefore, therapeutic inhibition of miR-21 for the treatment of cancer is unlikely to affect normal tissue types. Finally, the sensitization of *miR-21*$^{-/-}$ tumor cells to the chemotherapeutic agent doxorubicin suggests that this therapeutic strategy may also synergize with current treatment regimes, reducing the necessary doses of potentially toxic agents. Future studies

should employ the use of microRNA inhibitors, which may be clinically useful for the treatment of human cancers.

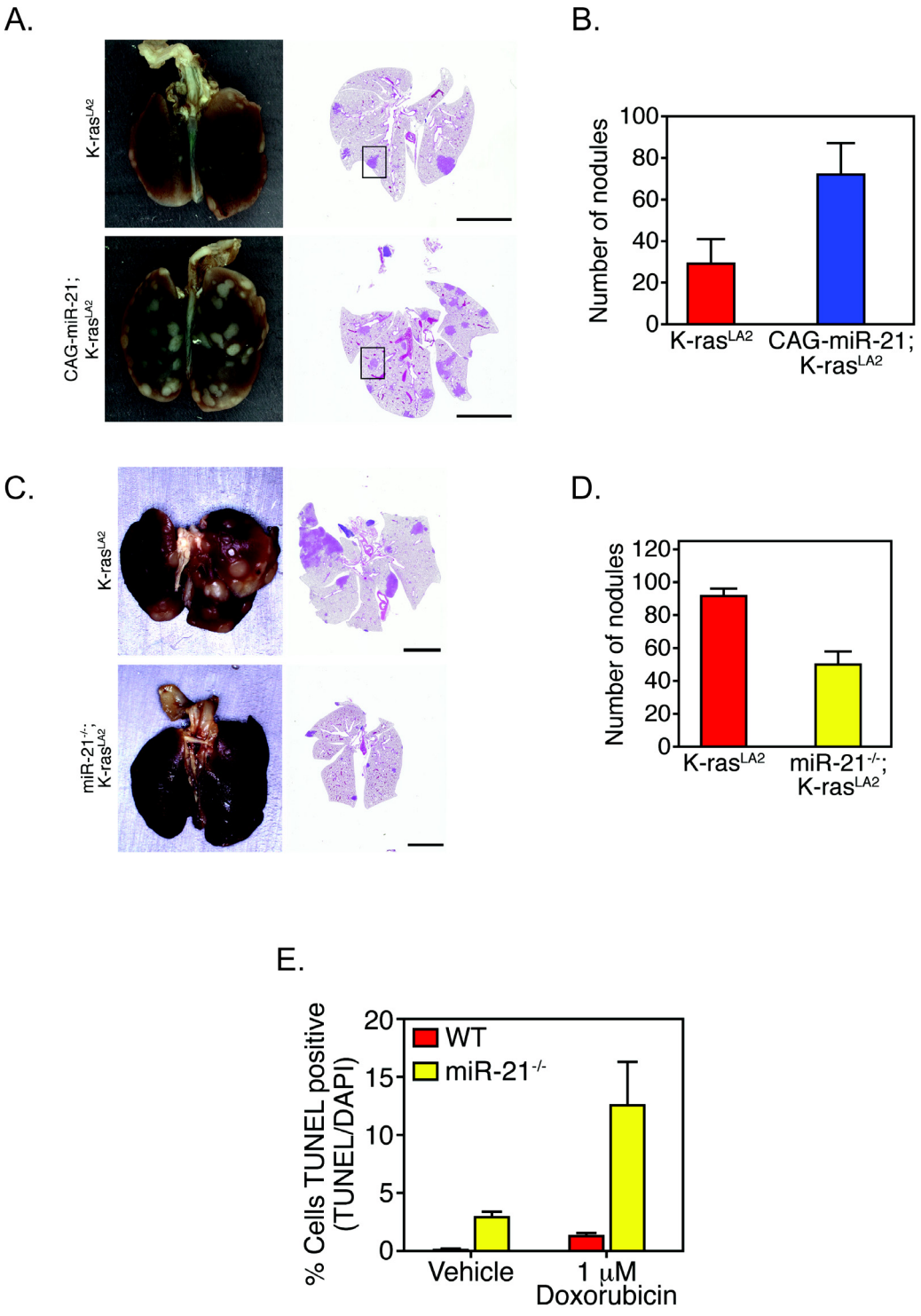

Figure 4.1. *(Legend continued on following page)*

Figure 4.1. Modulation of miR-21 affects NSLC tumorigenesis and chemosensitivity. *(A)* Gross and cross sectional H&E histology of lungs isolated from a NSLC mouse that is either wild-type for miR-21 (*K-ras*^{LA2}) or overexpresses miR-21 globally (*CAG-miR-21;K-ras*^{LA2}). These data show an increase in the number of tumors in animals that overexpress miR-21. *(B)* Surface nodules were counted from *K-ras*^{LA2} animals (n=4) or *CAG-miR-21;K-ras*^{LA2} animals (n=5). p = 0.013. *(C)* Gross and cross sectional H&E histology of lungs isolated from a NSLC mouse that is either wild-type for miR-21 (*K-ras*^{LA2}) or mutant for miR-21 globally (*miR-21*$^{-/-}$*;K-ras*^{LA2}). These data show significantly fewer nodules in the miR-21 mutant animals. *(D)* Surface nodules were counted from *K-ras*^{LA2} (n=3) and *miR-21*$^{-/-}$*;K-ras*^{LA2} animals (n=5). p = 0.008. *(E)* TUNEL assay of wild-type (WT) or *miR-21*$^{-/-}$ mouse embryonic fibroblasts treated with vehicle or 1 μM doxorubicin for 12 hours. *miR-21*$^{-/-}$ are sensitized to doxorubicin induced apoptosis, n = 6. All data are represented as mean ± SEM. Figure is adapted from (Hatley et al. 2010). For further experimental detail, please refer to this report.

MIR-451

MiR-451 mechanistic insights

MiR-451 is most abundant in TER119^{+} erythrocytes and erythrocyte precursors (Merkerova et al. 2008; Merkerova et al. 2010). In fact, deep sequencing analysis of both TER119^{-} CFU-E erythrocyte precursors and the more differentiated TER119^{+} erythcrocyte precursors revealed a 5-fold increase in miR-451 expression. This report also revealed that miR-451 is the most abundant microRNA in late erythrocyte precursors and mature erythrocytes, composing approximately 60% of all microRNAs in these cells (Zhang et al. 2011). Cell type specific function of miR-451 may also be inferred from the aforementioned Ago2$^{fl/fl}$;MX1-Cre bone marrow reconstitution experiments which identify only an erythroid differentiation defect upon Ago2 deletion (O'Carroll et al. 2007). Finally, miR-451 knockout mice do not display any obvious abnormalities aside from an erythroid differentiation defect.

The erythroid differentiation defect observed in *miR-451*$^{-/-}$ mice very closely resembles the STAT5A/B mutant phenotype. Neither mouse line displays obvious abnormalities at baseline. Both lines display a moderate reduction in hematocrit, an inability to sustain a high erythropoietic rate, and an erythroid differentiation defect (Socolovsky et al. 1999; Socolovsky et al. 2001). The similarity of these phenotypes is interesting due to the role of STAT5 as a transcriptional regulator of cell survival and terminal erythrocyte differentiation. Future studies should investigate the role of 14-3-3ζ as a regulator of STAT5 localization and function. Also, due to the role of STAT5 as potent downstream effector of JAK2, the role of 14-3-3ζ as regulator of JAK2 activity should also be examined. These striking phenotypic similarities and the

specificity of miR-451 expression strongly support the therapeutic potential of miR-451 for the treatment of the myeloproliferative disorder polcytythemia vera.

Polcythemia vera

Polycythemia vera (PV) is classified as a chronic myeloproliferative disorder. This disease is primarily characterized by the clonal expansion of hematopoietic stem cells which results in excessive production of erythrocytes specifically, but may also include the overproduction of white blood cells and/or platelets (Ma et al. 2008). Recently, the etiology of PV was identified as a clonal expansion of hematopoietic stem cells which harbor a mutation in JAK2. In fact, 97% of all patients presenting with PV harbor the V617F JAK2 mutation which renders the kinase constitutively active (Levine et al. 2005). The primary disease causing parameter in PV is a dramatically increased HCT which increases blood viscosity and thus coagulability. Symptoms also include fatigue, diaphoresis, and splenomegaly. PV patients die approximately 13 years post diagnosis due to secondary complications of hypercoagulability such as myocardial infarction or cerbrovascular events (Finazzi and Barbui 2007; Ma et al. 2008). First line therapy for PV is periodic phlebotomy which reduces hematocrit temporarily. Patients that do not respond to phlebotomy are then treated with chemotherapeutic agents (Finazzi and Barbui 2007). Currently, therapies are being developed which specifically target JAK2, however, due to the ubiquitous expression of JAK2 and its importance in many physiological processes, significant toxicity has been observed (Pardanani et al. 2011a; Pardanani et al. 2011b; Santos and Verstovsek 2011).

Interestingly, a study profiling microRNA expression in human PV peripheral erythrocytes identified microRNA-451 as the most abundant microRNA. In this study, miR-451

was also shown to be modestly upregulated during the differentiation of PV HSCs when compared to normal HSCs (Bruchova et al. 2007). Due to the profound effect of miR-451 inhibition on erythrocyte production, the cell-type specificity of its expression, the similarity of *miR-451*$^{-/-}$ animals to STAT5A/B mutant animals, and the regulation of miR-451 in PV, we hypothesized that inhibition of miR-451 may be therapeutically useful for the treatment of PV and may be an attractive alternative to current therapeutic regimes.

MiR-451 inhibition reduces disease burden in a mouse model of PV

To examine the effect of miR-451 inhibition on PV progression, we utilized an accepted xenograft mouse model of PV. This model employs a bone marrow transplantation technique whereby hematopoietic stem cells (HSCs) are collected from donor mice, infected with either wild-type human JAK2 (JAK2-WT) or human JAK2V617F (JAK2-VF). JAK2-VF animals develop a disease which very closely resembles human PV within 4-6 weeks post-transplantation which includes very high HCT values and splenomegaly (Wernig et al. 2006). JAK2-WT animals display no abnormalities and are therefore used as a control.

To inhibit miR-451 we utilized an LNA/DNA hybrid (antimiR-451) antimiR developed by Miragen Therapeutics. To examine the ability of miR-451 inhibition to effect disease parameters we performed bone marrow transplantation and allowed for the disease phenotype to fully manifest for 5 weeks. We then treated both JAK2-WT and JAK2-VF transplanted mice with either saline, a mismatch control antimiR, or antimiR-451. Animals were first injected with a high loading dose of 25 mg/kg on two concomitant days and were then maintained with a dose of 10 mg/kg every three days for 9 weeks. To follow disease progression, animals were bled once per week and hematologic parameters were measured.

Over the 9-week period, HCT levels in JAK2-WT animals were not modified across groups. JAK2-VF mice treated with both saline and mismatch did not show a significant reduction in HCT, however, JAK2-VF animals treated with antimiR-451 displayed a significant reduction in HCT compared to mismatch and saline animals combined (Fig. 4.2A,B). Animals were sacrificed after 9-weeks of treatment and spleen weight was analyzed. While the reduction in spleen weight was not statistically significant, the trend strongly suggests a protective effect of antimiR-451 on PV associated splenomegaly (Fig. 4.2C). Finally, to confirm inhibition of miR-451 in antimiR-451 treated animals, $TER119^{+}$ cells from spleen were purified by MACS, RNA was harvested, and northern blots were performed. Interestingly, antimiR-451 significantly reduced the levels of functional miR-451 in antimiR-451 treated animals (Fig. 4.2D). These studies implicate the therapeutic efficacy of antimiR-451 inhibition for the treatment of PV. Future studies should focus on confirming these data and determining the toxicology profiles of antimiR-451 for the use of this molecule in human PV patients.

A.

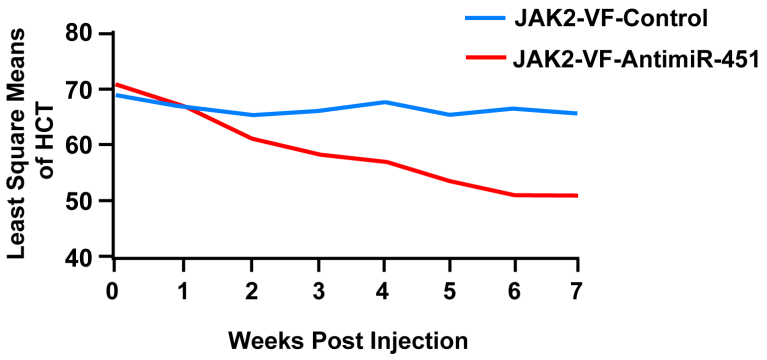

B.

Week	p-value
0	0.7288
1	0.7040
2	0.1616
3	0.0590
4	0.0383
5	0.0080
6	0.0025
7	0.0023

C.

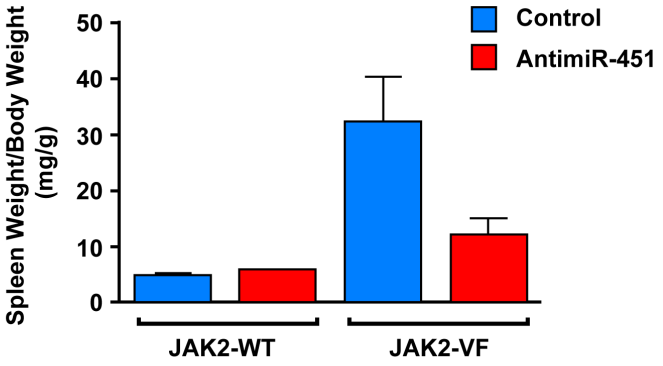

D.

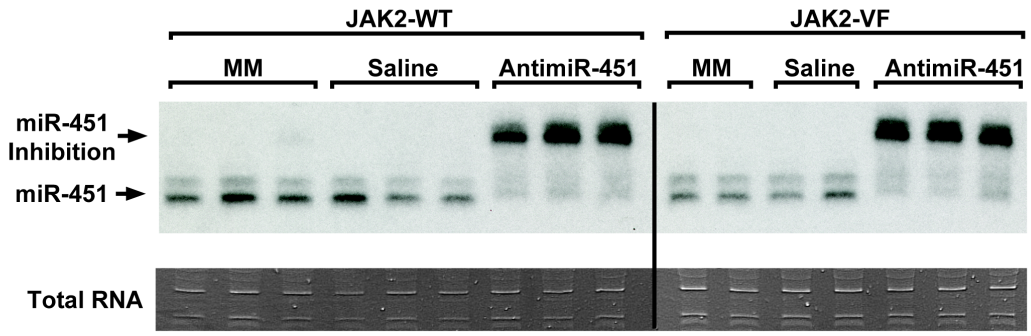

Figure 4.2. *(Figure legend continued on next page)*

Figure 4.2. AntimiR-451 inhibitis miR-451 and reduces disease burden in a mouse model of PV. *(A)* Least mean squares of HCT taken weekly from JAK2-VF animals treated with either antimiR-451 or saline/mismatch (control). These data show a significant reduction in HCT in the anitmiR-451 treated group when compared to control. *(B)* Table showing the p-Values of the difference between the groups in *(A)* at each time point. These data show that HCT is significantly reduced after 4-weeks of antimiR-451 treatment and is maintained. control (n=4); antimiR (n=3). *(C)* Spleen weight/body weight ratios of JAK2-WT and JAK2-VF mice treated with either saline/mismatch (control) or antimiR-451. These data show that antimiR-451 may reduce spleen size. Control (n=4); antimiR (n=3). Data represented as mean ± SEM. *(D)* RNA was harvested from TER119^{+} cells purified from spleen by MACS from all animals treated. miR-451 inhibition is observed only in antimiR-451 treated groups and not in saline or mismatch-antimiR (MM) treated groups. Total RNA is used as a loading control.

LESSONS LEARNED FROM MICRORNA INHIBITORS AND MICRORNA MUTANT ANIMALS

The roles of microRNAs in biology are controversial. Much of the dogma describing microRNA function that was determined upon the discovery of microRNAs has been modified or amended upon. Originally, microRNAs were known to be generalized repressors of mRNA expression however the mechanism of these repressive functions have been debated. A number of studies have reported that the primary function of microRNAs is mRNA destabilization, however, these studies are not supported by others showing the clear accumulation of translational repressors in P-bodies (Fenger-Gron et al. 2005; Jang et al. 2006; Guo et al. 2010). Similarly, both published and unpublished work from our own laboratory suggest that microRNA targets display significant microRNA-responsiveness at the protein level but not at the mRNA level (Xin et al. 2009). Recent work has also suggested that microRNAs may function to increase the expression of target mRNAs (Vasudevan et al. 2007). Finally, new techniques used to identify microRNA-target interactions in vivo have clearly shown that target prediction is imperfect (Karginov et al. 2007; Chi et al. 2009). Highly conserved microRNA binding sites in target transcripts may in fact not be occupied by the predicted microRNA due to unknown reasons. Moreover, it is also clear that most, if not all mRNAs are targeted by multiple microRNAs.

Recently, it has been suggested that microRNAs may in fact play highly redundant roles in a sequence unspecific manner. Studies performed in *C. elegans* have recently shown the likely redundant role of microRNAs as a class of combinatorial regulators of gene expression (Alvarez-Saavedra and Horvitz 2010; Ambros 2010; Brenner et al. 2010). The majority of single

microRNA or microRNA-family mutant worms do not display overt phenotypes. However, when these worms were crossed with worms which were haploinsufficient for the equivalent of Argonaute proteins and were thus haploinsufficient for microRNA function, they displayed mutant-specific phenotypes (Alvarez-Saavedra and Horvitz 2010; Brenner et al. 2010). These studies suggest that a significant amount of microRNA redundancy has evolved and that mutating single microRNAs may result in compensation by unrelated microRNAs. These data may explain the lack of embryonic or developmental phenotypes in the majority of microRNA knockout mice. Perhaps a reduction in global microRNA function would unveil developmental phenotypes in the animals. Future studies should examine the effects of microRNA haploinsufficiency in specific microRNA knockout backgrounds such as the Dicer-Heterozygous mice mentioned above. Unfortunately, no methods currently exist to determine specific redundant microRNA species, however, a description of this process is critical for the understanding of microRNA biology.

Finally, it should be mentioned that the physiologic effects observed in vivo upon treatment of animals with microRNA inhibitors does not always recapitulate the observations of genetic knockout mice. Due to the unknown effects of microRNA inhibitors, it is important to employ the use of both untreated and mismatch treated control groups. Moreover, the lack of genetic loss-of-function confirmation studies represents a significant weakness in the study of microRNA biology in vivo. Both of the studies presented here employed both the use of microRNA inhibitor molecules with concomitant confirmation in genetic knockout mice. These are the only studies that combine these strategies. Future analyses of microRNA inhibitors in vivo should be accompanied by confirmation in genetic knockout mice.

MATERIALS AND METHODS

Generation of PV mouse model

PV animals and WT control animals were generated as previously described (Wernig et al. 2006). Briefly: Adult congenic BALB/C animals were purchased. Donor mice were first injected with 5-fluoro uracil to stimulate division of primitive hematopoietic stem cells. Four days later, bone marrow was harvested from these animals, red cells were selectively lysed, and these cells were cultured in a medium containing a cocktail of cytokines designed to support growth and stimulate the expression of viral recognition proteins. The following day, these cells were infected with a retrovirus expressing either JAK2-V617F mutant human kinase or wild-type human JAK2 as a control. Both viral constructs express GFP from an internal ribosomal entry site. These cells were again cultured overnight to allow for viral genome insertion and expression of the respective JAK2 isoform. One day after infection, the infection procedure was repeated and the cells were suspended in a medium suitable for intravenous injection. Recipient animals were irradiated with 900 cGy and approximately 4-10 x 105 resuspended cells were injected intravenously into the donor animals. These animals were then housed in a sterile environment with administration of antibiotics. Animals were then phlebotomized every 7 days. At these times the percentage of GFP positive cells was monitored by flow cytometry and hematologic parameters were measured usin a Hemavet 850 (Drew Scientific, Dusseldorf Germany).

BIBLIOGRAPHY

Afonja, O., Juste, D., Das, S., Matsuhashi, S., and Samuels, H.H. 2004. Induction of PDCD4 tumor suppressor gene expression by RAR agonists, antiestrogen and HER-2/neu antagonist in breast cancer cells. Evidence for a role in apoptosis. *Oncogene* **23**(49): 8135-8145.

Aitken, A. 2006. 14-3-3 proteins: a historic overview. *Semin Cancer Biol* **16**(3): 162-172.

Alevizos, I. and Illei, G.G. 2010. MicroRNAs as biomarkers in rheumatic diseases. *Nat Rev Rheumatol* **6**(7): 391-398.

Alvarez-Saavedra, E. and Horvitz, H.R. 2010. Many families of C. elegans microRNAs are not essential for development or viability. *Curr Biol* **20**(4): 367-373.

Ambros, V. 2001. microRNAs: tiny regulators with great potential. *Cell* **107**(7): 823-826.

-. 2010. MicroRNAs: genetically sensitized worms reveal new secrets. *Curr Biol* **20**(14): R598-600.

Andersson, K.B., Winer, L.H., Mork, H.K., Molkentin, J.D., and Jaisser, F. 2010. Tamoxifen administration routes and dosage for inducible Cre-mediated gene disruption in mouse hearts. *Transgenic Res* **19**(4): 715-725.

Andrei, M.A., Ingelfinger, D., Heintzmann, R., Achsel, T., Rivera-Pomar, R., and Luhrmann, R. 2005. A role for eIF4E and eIF4E-transporter in targeting mRNPs to mammalian processing bodies. *RNA* **11**(5): 717-727.

Asangani, I.A., Rasheed, S.A., Nikolova, D.A., Leupold, J.H., Colburn, N.H., Post, S., and Allgayer, H. 2008. MicroRNA-21 (miR-21) post-transcriptionally downregulates tumor suppressor Pdcd4 and stimulates invasion, intravasation and metastasis in colorectal cancer. *Oncogene* **27**(15): 2128-2136.

Barry, E.F., Felquer, F.A., Powell, J.A., Biggs, L., Stomski, F.C., Urbani, A., Ramshaw, H., Hoffmann, P., Wilce, M.C., Grimbaldeston, M.A. et al. 2009. 14-3-3:Shc scaffolds integrate phosphoserine and phosphotyrosine signaling to regulate phosphatidylinositol 3-kinase activation and cell survival. *J Biol Chem* **284**(18): 12080-12090.

Bartel, D.P. 2004. MicroRNAs: genomics, biogenesis, mechanism, and function. *Cell* **116**(2): 281-297.

-. 2009. MicroRNAs: target recognition and regulatory functions. *Cell* **136**(2): 215-233.

Bitomsky, N., Wethkamp, N., Marikkannu, R., and Klempnauer, K.H. 2008. siRNA-mediated knockdown of Pdcd4 expression causes upregulation of p21(Waf1/Cip1) expression. *Oncogene* **27**(35): 4820-4829.

Boland, A., Tritschler, F., Heimstadt, S., Izaurralde, E., and Weichenrieder, O. 2010. Crystal structure and ligand binding of the MID domain of a eukaryotic Argonaute protein. *EMBO Rep* **11**(7): 522-527.

Braun, B.S., Tuveson, D.A., Kong, N., Le, D.T., Kogan, S.C., Rozmus, J., Le Beau, M.M., Jacks, T.E., and Shannon, K.M. 2004. Somatic activation of oncogenic Kras in hematopoietic cells initiates a rapidly fatal myeloproliferative disorder. *Proc Natl Acad Sci U S A* **101**(2): 597-602.

Brennecke, J., Stark, A., Russell, R.B., and Cohen, S.M. 2005. Principles of microRNA-target recognition. *PLoS Biol* **3**(3): e85.

Brenner, J.L., Jasiewicz, K.L., Fahley, A.F., Kemp, B.J., and Abbott, A.L. 2010. Loss of individual microRNAs causes mutant phenotypes in sensitized genetic backgrounds in C. elegans. *Curr Biol* **20**(14): 1321-1325.

Bruchova, H., Yoon, D., Agarwal, A.M., Mendell, J., and Prchal, J.T. 2007. Regulated expression of microRNAs in normal and polycythemia vera erythropoiesis. *Exp Hematol* **35**(11): 1657-1667.

Brummer, T., Larance, M., Herrera Abreu, M.T., Lyons, R.J., Timpson, P., Emmerich, C.H., Fleuren, E.D., Lehrbach, G.M., Schramek, D., Guilhaus, M. et al. 2008. Phosphorylation-dependent binding of 14-3-3 terminates signalling by the Gab2 docking protein. *EMBO J* **27**(17): 2305-2316.

Calin, G.A. and Croce, C.M. 2006. MicroRNA signatures in human cancers. *Nat Rev Cancer* **6**(11): 857-866.

Chan, J.A., Krichevsky, A.M., and Kosik, K.S. 2005. MicroRNA-21 is an antiapoptotic factor in human glioblastoma cells. *Cancer Res* **65**(14): 6029-6033.

Cheloufi, S., Dos Santos, C.O., Chong, M.M., and Hannon, G.J. 2010. A dicer-independent miRNA biogenesis pathway that requires Ago catalysis. *Nature*.

Chen, J.F., Murchison, E.P., Tang, R., Callis, T.E., Tatsuguchi, M., Deng, Z., Rojas, M., Hammond, S.M., Schneider, M.D., Selzman, C.H. et al. 2008. Targeted deletion of Dicer in the heart leads to dilated cardiomyopathy and heart failure. *Proc Natl Acad Sci U S A* **105**(6): 2111-2116.

Cheng, Y., Ji, R., Yue, J., Yang, J., Liu, X., Chen, H., Dean, D.B., and Zhang, C. 2007. MicroRNAs are aberrantly expressed in hypertrophic heart: do they play a role in cardiac hypertrophy? *Am J Pathol* **170**(6): 1831-1840.

Cheng, Y., Liu, X., Zhang, S., Lin, Y., Yang, J., and Zhang, C. 2009. MicroRNA-21 protects against the H(2)O(2)-induced injury on cardiac myocytes via its target gene PDCD4. *J Mol Cell Cardiol* **47**(1): 5-14.

Chi, S.W., Zang, J.B., Mele, A., and Darnell, R.B. 2009. Argonaute HITS-CLIP decodes microRNA-mRNA interaction maps. *Nature* **460**(7254): 479-486.

Chiang, H.R., Schoenfeld, L.W., Ruby, J.G., Auyeung, V.C., Spies, N., Baek, D., Johnston, W.K., Russ, C., Luo, S., Babiarz, J.E. et al. 2010. Mammalian microRNAs: experimental evaluation of novel and previously annotated genes. *Genes Dev* **24**(10): 992-1009.

Ciafre, S.A., Galardi, S., Mangiola, A., Ferracin, M., Liu, C.G., Sabatino, G., Negrini, M., Maira, G., Croce, C.M., and Farace, M.G. 2005. Extensive modulation of a set of microRNAs in primary glioblastoma. *Biochem Biophys Res Commun* **334**(4): 1351-1358.

Cifuentes, D., Xue, H., Taylor, D.W., Patnode, H., Mishima, Y., Cheloufi, S., Ma, E., Mane, S., Hannon, G.J., Lawson, N. et al. 2010. A Novel miRNA Processing Pathway Independent of Dicer Requires Argonaute2 Catalytic Activity. *Science*.

Cimmino, A., Calin, G.A., Fabbri, M., Iorio, M.V., Ferracin, M., Shimizu, M., Wojcik, S.E., Aqeilan, R.I., Zupo, S., Dono, M. et al. 2005. miR-15 and miR-16 induce apoptosis by targeting BCL2. *Proc Natl Acad Sci U S A* **102**(39): 13944-13949.

Constantinescu, S.N., Ghaffari, S., and Lodish, H.F. 1999. The Erythropoietin Receptor: Structure, Activation and Intracellular Signal Transduction. *Trends Endocrinol Metab* **10**(1): 18-23.

Cougot, N., Babajko, S., and Seraphin, B. 2004. Cytoplasmic foci are sites of mRNA decay in human cells. *J Cell Biol* **165**(1): 31-40.
Croce, C.M. 2009. Causes and consequences of microRNA dysregulation in cancer. *Nat Rev Genet* **10**(10): 704-714.
da Costa Martins, P.A., Bourajjaj, M., Gladka, M., Kortland, M., van Oort, R.J., Pinto, Y.M., Molkentin, J.D., and De Windt, L.J. 2008. Conditional dicer gene deletion in the postnatal myocardium provokes spontaneous cardiac remodeling. *Circulation* **118**(15): 1567-1576.
da Costa Martins, P.A., Salic, K., Gladka, M.M., Armand, A.S., Leptidis, S., el Azzouzi, H., Hansen, A., Coenen-de Roo, C.J., Bierhuizen, M.F., van der Nagel, R. et al. 2010. MicroRNA-199b targets the nuclear kinase Dyrk1a in an auto-amplification loop promoting calcineurin/NFAT signalling. *Nat Cell Biol* **12**(12): 1220-1227.
Danielian, P.S., Muccino, D., Rowitch, D.H., Michael, S.K., and McMahon, A.P. 1998. Modification of gene activity in mouse embryos in utero by a tamoxifen-inducible form of Cre recombinase. *Curr Biol* **8**(24): 1323-1326.
Ding, L. and Han, M. 2007. GW182 family proteins are crucial for microRNA-mediated gene silencing. *Trends Cell Biol* **17**(8): 411-416.
Dong, S., Cheng, Y., Yang, J., Li, J., Liu, X., Wang, X., Wang, D., Krall, T.J., Delphin, E.S., and Zhang, C. 2009. MicroRNA expression signature and the role of microRNA-21 in the early phase of acute myocardial infarction. *J Biol Chem* **284**(43): 29514-29525.
Dore, L.C., Amigo, J.D., Dos Santos, C.O., Zhang, Z., Gai, X., Tobias, J.W., Yu, D., Klein, A.M., Dorman, C., Wu, W. et al. 2008. A GATA-1-regulated microRNA locus essential for erythropoiesis. *Proc Natl Acad Sci U S A* **105**(9): 3333-3338.
Elmen, J., Lindow, M., Schutz, S., Lawrence, M., Petri, A., Obad, S., Lindholm, M., Hedtjarn, M., Hansen, H.F., Berger, U. et al. 2008a. LNA-mediated microRNA silencing in non-human primates. *Nature* **452**(7189): 896-899.
Elmen, J., Lindow, M., Silahtaroglu, A., Bak, M., Christensen, M., Lind-Thomsen, A., Hedtjarn, M., Hansen, J.B., Hansen, H.F., Straarup, E.M. et al. 2008b. Antagonism of microRNA-122 in mice by systemically administered LNA-antimiR leads to up-regulation of a large set of predicted target mRNAs in the liver. *Nucleic Acids Res* **36**(4): 1153-1162.
Felker, G.M., Thompson, R.E., Hare, J.M., Hruban, R.H., Clemetson, D.E., Howard, D.L., Baughman, K.L., and Kasper, E.K. 2000. Underlying causes and long-term survival in patients with initially unexplained cardiomyopathy. *N Engl J Med* **342**(15): 1077-1084.
Felli, N., Fontana, L., Pelosi, E., Botta, R., Bonci, D., Facchiano, F., Liuzzi, F., Lulli, V., Morsilli, O., Santoro, S. et al. 2005. MicroRNAs 221 and 222 inhibit normal erythropoiesis and erythroleukemic cell growth via kit receptor down-modulation. *Proc Natl Acad Sci U S A* **102**(50): 18081-18086.
Fenger-Gron, M., Fillman, C., Norrild, B., and Lykke-Andersen, J. 2005. Multiple processing body factors and the ARE binding protein TTP activate mRNA decapping. *Mol Cell* **20**(6): 905-915.
Finazzi, G. and Barbui, T. 2007. How I treat patients with polycythemia vera. *Blood* **109**(12): 5104-5111.
Frank, F., Sonenberg, N., and Nagar, B. 2010. Structural basis for 5'-nucleotide base-specific recognition of guide RNA by human AGO2. *Nature* **465**(7299): 818-822.

Frankel, L.B., Christoffersen, N.R., Jacobsen, A., Lindow, M., Krogh, A., and Lund, A.H. 2008. Programmed cell death 4 (PDCD4) is an important functional target of the microRNA miR-21 in breast cancer cells. *J Biol Chem* **283**(2): 1026-1033.

Fujita, S., Ito, T., Mizutani, T., Minoguchi, S., Yamamichi, N., Sakurai, K., and Iba, H. 2008. miR-21 Gene expression triggered by AP-1 is sustained through a double-negative feedback mechanism. *J Mol Biol* **378**(3): 492-504.

Ganau, A., Devereux, R.B., Roman, M.J., de Simone, G., Pickering, T.G., Saba, P.S., Vargiu, P., Simongini, I., and Laragh, J.H. 1992. Patterns of left ventricular hypertrophy and geometric remodeling in essential hypertension. *J Am Coll Cardiol* **19**(7): 1550-1558.

Ghaffari, S., Kitidis, C., Fleming, M.D., Neubauer, H., Pfeffer, K., and Lodish, H.F. 2001. Erythropoiesis in the absence of janus-kinase 2: BCR-ABL induces red cell formation in JAK2(-/-) hematopoietic progenitors. *Blood* **98**(10): 2948-2957.

Gilbert, S.F. 2000. Sites of Hematopoiesis. in *Developmental Biology*. Sinauer Associates, Sunderland (MA).

Guo, H., Ingolia, N.T., Weissman, J.S., and Bartel, D.P. 2010. Mammalian microRNAs predominantly act to decrease target mRNA levels. *Nature* **466**(7308): 835-840.

Hafner, M., Landgraf, P., Ludwig, J., Rice, A., Ojo, T., Lin, C., Holoch, D., Lim, C., and Tuschl, T. 2008. Identification of microRNAs and other small regulatory RNAs using cDNA library sequencing. *Methods* **44**(1): 3-12.

Hatley, M.E., Patrick, D.M., Garcia, M.R., Richardson, J.A., Bassel-Duby, R., van Rooij, E., and Olson, E.N. 2010. Modulation of K-Ras-dependent lung tumorigenesis by MicroRNA-21. *Cancer Cell* **18**(3): 282-293.

Hill, J.A., Karimi, M., Kutschke, W., Davisson, R.L., Zimmerman, K., Wang, Z., Kerber, R.E., and Weiss, R.M. 2000. Cardiac hypertrophy is not a required compensatory response to short-term pressure overload. *Circulation* **101**(24): 2863-2869.

Hill, J.A. and Olson, E.N. 2008. Cardiac plasticity. *N Engl J Med* **358**(13): 1370-1380.

Hipfner, D.R., Weigmann, K., and Cohen, S.M. 2002. The bantam gene regulates Drosophila growth. *Genetics* **161**(4): 1527-1537.

Ikeda, S., Kong, S.W., Lu, J., Bisping, E., Zhang, H., Allen, P.D., Golub, T.R., Pieske, B., and Pu, W.T. 2007. Altered microRNA expression in human heart disease. *Physiol Genomics* **31**(3): 367-373.

Ingelfinger, D., Arndt-Jovin, D.J., Luhrmann, R., and Achsel, T. 2002. The human LSm1-7 proteins colocalize with the mRNA-degrading enzymes Dcp1/2 and Xrnl in distinct cytoplasmic foci. *RNA* **8**(12): 1489-1501.

Jaenisch, R. and Bird, A. 2003. Epigenetic regulation of gene expression: how the genome integrates intrinsic and environmental signals. *Nat Genet* **33 Suppl**: 245-254.

Jang, L.T., Buu, L.M., and Lee, F.J. 2006. Determinants of Rbp1p localization in specific cytoplasmic mRNA-processing foci, P-bodies. *J Biol Chem* **281**(39): 29379-29390.

Johnson, L., Mercer, K., Greenbaum, D., Bronson, R.T., Crowley, D., Tuveson, D.A., and Jacks, T. 2001. Somatic activation of the K-ras oncogene causes early onset lung cancer in mice. *Nature* **410**(6832): 1111-1116.

Jopling, C.L., Yi, M., Lancaster, A.M., Lemon, S.M., and Sarnow, P. 2005. Modulation of hepatitis C virus RNA abundance by a liver-specific MicroRNA. *Science* **309**(5740): 1577-1581.

Kanellopoulou, C., Muljo, S.A., Kung, A.L., Ganesan, S., Drapkin, R., Jenuwein, T., Livingston, D.M., and Rajewsky, K. 2005. Dicer-deficient mouse embryonic stem cells are defective in differentiation and centromeric silencing. *Genes Dev* **19**(4): 489-501.

Karginov, F.V., Conaco, C., Xuan, Z., Schmidt, B.H., Parker, J.S., Mandel, G., and Hannon, G.J. 2007. A biochemical approach to identifying microRNA targets. *Proc Natl Acad Sci U S A* **104**(49): 19291-19296.

Kim, V.N. 2005. MicroRNA biogenesis: coordinated cropping and dicing. *Nat Rev Mol Cell Biol* **6**(5): 376-385.

Krek, A., Grun, D., Poy, M.N., Wolf, R., Rosenberg, L., Epstein, E.J., MacMenamin, P., da Piedade, I., Gunsalus, K.C., Stoffel, M. et al. 2005. Combinatorial microRNA target predictions. *Nat Genet* **37**(5): 495-500.

Krutzfeldt, J., Kuwajima, S., Braich, R., Rajeev, K.G., Pena, J., Tuschl, T., Manoharan, M., and Stoffel, M. 2007. Specificity, duplex degradation and subcellular localization of antagomirs. *Nucleic Acids Res* **35**(9): 2885-2892.

Krutzfeldt, J., Rajewsky, N., Braich, R., Rajeev, K.G., Tuschl, T., Manoharan, M., and Stoffel, M. 2005. Silencing of microRNAs in vivo with 'antagomirs'. *Nature* **438**(7068): 685-689.

Kuhnert, F., Mancuso, M.R., Hampton, J., Stankunas, K., Asano, T., Chen, C.Z., and Kuo, C.J. 2008. Attribution of vascular phenotypes of the murine Egfl7 locus to the microRNA miR-126. *Development* **135**(24): 3989-3993.

Kung, H.C., Hoyert, D.L., Xu, J., and Murphy, S.L. 2008. Deaths: final data for 2005. *Natl Vital Stat Rep* **56**(10): 1-120.

Kwon, C., Han, Z., Olson, E.N., and Srivastava, D. 2005. MicroRNA1 influences cardiac differentiation in Drosophila and regulates Notch signaling. *Proc Natl Acad Sci U S A* **102**(52): 18986-18991.

Lagos-Quintana, M., Rauhut, R., Lendeckel, W., and Tuschl, T. 2001. Identification of novel genes coding for small expressed RNAs. *Science* **294**(5543): 853-858.

Lanford, R.E., Hildebrandt-Eriksen, E.S., Petri, A., Persson, R., Lindow, M., Munk, M.E., Kauppinen, S., and Orum, H. 2010. Therapeutic silencing of microRNA-122 in primates with chronic hepatitis C virus infection. *Science* **327**(5962): 198-201.

Lau, N.C., Lim, L.P., Weinstein, E.G., and Bartel, D.P. 2001. An abundant class of tiny RNAs with probable regulatory roles in Caenorhabditis elegans. *Science* **294**(5543): 858-862.

Lee, R.C. and Ambros, V. 2001. An extensive class of small RNAs in Caenorhabditis elegans. *Science* **294**(5543): 862-864.

Lee, R.C., Feinbaum, R.L., and Ambros, V. 1993. The C. elegans heterochronic gene lin-4 encodes small RNAs with antisense complementarity to lin-14. *Cell* **75**(5): 843-854.

Lee, Y., Jeon, K., Lee, J.T., Kim, S., and Kim, V.N. 2002. MicroRNA maturation: stepwise processing and subcellular localization. *EMBO J* **21**(17): 4663-4670.

Lennox, K.A. and Behlke, M.A. 2010. A direct comparison of anti-microRNA oligonucleotide potency. *Pharm Res* **27**(9): 1788-1799.

Levine, R.L., Wadleigh, M., Cools, J., Ebert, B.L., Wernig, G., Huntly, B.J., Boggon, T.J., Wlodarska, I., Clark, J.J., Moore, S. et al. 2005. Activating mutation in the tyrosine kinase JAK2 in polycythemia vera, essential thrombocythemia, and myeloid metaplasia with myelofibrosis. *Cancer Cell* **7**(4): 387-397.

Lewis, B.P., Burge, C.B., and Bartel, D.P. 2005. Conserved seed pairing, often flanked by adenosines, indicates that thousands of human genes are microRNA targets. *Cell* **120**(1): 15-20.
Lewis, B.P., Shih, I.H., Jones-Rhoades, M.W., Bartel, D.P., and Burge, C.B. 2003. Prediction of mammalian microRNA targets. *Cell* **115**(7): 787-798.
Liu, M., Wu, H., Liu, T., Li, Y., Wang, F., Wan, H., Li, X., and Tang, H. 2009. Regulation of the cell cycle gene, BTG2, by miR-21 in human laryngeal carcinoma. *Cell Res* **19**(7): 828-837.
Liu, N., Okamura, K., Tyler, D.M., Phillips, M.D., Chung, W.J., and Lai, E.C. 2008. The evolution and functional diversification of animal microRNA genes. *Cell Res* **18**(10): 985-996.
Lopez-Romero, P., Gonzalez, M.A., Callejas, S., Dopazo, A., and Irizarry, R.A. 2010. Processing of Agilent microRNA array data. *BMC Res Notes* **3**: 18.
Lu, J., Getz, G., Miska, E.A., Alvarez-Saavedra, E., Lamb, J., Peck, D., Sweet-Cordero, A., Ebert, B.L., Mak, R.H., Ferrando, A.A. et al. 2005. MicroRNA expression profiles classify human cancers. *Nature* **435**(7043): 834-838.
Lu, J., Guo, S., Ebert, B.L., Zhang, H., Peng, X., Bosco, J., Pretz, J., Schlanger, R., Wang, J.Y., Mak, R.H. et al. 2008. MicroRNA-mediated control of cell fate in megakaryocyte-erythrocyte progenitors. *Dev Cell* **14**(6): 843-853.
Ma, X., Vanasse, G., Cartmel, B., Wang, Y., and Selinger, H.A. 2008. Prevalence of polycythemia vera and essential thrombocythemia. *Am J Hematol* **83**(5): 359-362.
Maeda, T., Ito, K., Merghoub, T., Poliseno, L., Hobbs, R.M., Wang, G., Dong, L., Maeda, M., Dore, L.C., Zelent, A. et al. 2009. LRF is an essential downstream target of GATA1 in erythroid development and regulates BIM-dependent apoptosis. *Dev Cell* **17**(4): 527-540.
Matkovich, S.J., Van Booven, D.J., Youker, K.A., Torre-Amione, G., Diwan, A., Eschenbacher, W.H., Dorn, L.E., Watson, M.A., Margulies, K.B., and Dorn, G.W., 2nd. 2009. Reciprocal regulation of myocardial microRNAs and messenger RNA in human cardiomyopathy and reversal of the microRNA signature by biomechanical support. *Circulation* **119**(9): 1263-1271.
Medina, P.P., Nolde, M., and Slack, F.J. 2010. OncomiR addiction in an in vivo model of microRNA-21-induced pre-B-cell lymphoma. *Nature* **467**(7311): 86-90.
Meister, G., Landthaler, M., Patkaniowska, A., Dorsett, Y., Teng, G., and Tuschl, T. 2004. Human Argonaute2 mediates RNA cleavage targeted by miRNAs and siRNAs. *Mol Cell* **15**(2): 185-197.
Meister, G., Landthaler, M., Peters, L., Chen, P.Y., Urlaub, H., Luhrmann, R., and Tuschl, T. 2005. Identification of novel argonaute-associated proteins. *Curr Biol* **15**(23): 2149-2155.
Mendell, J.T. 2008. miRiad roles for the miR-17-92 cluster in development and disease. *Cell* **133**(2): 217-222.
Meng, F., Henson, R., Wehbe-Janek, H., Ghoshal, K., Jacob, S.T., and Patel, T. 2007. MicroRNA-21 regulates expression of the PTEN tumor suppressor gene in human hepatocellular cancer. *Gastroenterology* **133**(2): 647-658.
Merkerova, M., Belickova, M., and Bruchova, H. 2008. Differential expression of microRNAs in hematopoietic cell lineages. *Eur J Haematol* **81**(4): 304-310.
Merkerova, M., Vasikova, A., Belickova, M., and Bruchova, H. 2010. MicroRNA expression profiles in umbilical cord blood cell lineages. *Stem Cells Dev* **19**(1): 17-26.

Molkentin, J.D., Lu, J.R., Antos, C.L., Markham, B., Richardson, J., Robbins, J., Grant, S.R., and Olson, E.N. 1998. A calcineurin-dependent transcriptional pathway for cardiac hypertrophy. *Cell* **93**(2): 215-228.

Moss, E.G., Lee, R.C., and Ambros, V. 1997. The cold shock domain protein LIN-28 controls developmental timing in C. elegans and is regulated by the lin-4 RNA. *Cell* **88**(5): 637-646.

Mourelatos, Z., Dostie, J., Paushkin, S., Sharma, A., Charroux, B., Abel, L., Rappsilber, J., Mann, M., and Dreyfuss, G. 2002. miRNPs: a novel class of ribonucleoproteins containing numerous microRNAs. *Genes Dev* **16**(6): 720-728.

Nelson, P.T., De Planell-Saguer, M., Lamprinaki, S., Kiriakidou, M., Zhang, P., O'Doherty, U., and Mourelatos, Z. 2007. A novel monoclonal antibody against human Argonaute proteins reveals unexpected characteristics of miRNAs in human blood cells. *RNA* **13**(10): 1787-1792.

O'Carroll, D., Mecklenbrauker, I., Das, P.P., Santana, A., Koenig, U., Enright, A.J., Miska, E.A., and Tarakhovsky, A. 2007. A Slicer-independent role for Argonaute 2 in hematopoiesis and the microRNA pathway. *Genes Dev* **21**(16): 1999-2004.

Obad, S., Dos Santos, C.O., Petri, A., Heidenblad, M., Broom, O., Ruse, C., Fu, C., Lindow, M., Stenvang, J., Straarup, E.M. et al. 2011. Silencing of microRNA families by seed-targeting tiny LNAs. *Nat Genet*.

Pan, X., Wang, Z.X., and Wang, R. 2010. MicroRNA-21: a novel therapeutic target in human cancer. *Cancer Biol Ther* **10**(12): 1224-1232.

Pardanani, A., Gotlib, J.R., Jamieson, C., Cortes, J.E., Talpaz, M., Stone, R.M., Silverman, M.H., Gilliland, D.G., Shorr, J., and Tefferi, A. 2011a. Safety and Efficacy of TG101348, a Selective JAK2 Inhibitor, in Myelofibrosis. *J Clin Oncol* **29**(7): 789-796.

Pardanani, A., Vannucchi, A.M., Passamonti, F., Cervantes, F., Barbui, T., and Tefferi, A. 2011b. JAK inhibitor therapy for myelofibrosis: critical assessment of value and limitations. *Leukemia* **25**(2): 218-225.

Park, C.Y., Choi, Y.S., and McManus, M.T. 2010. Analysis of microRNA knockouts in mice. *Hum Mol Genet* **19**(R2): R169-175.

Parker, R. and Sheth, U. 2007. P bodies and the control of mRNA translation and degradation. *Mol Cell* **25**(5): 635-646.

Pase, L., Layton, J.E., Kloosterman, W.P., Carradice, D., Waterhouse, P.M., and Lieschke, G.J. 2009. miR-451 regulates zebrafish erythroid maturation in vivo via its target gata2. *Blood* **113**(8): 1794-1804.

Pedersen, I.M., Cheng, G., Wieland, S., Volinia, S., Croce, C.M., Chisari, F.V., and David, M. 2007. Interferon modulation of cellular microRNAs as an antiviral mechanism. *Nature* **449**(7164): 919-922.

Pevny, L., Simon, M.C., Robertson, E., Klein, W.H., Tsai, S.F., D'Agati, V., Orkin, S.H., and Costantini, F. 1991. Erythroid differentiation in chimaeric mice blocked by a targeted mutation in the gene for transcription factor GATA-1. *Nature* **349**(6306): 257-260.

Pogribny, I.P., Starlard-Davenport, A., Tryndyak, V.P., Han, T., Ross, S.A., Rusyn, I., and Beland, F.A. 2010. Difference in expression of hepatic microRNAs miR-29c, miR-34a, miR-155, and miR-200b is associated with strain-specific susceptibility to dietary nonalcoholic steatohepatitis in mice. *Lab Invest* **90**(10): 1437-1446.

Prchal, J.T. 2006. Production of Erythrocytes. in *Williams Hematology*, Columbus, (OH).

Raj, A. and van Oudenaarden, A. 2008. Nature, nurture, or chance: stochastic gene expression and its consequences. *Cell* **135**(2): 216-226.
Rao, P.K., Toyama, Y., Chiang, H.R., Gupta, S., Bauer, M., Medvid, R., Reinhardt, F., Liao, R., Krieger, M., Jaenisch, R. et al. 2009. Loss of cardiac microRNA-mediated regulation leads to dilated cardiomyopathy and heart failure. *Circ Res* **105**(6): 585-594.
Rehwinkel, J., Behm-Ansmant, I., Gatfield, D., and Izaurralde, E. 2005. A crucial role for GW182 and the DCP1:DCP2 decapping complex in miRNA-mediated gene silencing. *RNA* **11**(11): 1640-1647.
Ren, X.P., Wu, J., Wang, X., Sartor, M.A., Qian, J., Jones, K., Nicolaou, P., Pritchard, T.J., and Fan, G.C. 2009. MicroRNA-320 is involved in the regulation of cardiac ischemia/reperfusion injury by targeting heat-shock protein 20. *Circulation* **119**(17): 2357-2366.
Robertson, B., Dalby, A.B., Karpilow, J., Khvorova, A., Leake, D., and Vermeulen, A. 2010. Specificity and functionality of microRNA inhibitors. *Silence* **1**(1): 10.
Roccaro, A.M., Sacco, A., Thompson, B., Leleu, X., Azab, A.K., Azab, F., Runnels, J., Jia, X., Ngo, H.T., Melhem, M.R. et al. 2009. MicroRNAs 15a and 16 regulate tumor proliferation in multiple myeloma. *Blood* **113**(26): 6669-6680.
Rosenquist, M., Sehnke, P., Ferl, R.J., Sommarin, M., and Larsson, C. 2000. Evolution of the 14-3-3 protein family: does the large number of isoforms in multicellular organisms reflect functional specificity? *J Mol Evol* **51**(5): 446-458.
Santos, F.P. and Verstovsek, S. 2011. JAK2 inhibitors: What's the true therapeutic potential? *Blood Rev* **25**(2): 53-63.
Sayed, D., He, M., Hong, C., Gao, S., Rane, S., Yang, Z., and Abdellatif, M. 2010. MicroRNA-21 is a downstream effector of AKT that mediates its antiapoptotic effects via suppression of Fas ligand. *J Biol Chem* **285**(26): 20281-20290.
Sayed, D., Hong, C., Chen, I.Y., Lypowy, J., and Abdellatif, M. 2007. MicroRNAs play an essential role in the development of cardiac hypertrophy. *Circ Res* **100**(3): 416-424.
Sayed, D., Rane, S., Lypowy, J., He, M., Chen, I.Y., Vashistha, H., Yan, L., Malhotra, A., Vatner, D., and Abdellatif, M. 2008. MicroRNA-21 targets Sprouty2 and promotes cellular outgrowths. *Mol Biol Cell* **19**(8): 3272-3282.
Schluter, K.D. and Wenzel, S. 2008. Angiotensin II: a hormone involved in and contributing to pro-hypertrophic cardiac networks and target of anti-hypertrophic cross-talks. *Pharmacol Ther* **119**(3): 311-325.
Schneider, M.D., Najand, N., Chaker, S., Pare, J.M., Haskins, J., Hughes, S.C., Hobman, T.C., Locke, J., and Simmonds, A.J. 2006. Gawky is a component of cytoplasmic mRNA processing bodies required for early Drosophila development. *J Cell Biol* **174**(3): 349-358.
Sliva, D., Gu, M., Zhu, Y.X., Chen, J., Tsai, S., Du, X., and Yang, Y.C. 2000. 14-3-3zeta interacts with the alpha-chain of human interleukin 9 receptor. *Biochem J* **345 Pt 3**: 741-747.
Socolovsky, M., Fallon, A.E., Wang, S., Brugnara, C., and Lodish, H.F. 1999. Fetal anemia and apoptosis of red cell progenitors in Stat5a-/-5b-/- mice: a direct role for Stat5 in Bcl-X(L) induction. *Cell* **98**(2): 181-191.
Socolovsky, M., Nam, H., Fleming, M.D., Haase, V.H., Brugnara, C., and Lodish, H.F. 2001. Ineffective erythropoiesis in Stat5a(-/-)5b(-/-) mice due to decreased survival of early erythroblasts. *Blood* **98**(12): 3261-3273.

Stefani, G. and Slack, F.J. 2008. Small non-coding RNAs in animal development. *Nat Rev Mol Cell Biol* **9**(3): 219-230.

Stomski, F.C., Dottore, M., Winnall, W., Guthridge, M.A., Woodcock, J., Bagley, C.J., Thomas, D.T., Andrews, R.K., Berndt, M.C., and Lopez, A.F. 1999. Identification of a 14-3-3 binding sequence in the common beta chain of the granulocyte-macrophage colony-stimulating factor (GM-CSF), interleukin-3 (IL-3), and IL-5 receptors that is serine-phosphorylated by GM-CSF. *Blood* **94**(6): 1933-1942.

Su, H., Trombly, M.I., Chen, J., and Wang, X. 2009. Essential and overlapping functions for mammalian Argonautes in microRNA silencing. *Genes Dev* **23**(3): 304-317.

Tatsuguchi, M., Seok, H.Y., Callis, T.E., Thomson, J.M., Chen, J.F., Newman, M., Rojas, M., Hammond, S.M., and Wang, D.Z. 2007. Expression of microRNAs is dynamically regulated during cardiomyocyte hypertrophy. *J Mol Cell Cardiol* **42**(6): 1137-1141.

Thum, T., Chau, N., Bhat, B., Gupta, S.K., Linsley, P.S., Bauersachs, J., and Engelhardt, S. 2011. Comparison of different miR-21 inhibitor chemistries in a cardiac disease model. *J Clin Invest* **121**(2): 461-462; author reply 462-463.

Thum, T., Galuppo, P., Wolf, C., Fiedler, J., Kneitz, S., van Laake, L.W., Doevendans, P.A., Mummery, C.L., Borlak, J., Haverich, A. et al. 2007. MicroRNAs in the human heart: a clue to fetal gene reprogramming in heart failure. *Circulation* **116**(3): 258-267.

Thum, T., Gross, C., Fiedler, J., Fischer, T., Kissler, S., Bussen, M., Galuppo, P., Just, S., Rottbauer, W., Frantz, S. et al. 2008. MicroRNA-21 contributes to myocardial disease by stimulating MAP kinase signalling in fibroblasts. *Nature* **456**(7224): 980-984.

Urbich, C., Kuehbacher, A., and Dimmeler, S. 2008. Role of microRNAs in vascular diseases, inflammation, and angiogenesis. *Cardiovasc Res* **79**(4): 581-588.

van Rooij, E., Sutherland, L.B., Liu, N., Williams, A.H., McAnally, J., Gerard, R.D., Richardson, J.A., and Olson, E.N. 2006. A signature pattern of stress-responsive microRNAs that can evoke cardiac hypertrophy and heart failure. *Proc Natl Acad Sci U S A* **103**(48): 18255-18260.

van Rooij, E., Sutherland, L.B., Qi, X., Richardson, J.A., Hill, J., and Olson, E.N. 2007. Control of stress-dependent cardiac growth and gene expression by a microRNA. *Science* **316**(5824): 575-579.

Vasudevan, S., Tong, Y., and Steitz, J.A. 2007. Switching from repression to activation: microRNAs can up-regulate translation. *Science* **318**(5858): 1931-1934.

Ventura, A., Young, A.G., Winslow, M.M., Lintault, L., Meissner, A., Erkeland, S.J., Newman, J., Bronson, R.T., Crowley, D., Stone, J.R. et al. 2008. Targeted deletion reveals essential and overlapping functions of the miR-17 through 92 family of miRNA clusters. *Cell* **132**(5): 875-886.

Volinia, S., Calin, G.A., Liu, C.G., Ambs, S., Cimmino, A., Petrocca, F., Visone, R., Iorio, M., Roldo, C., Ferracin, M. et al. 2006. A microRNA expression signature of human solid tumors defines cancer gene targets. *Proc Natl Acad Sci U S A* **103**(7): 2257-2261.

Wang, Q., Huang, Z., Xue, H., Jin, C., Ju, X.L., Han, J.D., and Chen, Y.G. 2008a. MicroRNA miR-24 inhibits erythropoiesis by targeting activin type I receptor ALK4. *Blood* **111**(2): 588-595.

Wang, S., Aurora, A.B., Johnson, B.A., Qi, X., McAnally, J., Hill, J.A., Richardson, J.A., Bassel-Duby, R., and Olson, E.N. 2008b. The endothelial-specific microRNA miR-126 governs vascular integrity and angiogenesis. *Dev Cell* **15**(2): 261-271.

Wang, Y., Medvid, R., Melton, C., Jaenisch, R., and Blelloch, R. 2007. DGCR8 is essential for microRNA biogenesis and silencing of embryonic stem cell self-renewal. *Nat Genet* **39**(3): 380-385.

Wernig, G., Mercher, T., Okabe, R., Levine, R.L., Lee, B.H., and Gilliland, D.G. 2006. Expression of Jak2V617F causes a polycythemia vera-like disease with associated myelofibrosis in a murine bone marrow transplant model. *Blood* **107**(11): 4274-4281.

Xin, M., Small, E.M., Sutherland, L.B., Qi, X., McAnally, J., Plato, C.F., Richardson, J.A., Bassel-Duby, R., and Olson, E.N. 2009. MicroRNAs miR-143 and miR-145 modulate cytoskeletal dynamics and responsiveness of smooth muscle cells to injury. *Genes Dev* **23**(18): 2166-2178.

Yang, J.S., Maurin, T., Robine, N., Rasmussen, K.D., Jeffrey, K.L., Chandwani, R., Papapetrou, E.P., Sadelain, M., O'Carroll, D., and Lai, E.C. 2010. Conserved vertebrate mir-451 provides a platform for Dicer-independent, Ago2-mediated microRNA biogenesis. *Proc Natl Acad Sci U S A* **107**(34): 15163-15168.

Yu, D., dos Santos, C.O., Zhao, G., Jiang, J., Amigo, J.D., Khandros, E., Dore, L.C., Yao, Y., D'Souza, J., Zhang, Z. et al. 2010. miR-451 protects against erythroid oxidant stress by repressing 14-3-3zeta. *Genes Dev* **24**(15): 1620-1633.

Yuan, J.Y., Wang, F., Yu, J., Yang, G.H., Liu, X.L., and Zhang, J.W. 2009. MicroRNA-223 reversibly regulates erythroid and megakaryocytic differentiation of K562 cells. *J Cell Mol Med* **13**(11-12): 4551-4559.

Zhan, M., Miller, C.P., Papayannopoulou, T., Stamatoyannopoulos, G., and Song, C.Z. 2007. MicroRNA expression dynamics during murine and human erythroid differentiation. *Exp Hematol* **35**(7): 1015-1025.

Zhang, J., Liu, Y., Beard, C., Tuveson, D.A., Jaenisch, R., Jacks, T.E., and Lodish, H.F. 2007. Expression of oncogenic K-ras from its endogenous promoter leads to a partial block of erythroid differentiation and hyperactivation of cytokine-dependent signaling pathways. *Blood* **109**(12): 5238-5241.

Zhang, J. and Lodish, H.F. 2005. Identification of K-ras as the major regulator for cytokine-dependent Akt activation in erythroid progenitors in vivo. *Proc Natl Acad Sci U S A* **102**(41): 14605-14610.

-. 2007. Endogenous K-ras signaling in erythroid differentiation. *Cell Cycle* **6**(16): 1970-1973.

Zhang, J., Socolovsky, M., Gross, A.W., and Lodish, H.F. 2003. Role of Ras signaling in erythroid differentiation of mouse fetal liver cells: functional analysis by a flow cytometry-based novel culture system. *Blood* **102**(12): 3938-3946.

Zhang, L., Flygare, J., Wong, P., Lim, B., and Lodish, H.F. 2011. miR-191 regulates mouse erythroblast enucleation by down-regulating Riok3 and Mxi1. *Genes Dev* **25**(2): 119-124.

Zhao, G., Yu, D., and Weiss, M.J. 2010. MicroRNAs in erythropoiesis. *Curr Opin Hematol* **17**(3): 155-162.